INSTANTANEOUS BER ESTIMATION BASED LINK ADAPTATION AND SCHEDULING IN MULTI-BAND OFDM UWB WPANS

by

ENGİN MAŞAZADE

Submitted to the Graduate School of Engineering and Natural Sciences
in partial fulfillment of
the requirements for the degree of
Master of Science

Sabancı University
January 2006

INSTANTANEOUS BER ESTIMATION BASED LINK ADAPTATION AND SCHEDULING IN MULTI-BAND OFDM UWB WPANS

APPROVED BY:

Assist. Prof. Dr. Mehmet Keskinöz …….

(Thesis Supervisor)

Assist. Prof. Dr. Özgür Gürbüz …….

Prof. Dr. Hakan Deliç …….

Assist. Prof. Dr. İbrahim Tekin …….

Assoc. Prof. Dr. Yaşar Gürbüz …….

DATE OF APPROVAL: …….

INSTANTANEOUS BER ESTIMATION BASED LINK ADAPTATION AND SCHEDULING IN MULTI-BAND OFDM UWB WPANS

ABSTRACT

Ultra Wide Band (UWB) systems have gained interest because of their abilities to provide high data rate with low power transmission for WPANs. This thesis considers the Multi band OFDM UWB WPANs over time varying channels. Due to the channel impairments, the links are subject to degradations in quality varying with time and space. To maximize the link efficiency, we consider an immediate acknowledgement protocol with dynamically and optimally selected frame sizes according to the channels bit error rate (BER) estimates. The BER is first estimated in maximum likelihood sense, by applying Modiano's algorithm. Since, this makes the tracking of the channel difficult under fast fading conditions, we propose a new method to model and estimate the BER of the MB-OFDM UWB links based on the OFDM subcarrier signal to noise ratios.

In a wireless network, opportunistic scheduling improves the network performance by allocating more resources to good links. We also propose an opportunistic channel access scheme using IEEE 802.15.3 WPAN superframe structure to enhance the system throughput further. In this method, time allocations for individual links are proportionally determined with respect to their instantaneous efficiencies. Simulation results show that opportunistic scheduling along with frame size adaptation improves the individual link throughputs up to thirty percent for low number of links and up to hundred and ten percent for large number of links; and overall network throughputs by twenty seven percent up to eighteen simultaneously operating connections as compared to the equal-time scheduled links operating with fixed frame sizes.

ÇOK BANT OFDM WPAN'LER İÇİN ANLIK BİT HATA ORANI KESTİRİMİNE DAYALI BİR BAĞLANTI UYARLAMA VE BAĞLANTI ÇİZELGELEME YÖNTEMİ

ÖZET

MB-OFDM tabanlı UWB kablosuz iletişimi, düşük güçlü ve yüksek hızlı bağlantılara imkan vermesiyle, gelecek kablosuz kişisel alan ağları (WPAN) için iyi bir fiziksel katman seçimi olarak göze çarpar. Ne var ki, bu tür kablosuz bağlantıların verimi kanalın zamana bağlı değişen özelliklerine bağlıdır. Bu tezde MB-OFDM temelli WPAN'ların başarımı zamanla değişen gürültülü kanallarda incelenmektedir. Ağ içerisindeki her bir bağlantının veriminin en çoklanması için kullanılan paket boyunun kanalın anlık durumuna bağlı olarak seçilmesi önerilmektedir. Kanalın anlık durumu bit hata oranı (BER) cinsinden ifade edilmiş, anlık BER'i kestirebilmek için ilk etapta kanalın fiziksel özelliklerinden bağımsız Modiano'nun algoritması (MA) uygulanmıştır. MA, BER kestirimi için belli miktarda veri paketinin önceden iletimine ihtiyaç duymasından dolayı çok hızlı değişen kanallar bu yöntemle takip edilemez. Yaptığımız çalışmada kanal BER'inin OFDM taşıyıcılarının işaret gürültü oranı dağılımıyla yüksek ilişkili olduğu sonucuna varılmış ve bu ilişki kullanılarak MB-OFDM sistemler için yeni bir BER kestirim yöntemi sunulmuştur.

Bu tezde ayrıca IEEE 802.15.3 çerçeve yapısı temelinde, ağ içindeki herhangi bir bağlantıya tahsis edilen süreyi, o bağlantının kestirilmiş kanal verimi ile orantılı olarak belirleyen yeni bir zaman çizelgeleme yöntemi sunulmuştur. Bu yöntemin başarımı, her bir bağlantıya çerçeve içerisinde eşit süre ayıran bir çizelgeleme ile karşılaştırılmıştır. Verilen benzetim parametrelerine göre, önerilen çizelgeleme, paket boyu uyarlamasıyla beraber kullanıldığında, sabit uzunlukta paket kullanılan eşit zaman çizelgelemeli bir duruma göre genel ağ net iletim hızını aynı anda haberleşen onsekiz bağlantıya kadar yüzde yirmiyedi, ağ içindeki her bir bağlantının net iletim hızını düşük sayıda bağlantı için yüzde otuz, çok sayıda bağlantı için yüzde yüzona kadar arttırmaktadır.

ACKNOWLEDGEMENTS

I would like to thank everybody who has contributed to the realization of this thesis. Special thanks go to my supervisor Assist. Prof. Dr. Mehmet Keskinöz for his invaluable guidance and support all through my stay at the Department Electrical Engineering and Computer Science. I am also grateful to Assist. Prof. Dr. Özgür Gürbüz for her contributions to this thesis.

I want to express my gratitude to my colleagues and members of Sabancı University for creating stimulating work environment. I am indebted to the members of the jury of my thesis: Prof. Dr. Hakan Deliç, Assoc. Prof. Dr. Yaşar Gürbüz and Assist. Prof. Dr. İbrahim Tekin for reviewing my thesis and for their useful remarks.

Especially, I would like to thank my family for their endless support during all my studies. It would not have been possible to manage everything without them.

TABLE OF CONTENTS

TABLE OF FIGURES

1. INTRODUCTION

In the information age, the demand for wireless communications and Internet/multimedia communications is growing drastically. The research and development in this field is taking place to define the next generation wireless broadband networks. This type of networks brings both wireless and multimedia applications together. Today there are three important wireless technologies is in use, namely Wireless Wide Area Networks (WWAN), Wireless Local Area Networks (WLAN), and Wireless Personal Area Networks (WPAN) [1].

As depicted in Figure 1. 1, these technologies are not competing but they are complementing each other. The growth in WWAN area has been amazing over the last decade. Second generation (2G) and third generation (3G) systems are in use today [1],[2]. The existing 2G systems are essentially designed for voice purposes. On the other hand, as a result of the incredible expansion of the Internet, support for data services like Wireless Application Protocol (WAP) is also developed [1],[2]. Further services, like 3G, provide additional opportunities for data services with varying Quality of Service (QoS) requirements. WLANs provide higher data rates as compared to WWANs for slower mobile channels and they are mainly used for transmission of Internet protocol packets. WLANs provide network access as a complement to the wireline systems. Today Institute of Electrical and Electronics Engineering (IEEE) 802.11 based protocols are widely used, which support up to 54 Mbps data rates inside a several hundred meters cell radius [3]. WPANs, such as Bluetooth, are used for short distance communications (~10 meters) with low data rates (721 Kbps) [1],[2]. Meanwhile, IEEE 802.15.3 [4] based WPAN standards are developed to provide higher data rates greater than 55 Mbps, which opens a path towards to broadband WPANs. In this area, Ultra-wide band (UWB) systems have recently gained a lot of interest because of their abilities to provide high data rate transmission with low power consumption and cost.

Following sections are devoted to discuss UWB based PAN and PAN MAC .

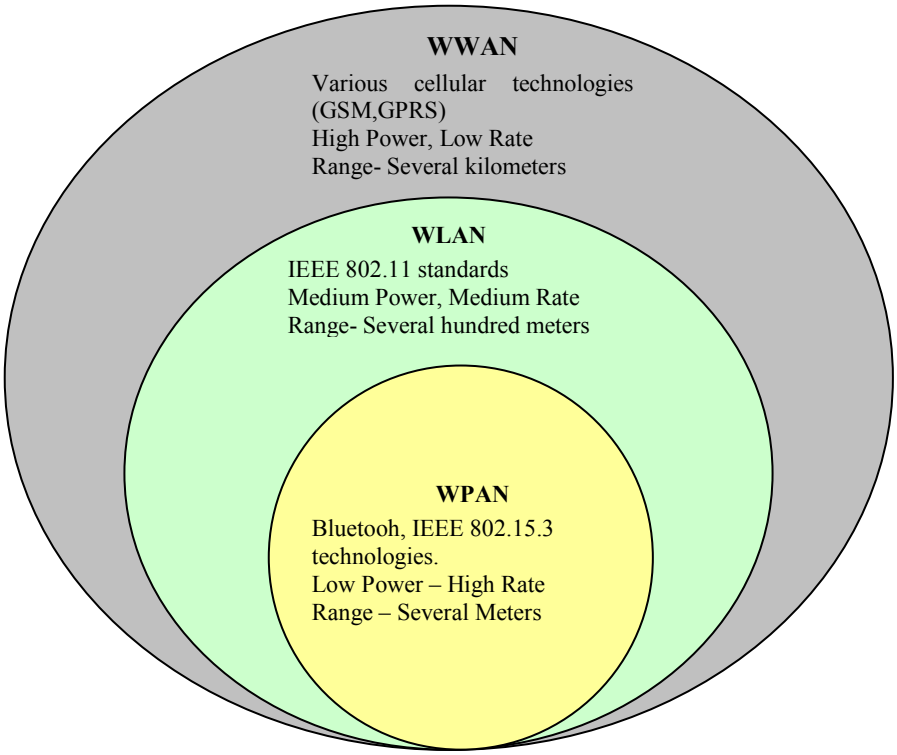

Figure 1. 1 Partition among wireless systems

1.1. UWB Systems

The common agreement on UWB definition comes from the UWB radar world. The instantaneous energy bandwidth of a waveform is defined by the frequencies f_L and f_H, which describe the interval where most of the waveform energy (over 90%) falls. The width of this interval is called as *energy bandwidth*. The *fractional bandwidth* is then defined as the ratio of the energy bandwidth to the center frequency as,

$$\text{fractional bandwidth} = \frac{f_H - f_L}{\left(\frac{f_H + f_L}{2}\right)} \tag{1.1}$$

If the fractional bandwidth is greater than 0.2-0.25 the signal is said to be UWB [5]

In February 2002, the Federal Communications Commissions (FCC) [6] defined that a signal is UWB if its bandwidth is greater than 500 MHz, and opened the unlicensed

spectrum between 3.1 GHz and 10.6 GHz for the use of UWB. The FCC has set an upper limit of -41.3 dBm/MHz on the transmitted power. The low transmit power is meant to avoid interfering other services, like 802.11, which operate inside the UWB spectrum.

Standardization of the UWB physical layer is still under development under the control of IEEE 802.15.3a task group [7]. The submitted UWB physical layer proposals focus on three techniques. One method is based on Direct Sequence UWB (DS-UWB) [8], another is based on Time Division / Frequency Division Multiple Access (TD/FDMA) pulse approach [9], and the third method is based on Orthogonal Frequency Division Multiplexing (OFDM) [10],[11]. Each approach is described briefly in the coming subsections.

1.1.1. DS-UWB Approach

In direct sequence spread spectrum (DS-SS), users can simultaneously occupy a large common channel and they are separated by digital codes rather than the waveform frequency. Unlike conventional carrier based DS-SS, the DS-UWB approach uses non-sinusoidal wavelets, which are designed to occupy the allowed UWB spectrum [8]. Figure 1. 2, shows two sample wavelets with spectral contents in 3.1 GHz to 5.1 GHz band and 5.8 GHz to 10.6 GHz band. To avoid interfering IEEE 802.11 based systems the band around 5 GHz is restricted. Both bands can be used together or independently to achieve different levels of performance.

The sequences of wavelets are multiplied with a 32-length orthogonal sequence that is composed of –1,0,1 where this modulation scheme is referred as Multi-level Bi-Orthogonal Keying (*M-BOK*). The wavelets are generated at 1.368 Giga cycles per second (Gcps). Since each symbol is composed of 32 wavelets, the symbol rate becomes 42.75 Mega symbols per second (Msym/s). For a *64-BOK* modulation, each symbol carries 6 bit information, so the data rate becomes 42.75 Msym/s x 6 = 256.5 Mbps. Using a rate 0.44 error-correction code results 112 Mbps data rate. This channel capacity is obtained by utilizing the lower frequency band. Other possible data rates are 224 Mbps and 448 Mbps. Using the parameters of 112 Mbps data rate, 224 Mbps data

rate is obtained by simultaneously using upper and lower frequency bands. Similarly in order to achieve 448 Mbps data rate, the coding rate is selected as 0.87.

Although DS-UWB achieves very high data rates, there are some practical disadvantages. Since DS-UWB uses very narrow wavelets in time domain, system needs an accurate timing generator. For the symbol transmission and reception digital to analog (DAC) and analog to digital converters (ADC) must have very high sampling rates. For such systems the channel estimation algorithms become complex and channel-matching filter is needed to be long to capture all the major channel energy [12],[13].

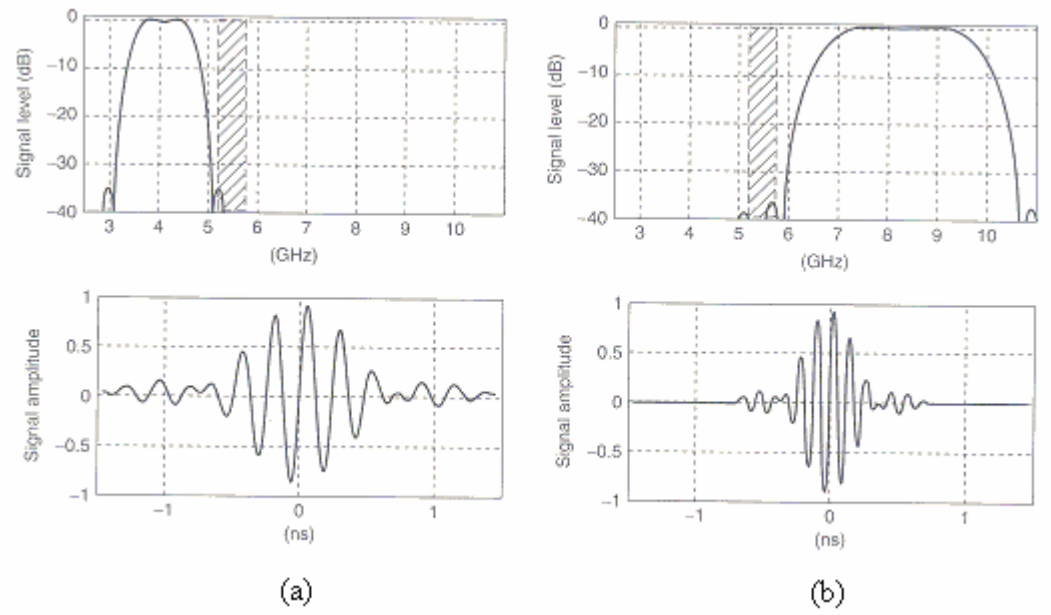

Figure 1. 2 DS-UWB Wavelet and its spectrum (a) in the 3.1GHz to 5GHz (b) in the 6 GHz to 10.6 GHz (Reprinted from Ultra Wideband Radio Technology Swiak, K;McKeown, D. John Wiley & Sons, 2004).

1.1.2. TD/FDMA Approach

A second approach to implement UWB systems is Time Domain / Frequency Domain Multiple Access (TD/FDMA). In this approach the wavelets are centered at frequencies that are spaced by 550 MHz and each wavelet occupies a 700 MHz bandwidth. Figure 1. 3 shows the wavelets for the first four bands and the corresponding spectral occupancy. This approach alleviates the multipath propagation hence intersymbol

interference by increasing the time intervals between successive wavelets that share the same channel. Also by using TD/FDMA approach each sub-band needs lower ADC sampling rate and the length of the digital filters needed for channel equalization is reduced. [14]

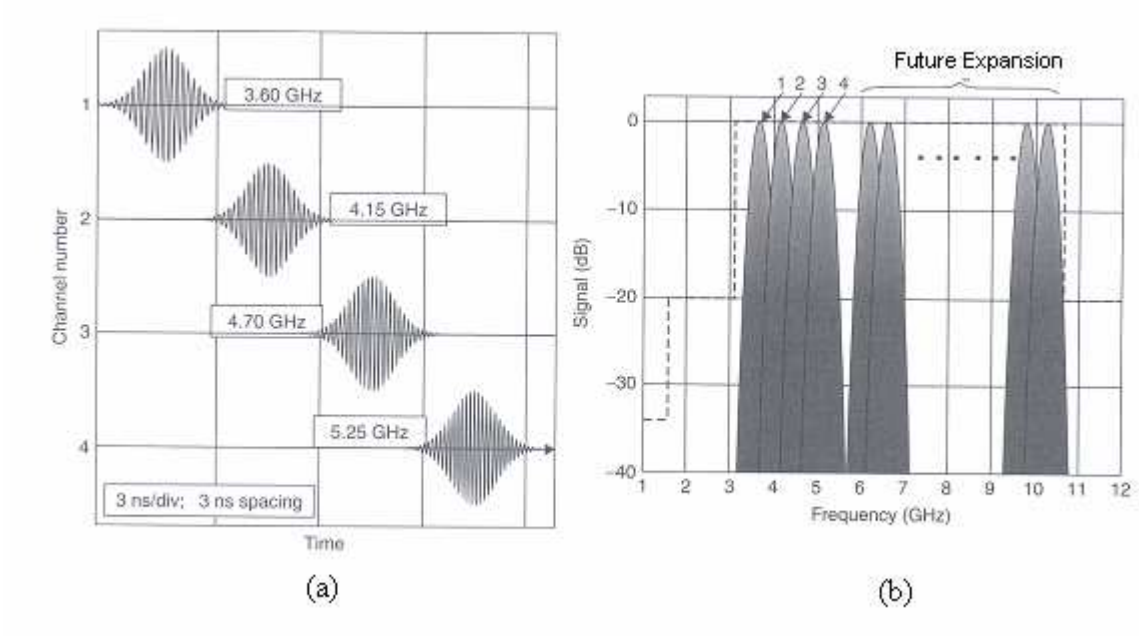

Figure 1. 3 (a) Wavelets (b) Spectrum occupancy for a TD/FDMA UWB system (Reprinted from Ultra Wideband Radio Technology Swiak, K;McKeown, D. John Wiley & Sons, 2004).

1.1.3. MB-OFDM Based UWB

OFDM technology appears in many wired and wireless communication services. Asymmetric Digital Subscriber Line (ADSL) service uses OFDM over wireline telephone networks. OFDM is also used in IEEE 802.11a/g WLAN standards and terrestrial Digital Audio Broadcasting (DAB), Digital Video Broadcasting (DVB) systems.

1.1.3.1.OFDM Fundamentals

The idea behind OFDM is splitting a high rate data stream into many lower rate substreams. The data substreams are then transmitted on subcarriers which are orthogonal to each other. Namely, OFDM divides the allocated frequency range into many parallel orthogonal subcarriers. OFDM's beauty originates from its spectral

efficiency. In traditional Frequency Division Multiplexing Schemes (FDM) the spectrum is divided into channels with some guard band between them. On the other hand OFDM allows subcarriers to overlap while they can be still received without any adjacent subcarrier interference. Figure 1. 4 shows the spectral efficiency of OFDM.

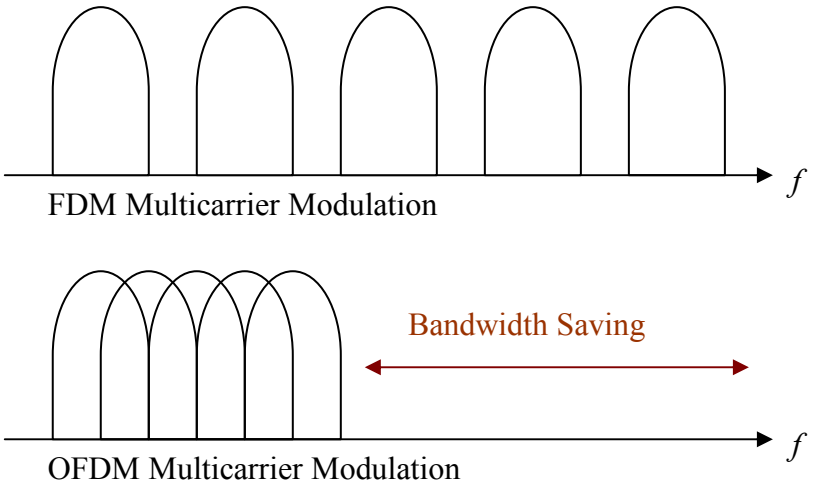

Figure 1. 4 Spectrum utilization of FDM and OFDM

Let a QPSK modulated serial symbols with symbol period T, is divided into N parallel substreams. After the N parallel conversion the symbol period on each substream increases to $T_s = T$ x N. The baseband equivalent of the signal that is composed of N parallel subcarriers is can be given as,

$$s(t) = \sum_{n=-\infty}^{\infty} \sum_{k=0}^{N-1} X_{n,k} e^{j2\pi f_k (t-T_s)} \qquad (1.2)$$

where $X_{n,k}$ is the QPSK modulated symbol transmitted on k^{th} subcarrier of the n^{th} OFDM symbol and f_k is the central frequency of the k^{th} subcarrier.

If the frequency spacing between any two subcarriers is a multiple of $1/T_s$, namely

$$f_k = \frac{k}{T_s} \qquad (1.3)$$

The subcarriers become perfectly orthogonal to each other. Since the frequency of each subcarrier is an integer multiple of $1 / T_s$ each subcarrier carriers integer number of periods inside the T_s duration.

To verify this property lets find the receiver output at each subcarrier. Let $c_k(t) = e^{j2\pi f_k t}$ Down-converting the received signal by $c_k^*(t)$ and integrating over T_s seconds performs the demodulation as,

$$\hat{X}_k = \frac{1}{T_s}\int_0^{T_s}\left[\sum_{k=0}^{N-1} X_k c_k(t)\right] c_k^*(t)\,dt = \frac{1}{T_s}\int_0^{T_s}\left[\sum_{k=0}^{N-1} X_k e^{j2\pi\frac{k}{T_s}t}\right] e^{-j2\pi\frac{l}{T_s}t}\,dt \quad k,l \text{ integer}$$

$$\hat{X}_k = \frac{1}{T_s}\int_0^{T_s}\sum_{k=0}^{N-1} X_k e^{j2\pi\frac{(k-l)}{T_s}t}\,dt = \frac{1}{T_s}\sum_{k=0}^{N-1} X_k \int_0^{T_s} e^{j2\pi\frac{(k-l)}{T_s}t}\,dt$$

$$\hat{X}_k = \frac{1}{T_s}\sum_{k=0}^{N-1} X_k \left[\int_0^{T_s}\cos(2\pi(k-l)\frac{t}{T_s})dt + j\int_0^{T_s}\sin(2\pi(k-l)\frac{t}{T_s})dt\right]$$

$$\hat{X}_k = \sum_{k=0}^{N-1} X_k \frac{\sin(2\pi(k-l))}{2\pi(k-l)}$$

(1.4)

So that,

$$\hat{X}_k = \begin{cases} X_k & k = l \\ 0 & k \neq l \end{cases} \tag{1.5}$$

The OFDM modulation given in Eq.(1.2) can be implemented efficiently by using the Inverse Fast Fourier Transform (IFFT) algorithms.

Another point of view, lets assume the symbols of first subcarrier are represented with ideal square pulses and subcarrier frequency is $1/T_s$. The output signal can be written as,

$$s_k(t) = \frac{1}{T_s}\Pi(\frac{t}{T_s}) \tag{1.6}$$

The Fourier transform of the signal then becomes,

$$S_k(f) = \text{sinc}(\pi f T_s) \tag{1.7}$$

As shown in Figure 1. 5, the above equation gives one at $f = 0$ and zero for integer multiples of $1/T_s$. Thus subcarrier spacing with $1/T_s$ allows subcarriers to overlap but symbols can be still received without adjacent carrier interference.

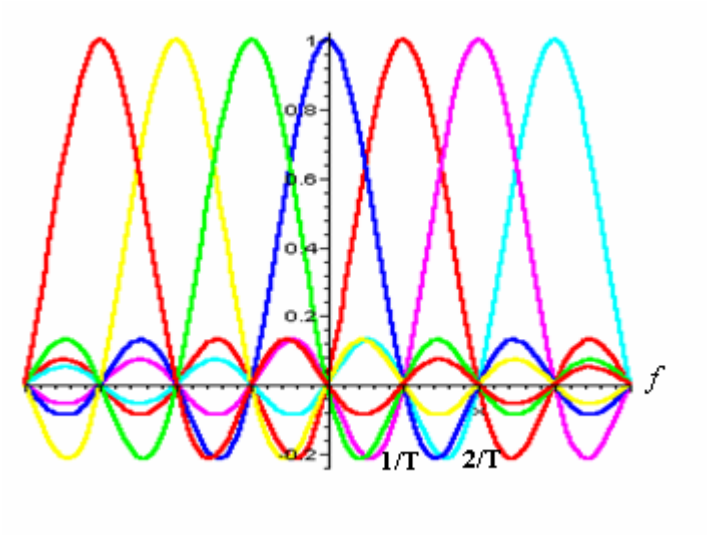

Figure 1. 5 Spectrum of individual subcarriers

Over multipath fading channels receiver not only captures the direct line-of-sight (LOS) signal, but also captures many signal reflections coming from different propagation paths. Such dispersive channels result intersymbol interference (ISI) between adjacent symbols. The channel does not introduce ISI when $\sigma_\tau << T$, where σ_τ is the RMS delay spread of the channel, and T is the symbol period. By dividing the spectrum into N parallel substreams the symbol period increases to T_s. Since the data throughput is the sum of all parallel substreams throughput, OFDM allows designing high data rate systems without exceeding the delay spread of the channel. On the other hand, under such dispersive channels, the signals received with some propagation delay do not carry integer number of periods inside the T_s interval. Hence orthogonality is violated and intercarrier interference (ICI) is introduced.

In order to mitigate with ISI and ICI, OFDM brings *cyclic prefix* (CP), as a guard interval between adjacent OFDM symbols. Appending the last part of the time domain OFDM symbol to the beginning of the OFDM symbol as shown in Figure 1. 6 creates the cyclic prefix.

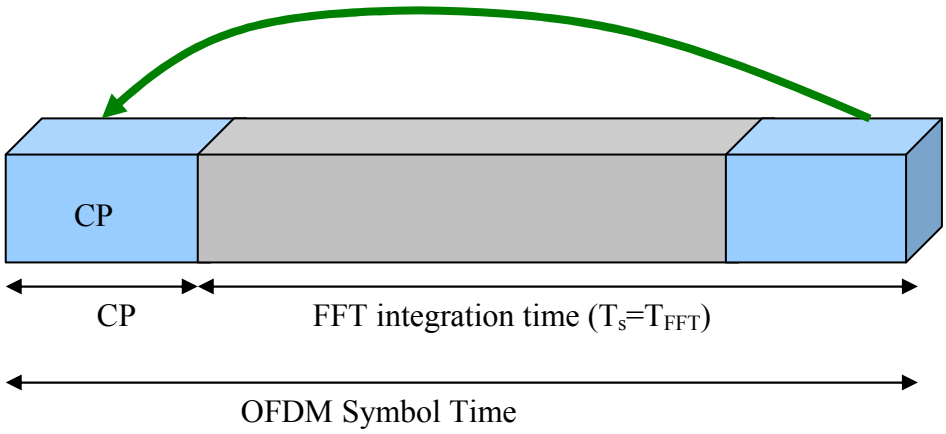

Figure 1. 6 OFDM symbol with cyclic prefix

The length of the cyclic prefix should be selected at least the excess delay of the channel. So the incoming multipath arrivals disappear before the beginning of the information carrying part of the OFDM symbol. Hence CP ensures no ISI between consecutive OFDM symbols. Similarly, since the CP duration is longer than the channel's excess delay, entire multipath components arrive inside the CP. Therefore; OFDM symbols always carry integer number of cycles within the FFT integration time and avoid the ICI.

1.1.3.2.MB-OFDM Approach

In this approach UWB waveforms are generated with conventional OFDM modulation. The 500 MHz bandwidth regulation of FCC is met by 128 subcarriers that are spaced 4.125 MHz apart from each other. Hence, a single MB-OFDM signal occupies a 528 MHz wide channel. The 528 MHz wide signal is then upconverted to the one of the frequency band inside the UWB spectrum as shown in Figure 1. 7. The MB-OFDM approach simultaneously uses at least three bands at a time in a time-frequency hopping manner. As shown in Figure 1. 8, The MB-OFDM symbol remains at Band 1 for a FFT integration period ($1/T_{FFT}$) 242.42 ns plus a cyclic prefix period 60.6 ns. The MB-OFDM symbol is then switched to Band 2 within 9.5 ns. After a 312.5 ns the MB-OFDM symbol is now in Band 3 and resumes accordingly.

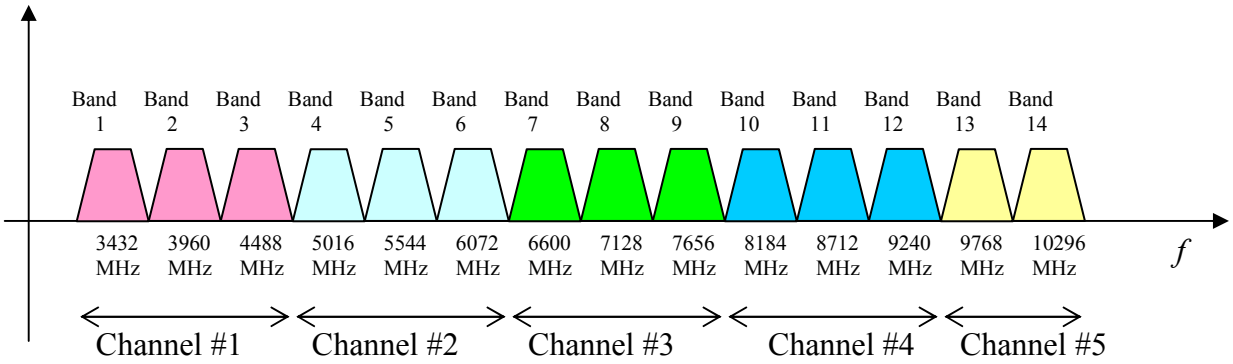

Figure 1. 7 MB-OFDM Band Occupancy

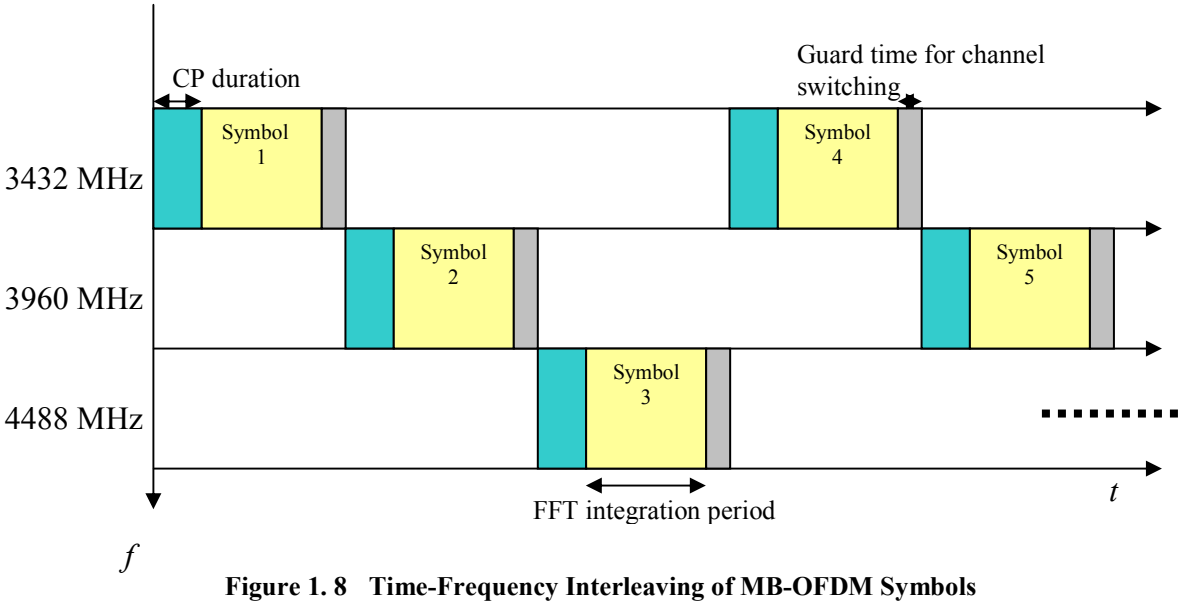

Figure 1. 8 Time-Frequency Interleaving of MB-OFDM Symbols

MB-OFDM based UWB proposal support maximum 480Mbps data rate with QPSK modulated symbols on each subcarrier. The initial MB-OFDM systems utilize Channel 1 bands since the hardware technology is already available for this spectrum. The bands beyond Channel 1 are reserved for future growth.

MB-OFDM approach is much different from the traditional UWB schemes. It does not implement the impulse radio concept [15]. Instead, it uses conventional communication techniques to access the FCC's 7.5 GHz unlicensed spectrum. By the help of cyclic prefix OFDM is an efficient way to deal with multipath propagation. The cyclic prefix also eases the equalizer implementation as compared to the DS-UWB approach. OFDM is also robust against narrowband interference because such interference only affects a number of subcarriers. Using error correction coding, the errors originated by the interfered subcarriers can be recovered up to some limit. OFDM is also well analyzed

for high rate WLANs and DVB. Finally MB-OFDM has a great flexibility by turning off subcarriers and turning off bands in order to coexist with already allocated services in different parts of the world. Therefore, due to these nice virtues of OFDM (e.g., simple equalization, multipath and interference resilience), in this thesis, we concentrate on the MB-OFDM approach of Texas Instruments (TI) [10][11]

1.2. WPAN Medium Access Control

For the usage of WPANs there are two Medium Access Control Standards: The Bluetooth MAC [1]and the IEEE 802.15.3 MAC [4]. Briefly, Bluetooth MAC has a star topology and point-to-point communications between devices is not allowed. Instead point-to-point links between the master and slave devices are allowed. On the other hand IEEE 802.15.3 MAC, the network management is centralized but data transfer is performed in an ad-hoc manner. Master device grants channel access for each link on a TDMA fashion and only schedules the transmission time for point-to-point links between the slave devices and it is not involved in data exchange.

1.3. Motivations for the Thesis

Fortunately, the MB-OFDM UWB physical layer proposal and IEEE 802.15.3 MAC standard presents some flexible parameters (e.g. data rate, frame size, superframe duration), so selecting appropriate values provide performance improvements in the data link and access layers of WPANs. Due to impairments in wireless environments (e.g. multi-path fading, shadowing, multi-user interference etc.), wireless links are subject to severe degradation in quality that varies with time and space. Since, the physical layer proposal leaves the frame size decision to designers, selecting the frame size dynamically based on the instantaneous link conditions enhances link throughput. Also in a multi-user scenario, the lack of link status knowledge can result channel allocation for the deep-faded connections, which causes resource wastage. A priori information about the instantaneous link conditions provides a powerful tool to the network controller while managing the medium access. Selecting the links that have best conditions increases the network's overall performance.

1.4. Literature Overview

The physical layer performance of MB-OFDM systems are studied in [16]-[21] over the UWB channel models. [16],[17]concentrate on the co-channel interference between MB-OFDM based simultaneously operating piconets (WPANs). (SOP). Different piconets employ different time-frequency hopping patterns. On the other hand collusions can occur when two of the patterns hop to the same frequency at the same time. [16] proposed a symbol repeater following to the interleaver. Transmitting a MB-OFDM symbol in two consecutive bands decreases the collision probability and enhances the diversity. Using symbol repeating [17] added bit reversal interleaving to consecutive OFDM symbols. This method prevents the transmission of information bits at the same subcarrier in both MB-OFDM symbols. In the repeating symbol, coded bits within the OFDM symbol is reversed and then fed into the interleaver. The original MB-OFDM physical layer proposal introduces two stages of interleaver which provides diversity across the transmission bands and subcarriers. [18], [19] verify the performance improvement due this diversity gain and propsed additional methods to improve the diversity gain In this thesis we do not deal with the interference problem. We assume that the MB-OFDM links are only subject to additive White Gaussian Noise (AWGN), multipath fading and shadowing.

Coded Multiband-OFDM systems are studied in [20], and [21]. [20] measures the performance of MB-OFDM links under Bose-Chaudhuri-Hocquengem (BCH) coding and Convolutional Coding with different coding rates. On the other hand, this work employs well known coding rates and it does not implement the coding structure puncturing pattern and interleaving procedure defined in the actual proposal. Similarly [21] obtains BER versus E_b/N_0 graphs for different UWB channel models under well known convolution codes. However these curves are obtained, after averaging the performance of large number of realizations. This work also comes up with a mathematical bound to model the BER versus E_b/N_0 performance. As we show in this thesis, for a given E_b/N_0, averaging the empirical BERs gives a BER estimate with large standard deviation. Thus, we search for additional methods in order to reduce the estimation error.

Under erroneous wireless channels with Rayleigh fading, [22] discusses about the optimal frame size by taking the data throughput as the performance criteria. Under explicit mathematical channel models and given mobility characteristics, this work finds the optimal frame size for the entire link. In other words frame size optimization is performed only at design time. Similar to our objective, [23] used Stop and Wait (S&W) ARQ protocol with adaptive frame size selection. Frame size adaptation is performed according to the measured frame error rate using ACK and NACK frames.

In order to obtain the instantaneous channel conditions, Modiano [24] presented an adaptive algorithm, which finds the most likely bit error rate (BER) from the number of erroneous frames inside a number of transmitted frames. This procedure is simple to implement because it does not considers the type of the transmission and the receiver structure. Since, the algorithm has to transmit a number of frames prior to make estimation about the link's instantaneous BER, the channel tracking capability decreases as the mobility increases.

The current IEEE 802.15.3 WPAN MAC specification does not include any scheduling scheme, but leaves this feature optional to system designers. Recent studies propose scheduling methods for WPANs, mostly concentrating on service differentiation [25], [26] . These schemes deal with the allocation of fixed time slots within a superframe according to the Quality of Service (QoS) requirements of different service applications. These schemes do not consider the channel conditions or the physical layer information.

Opportunistic scheduling schemes exploits the time varying nature of the wireless channel to decide which time slot to transmit data for each user. [27],[28],[29]. Liu [27],[28] described a framework for opportunistic scheduling to exploit the diversity in time domain while keeping various QoS and fairness constraints. Opportunistic Scheduler for Multi-user OFDM systems [29] decides not only the time-slot but also the sub-carrier to allocate to each user under the given constraints. In these cases, OFDM is used for multiple access. In this thesis we do not put any constraints to the ongoing communication. Instead we try to improve the throughputs of individual links by assigning the durations of each link's time-slot in an opportunistic and fair manner.

1.5. Thesis Contributions

In this thesis, we improve the efficiency of a MB-OFDM UWB link by optimizing the size of the transmitted frames based on channel state and physical layer information. Specifically, we propose a new method to estimate the BER of the MB-OFDB UWB link, and to accordingly optimize the frame size used in ARQ policies. We first try to optimize the frame size according to Modiano's simple algorithm. In order to reduce the channel adaptation duration, next we try to find a method to obtain a precise BER estimate for the MB-OFDM systems.

After estimating the instantaneous channel conditions, we propose an opportunistic multi-link-time scheduling scheme for MB-OFDM UWB WPANs. In this scheme, the network controller uses the measured or estimated knowledge of link ARQ efficiencies while allocating time to channel requesting links. Last but not least, we want to show that combining frame size optimization with opportunistic scheduling further increases the total network performance.

To evaluate our proposed schemes, namely optimal frame size adaptation and opportunistic link scheduling, we simulate the fundamental building blocks of the MB-OFDM UWB physical layer proposal and IEEE 802.15.3 WPAN MAC standard.

1.6. Thesis Organization

This thesis is organized as follows:

Chapter II presents the system model, with complete transmitter and receiver architectures. In this chapter, we mention about the channel estimation and Viterbi decoding procedures in detail. We also cover the IEEE channel model and give the path loss model for the MB-OFDM links. This section concludes with the description of MB-OFDM frame structure.

In Chapter III, Automatic Repeat reQuest (ARQ) policies of IEEE 802.15.3 networks are introduced. We consider the MB-OFDM links under erroneous time-varying channels and maximize the link efficiency by selecting the optimum frame size. In this section, we visit the Modiano's algorithm to make a BER estimate based on the frame

retransmission history. Next we derive another BER estimation method based on the distribution of signal to noise ratio's on each subcarrier. This section concludes with the simulation results that show the theoretical performance for ideal link adaptation, performance of the proposed link adaptation methods, and the performance of fixed frame size selections.

In Chapter IV, we describe the IEEE 802.15.3 MAC standard in detail. We first employ equal time sharing to simultaneously operating MB-OFDM links. A new time-sharing scheme is proposed where the time allocations are performed according to the instantaneous link qualities. The performance of equal time-sharing and proportional time-sharing schemes with fix and adaptive frame size selections is investigated for different numbers of simultaneously operating links.

And finally, Chapter V is devoted to our conclusions and possible research directions.

2. MB-OFDM UWB SYSTEM MODEL

In this chapter, we explain the transmitter and receiver architectures of MB-OFDM based on TI's physical layer (PHY) proposal [10],[11]. In addition, IEEE's UWB channel model is presented. Also, we explain the channel estimation and decoding procedures and finally give the structure of the MB-OFDM frame format as defined in MB-OFDM PHY proposal.

2.1. Transmitter Architecture

In MB-OFDM UWB, the binary information stream is first convolutionally encoded as shown in Figure 2. 1 . Then, puncturing is employed to achieve the desired data rate. Following that, the encoded and punctured data stream is subsequently passed through a two-stage interleaver: a block interleaver in time followed by a block interleaver across frequency subbands. After that, the interleaved bit stream is mapped into QPSK, converted into parallel streams and pilot tones are inserted. After obtaining the time domain MB-OFDM signal via IFFT, the signal is reconverted to serial, guard periods are added. Following the Digital-to-analog (DAC), the signal sent through the transmit antenna. We will briefly explain the functions of each blocks of the transmitter in the next subsections.

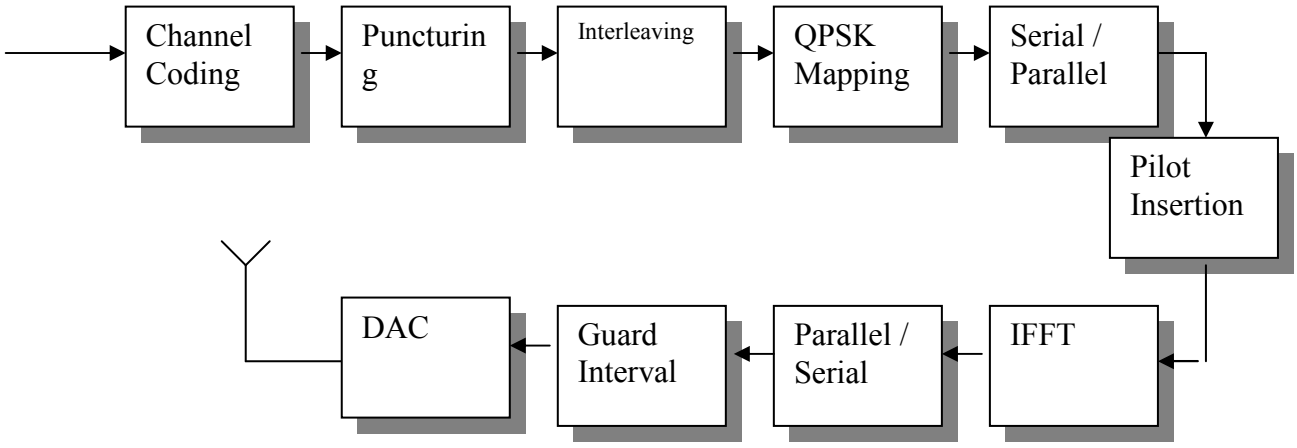

Figure 2. 1 Schematic of MB-OFDM UWB transmitter

2.1.1. Channel Coding

Channel coding is used to improve the bit error rate (BER) performance of the system. Since the channel introduces bit errors, channel coding detects and corrects these errors to a certain limit. In a multipath fading channel, the channel affects the OFDM subcarriers differently. For instance, some of the subcarriers arrive at the receiver with very small amplitudes and some of them are completely lost because of deep fades. Since weak subcarriers dominate the bit errors, channel coding corrects these errors to a certain extent depending on the correction ability of the code. The performance of the channel coding is limited by the Shannon's channel capacity formula [30] Although Reed-Solomon (RS) Codes is one of the most popular block codes for different applications such as CD, DVD etc. to combat with burst errors [30], instead of RS codes, convolutional codes are the most widely used channel code in wireless systems. All major cellular systems (GSM, IS-95), Wireless Local Area Network standards (IEEE 802.11a, HiperLAN/2) use convolutional codes [30], [46].

In the MB-OFDM UWB, a mother convolutional code with rate of 1/3, the constraint length (K) of seven, and generator polynomials of $g_0 = [133]_8$, $g_1 = [145]_8$, $g_2 = [175]_8$ is proposed. As shown in Figure 2. 2, the bit denoted as "A" is the first generated by the encoder, following that the bit denoted as "B", and finally, the bit denoted as "C" are generated.

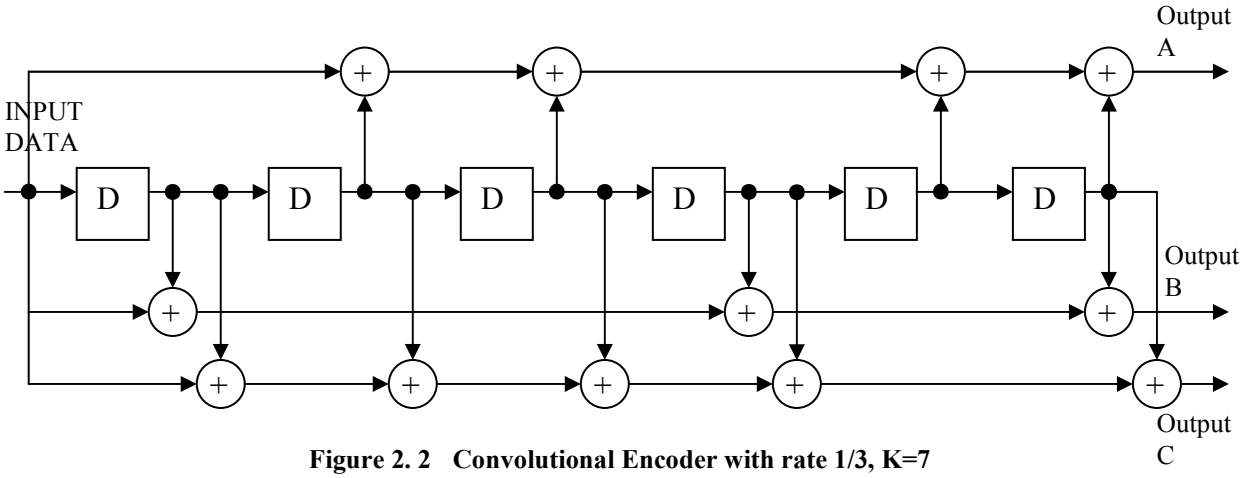

Figure 2. 2 Convolutional Encoder with rate 1/3, K=7

The MB-OFDM PHY supports data rates 55 Mbps, 80 Mbps, 110 Mbps, 160 Mbps, 200 Mbps, 320 Mbps and 480Mbps. The desired data rate is obtained by employing "puncturing", which is a process of omitting some of the coded bits in the transmitter.

Therefore puncturing reduces the number of transmitted bits and increases the coding rate. Since, in this thesis, we focus on the increasing the capacity of MB-OFDM UWB system with the highest 480Mbps data rate, all our subsequent simulations and analysis consider this rate only. The puncturing pattern for this data rate is illustrated in Figure 2. 3

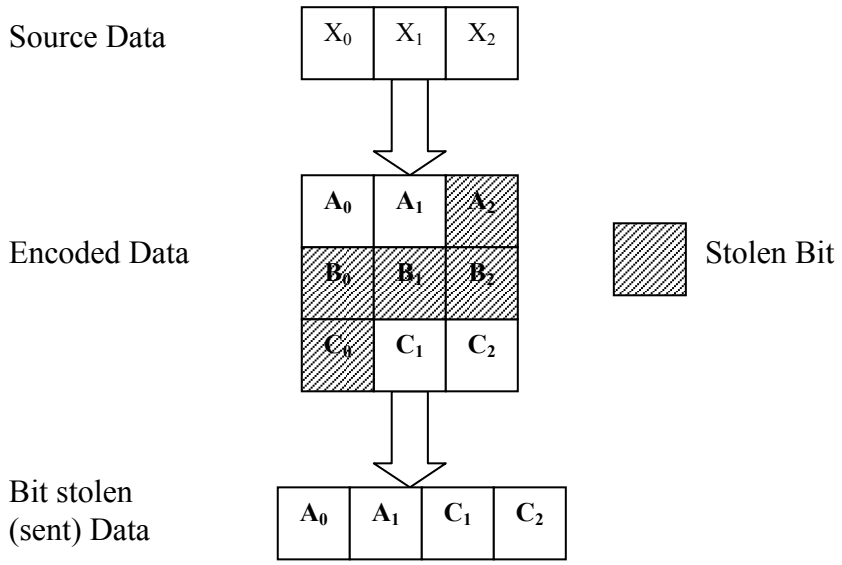

Figure 2. 3 Bit stealing (puncturing) procedure of rate ¾ coding to achieve 480 Mbps data rate.

This puncturing pattern provides a coding rate of ¾. Each MB-OFDM symbol contains 150 data bits at a time. Following the coding operation the number of bits carried inside an OFDM symbol increases to 200 bits. The output of the QPSK modulator produces 100 input symbols to the IFFT block. The output of the size 128-IFFT block produces a complex signal, since the data subcarriers input to IFFT cannot be arranged conjugate symmetric. On the other hand, for the data rates of 200 Mbps, 160 Mbps and 110 Mbps, there are just 50 data subcarriers input to the IFFT block. So the data subcarriers can be arranged conjugate symmetrically to make the output signal real. The rate dependent parameters of the MB-OFDM system are tabulated below.

Table 2-1 MB-OFDM Rate dependent parameters

Data Rate *(Mbps)*	Modulation	Coding Rate	Conjugate Symmetric Input to IFFT	Coded bits per OFDM symbol (N_{CBPS})	Data bits per OFDM symbol (N_{DBPS})
55	QPSK	11/32	Yes	50	171,875
80	QPSK	1/2	Yes	50	25
110	QPSK	11/32	Yes	100	34,375
160	QPSK	1/2	Yes	100	50
200	QPSK	5/8	Yes	100	62,5
320	QPSK	1/2	No	200	100
480	QPSK	3/4	No	200	150

2.1.2. Interleaving

Interleaving distributes the transmitted bits in time or frequency to achieve a random bit error distribution after demodulation. If only AWGN is available in the channel, no interleaving would be required since relocating the bits does not change the error distribution. However in a wireless environment, channel introduces burst errors. By using interleaving, the burst errors are scattered to achieve higher coding gains.

The MB-OFDM specification employs two types of interleaving to achieve different levels of frequency diversity. In the outer symbol interleaver, N_{CBPS} coded information bits are interleaved in time over succeeding three MB-OFDM symbols to achieve frequency diversity between Channel 1 bands. The symbol interleaver is a block type interleaver with size 3xN_{CBPS} where the bits are written in row wise and read in column wise. Thus, the symbol interleaver accepts 3xN_{CBPS} bits at a time. If *A(i)* and *B(j)* represent the input and output bits of the symbol interleaver respectively at position *j*, the relationship between *A(i)* and *B(j)* is given by [10]

$$B(j) = A\left\{\left\lfloor \frac{i}{N_{CBPS}} \right\rfloor + 3\bmod(i, N_{CBPS})\right\} \tag{2.1}$$

where $i, j = 0,1,2,...,N_{CBPS}-1$, $\lfloor\ \rfloor$ gives the integer value smaller and closest to the value in the bracket and mod gives the remainder after division by N_{CBPS}.

The output *B(j)* bits are then passed through the tone interleaver block. The inner tone interleaver is used for interleaving bits in each OFDM symbol to exploit the frequency

diversity between subcarriers. The tone interleaver is also a block interleaver with size *Zx10* where $Z = N_{CBPS}/10$. If *B(i)* and *C(j)* represent the input and output bits of the tone interleaver respectively at position *j*, the relationship between *B(i)* and *C(j)* is given by

$$C(j) = B\left\{\left\lfloor \frac{i}{N_{CBPS}} \right\rfloor + 10 \bmod(i, N_{CBPS})\right\} \quad (2.2)$$

2.1.3. QPSK Mapping

The encoded and interleaved binary data stream is mapped to the complex symbols from the signal constellation. As mentioned previously, MB-OFDM specification uses QPSK modulation for all supported data rates. The bits are gray coded. The mapping from bits to I and Q samples is shown below

Table 2-2 QPSK constellation points

Input Bit	I out	Q out
00	-1	-1
01	-1	1
10	1	-1
11	1	1

.

In order to have QPSK symbols with unit energy, a normalization factor of $1/\sqrt{2}$ is used to multiply the complex symbols.

2.1.4. Pilot Insertion

Due to the frequency selective nature of the transmission environment along with frequency and timing offsets in the receiver, data symbols experience phase rotation and amplitude variation. Hence symbols can cross the decision boundaries and consequently they are detected incorrectly.

In order to mitigate with the channel variations, and enhance the detection of the received symbols, OFDM uses a special set of symbols called “pilots”. Pilots are known symbols, which are used to make channel estimation and make corrections on the received symbols. Prior to the pilot insertion, the serial symbol stream is divided into N_{SC} parallel streams, where N_{SC} denotes the number of data subcarriers in an OFDM symbol. After dividing the data symbol stream into parallel streams, the pilot symbols

are inserted. The pilot symbols are scattered inside an OFDM symbol according to the channel properties and the transmission type. In literature, two types of pilot insertion are recognized: comb-type pilots and block-type pilots [31],[32]

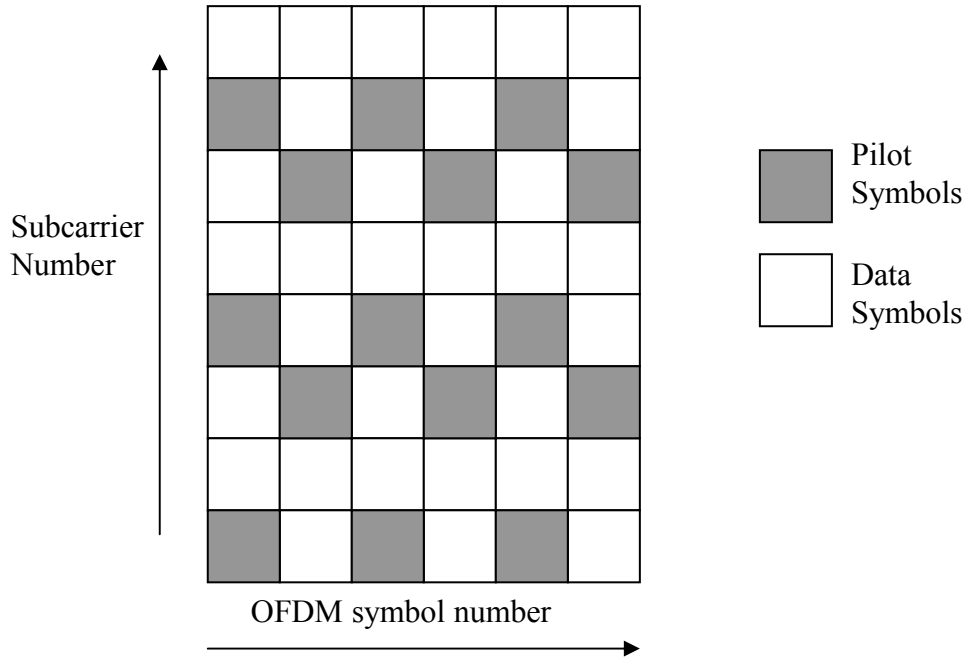

Figure 2. 4 Comb type pilot distribution (sample 6 OFDM symbols with 8 subcarriers)

Figure 2. 4 shows a sample comb-type pilot distribution. Such pilot distribution patterns are suitable for continuous transmission schemes like broadcasting (e.g. Digital Video Broadcasting, Digital Audio Broadcasting). The separation between pilot symbols in time and frequency is determined according to the coherence time and coherence bandwidth of the channel.

The coherence time characterizes the time varying nature of the frequency depressiveness of the channel in time domain. Namely it is the duration of time on which channel remains almost stable. According to [33], the coherence time is defined as,

$$T_C = \frac{9}{16\pi f_m} \tag{2.3}$$

where f_m is the maximum Doppler shift and defined as,

$$f_m = \frac{v}{\lambda} = \frac{v \times f_c}{c} \tag{2.4}$$

where c is the speed of light (3×10^8 m/s), and f_c is the geometric central frequency of a 3-band MB-OFDM signal defined later in Section 2.2.2 and v is the velocity of the mobile in m/s.

The coherence bandwidth is the range of frequencies over which the channel treats spectral components with equal gain and constant phase. In other words, two spectral components separated by an amount less than the coherence bandwidth are highly correlated. The coherence bandwidth of the channel can be defined as,

$$B_C = \frac{1}{50\sigma_\tau} \tag{2.5}$$

where σ_τ is the rms delay spread.

Let N_f and N_t denote the separation between two consecutive pilot symbols over frequency and time respectively. Than in comb-type pilot arrangement N_f and N_t should satisfy,

$$\begin{aligned} N_t &\le T_C \\ N_f &\le B_C \end{aligned} \tag{2.6}$$

For comb-type pilot pattern, channel is first estimated at pilot frequencies by employing several algorithms such as least square (LS), minimum mean square (MMSE), and least mean square (LMS).[31]. Channels impulse and frequency response to the entire subcarriers is then calculated using a 2-D interpolation both in time and frequency. For these purpose different algorithms such are linear interpolation, second order interpolation can be applied [32].

On the other hand, comb-type pilot insertion is not suitable for packet (frame) transmission schemes based on two reasons. First of all, in an indoor environment where the users have small velocity, the frame length is short enough to assume a constant channel during each frame period. So there is no need to estimate channel in time domain, which simplifies the channel estimation procedure. Secondly, using pilots scattered over several OFDM symbols brings a delay of several symbols before the calculation of first channel estimates. Hence, the systems effective throughput

decreases. Also comb-type pilot distribution needs to buffer several OFDM symbols, which requires additional hardware.

Therefore for packet transmission schemes such as 802.11a, and MB-OFDM PHY, block type pilots should be used. Figure 2. 5 shows a sample block-type pilot pattern.

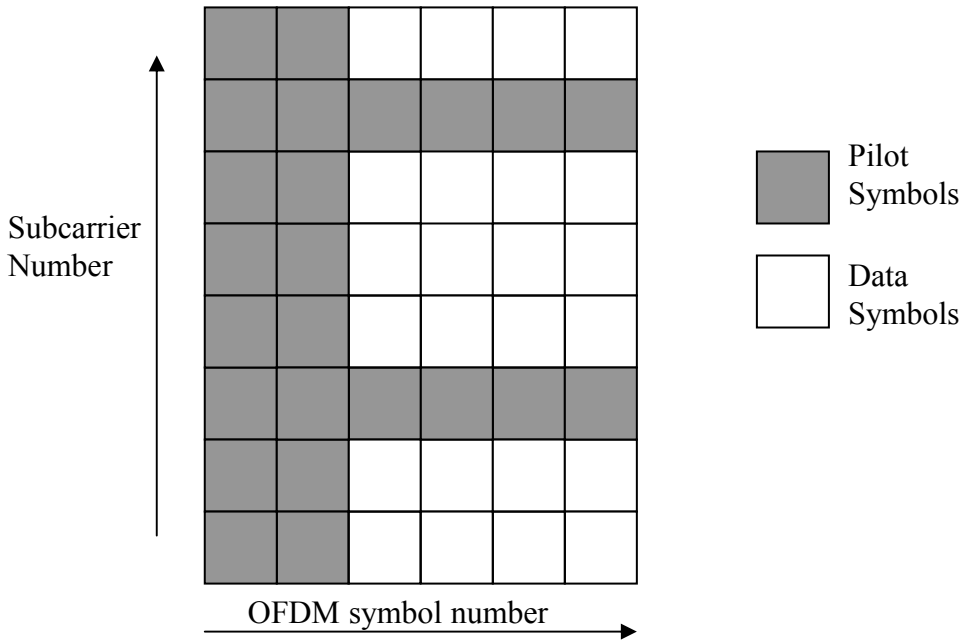

Figure 2. 5 Block type pilot distribution (sample 6 OFDM symbols with 8 subcarriers)

Block type pilot pattern consist a preamble of several OFDM symbols, where the pilots are sent over all subcarriers, called training symbols. The channels frequency response is estimated by using the training symbols. Based on this estimates, rest of the OFDM symbols are determined, since the channel is constant over frame duration.

The two rows of pilot symbols depicted in Figure 2. 5 are used for frequency-offset correction, which occurs as a result of the oscillator frequency mismatch between transmitter and receiver. Since frequency offsets affects all subcarriers are similarly there is no need to place so many pilot tones [31].

MB-OFDM PHY inserts 6 training symbols to the beginning of each frame. Inside each OFDM symbol 12 of subcarriers are reserved for standard pilot signals in order to make frequency offset correction. Also 10 of the subcarriers are left for user-defined pilot tones.

2.1.5. IFFT Block

Following the pilot insertion, *N* parallel symbol stream, is fed into the IFFT block where each stream is assigned to a single frequency of the inverse Fourier transform. The IFFT is performed according to,

$$x[n] = \frac{1}{\sqrt{N}} \sum_{k=0}^{N-1} X[k] e^{j(\frac{2\pi}{N})kn} \tag{2.7}$$

where scaling with $1/\sqrt{N}$ provides energy-invariance at the output i.e., makes the FFT orthonormal.

The physical layer proposal of TI uses 128 point IFFT to generate a MB-OFDM symbol at a single band. Out of 128 subcarriers, 100 subcarriers are used for transmitting data symbols, 12 for transmitting pilot symbols. The rest of the subcarrier inputs are set to zero. The symbol mapping is depicted at Figure 2. 6

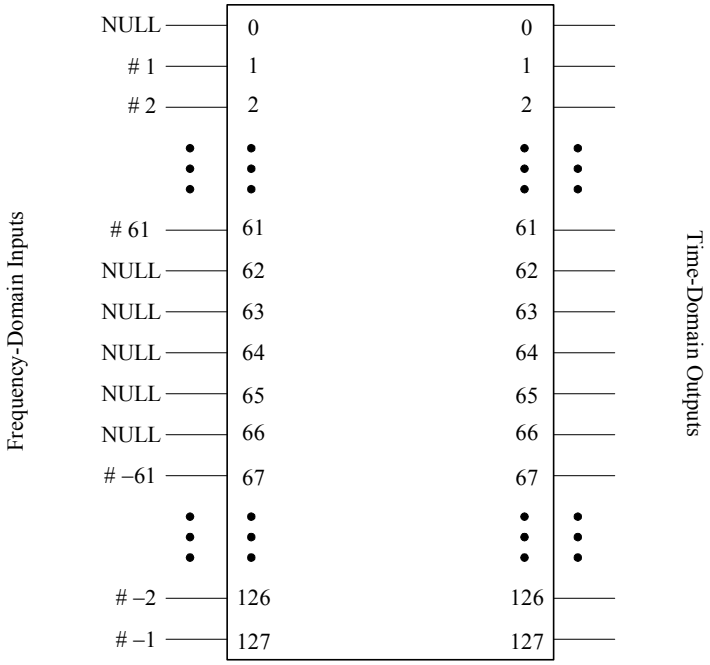

Figure 2. 6 Subcarrier assignment of the IFFT block

According to the IFFT block inputs from 1 to 56 are the positive subcarriers and inputs from 72 to 127 forms the negative subcarriers. Let $M(k)$ defines the mapping from the data subcarrier indices 0 to 99 to the IFFT inputs. Then the data rates for 480 and 320 Mbps, information symbol mapping is performed according to,

$$M(k)=\begin{cases} k-56 & k=0 \\ k-55 & 1\le k\le 9 \\ k-54 & 10\le k\le 18 \\ k-53 & 19\le k\le 27 \\ k-52 & 28\le k\le 36 \\ k-51 & 37\le k\le 45 \\ k-50 & 46\le k\le 49 \\ k-49 & 50\le k\le 53 \\ k-48 & 54\le k\le 62 \\ k-47 & 63\le k\le 71 \\ k-46 & 72\le k\le 80 \\ k-45 & 81\le k\le 89 \\ k-44 & 90\le k\le 98 \\ k-43 & k=99 \end{cases} \quad (2.8)$$

The standard pilot tones are put in subcarriers –55, -45, -35, -25,-15,-5,5,15,25,35,45,55 as $(1+j)/\sqrt{2}$ for $k=\pm 5,\pm 25$ and $(-1-j)/\sqrt{2}$ for $k=\pm 15,\pm 35,\pm 45,\pm 55$. The user defined pilot tones are defined at the IFFT inputs –61,-60,…,-57 and 57,58,….,61. In our simulations we set them to zero. In order to avoid unnecessary transmission, the physical layer proposal sets the DC subcarriers 62 to 66 to zero.

2.1.6. Guard Interval

The time domain MB-OFDM symbols are first converted to the serial form. In order to avoid intersymbol interference between two consecutive OFDM symbols and to keep the orthogonality between subcarriers, we append the last 32 samples of an OFDM symbol to the beginning of each symbol, based on the physical layer specification. The physical layer also introduces 5 zero samples between consecutive OFDM symbols as an additional guard interval, which allows some duration for frequency switching between bands.

Since the bandwidth of a MB-OFDM signal is 528 MHz, the subcarrier spacing between each subcarrier is 528MHz/128=4.125 MHz. Then, at the output of the parallel to serial converter each MB-OFDM symbol elapses 1 / 4.125 MHz = 242.42 ns. Appending 32-sample cyclic prefix (60.6 ns) to the beginning of each symbol and 5 zero sample (9.46ns) to the end of each sample increases the symbol duration (T_{SYM}) to 312.5 ns.

Table 2-3 summarizes the overall important physical layer parameters of MB-OFDM UWB for data rate of 480 Mbps.

Table 2-3 PHY parameters for data rate of 480 Mbps

Data Rate (*R*)	480 Mbps
Modulation	QPSK
Coding Rate	¾
Generator polynomials	g_0=[133]$_8$, g_1=[145]$_8$, g_2=[175]$_8$.
Constraint length (*K*)	7
N_{CBPS}: Coded bits per OFDM symbol	200
N_{DBPS}: Data bits per OFDM symbol	150
IFFT/FFT size (Total number of subcarriers)	128
Number of data subcarriers N_{SC}	100
Number of defined subcarriers	12
Number of undefined subcarriers	10
Number of zero subcarriers	6
Symbol bandwidth (*W*)	528 MHz
Subcarrier spacing between subcarriers	4.125 MHz
$T_{IFFT/FFT}$: IFFT/FFT duration	242.42 ns
T_{CP} : Cyclic prefix duration	60,61 ns
T_{GI} : Guard interval duration	9,47 ns
T_{SYM} : Symbol duration	312,5 ns
RC Filter roll-off factor	0.5
Sub-band 1 center frequency (f_1)	3432 MHz
Sub-band 2 center frequency (f_2)	3960 MHz
Sub-band 3 center frequency (f_3)	4488 MHz
Time & Freq. Int. Pattern	f_1 f_2 f_3 f_1 f_2 f_3

2.1.7. Digital to Analog Converter

The consecutive time domain samples are passed through a Raised Cosine Filter [30], with roll-of factor 0.5 to obtain the analog waveform at baseband. In most OFDM system, designers want to reduce the out of band power to avoid interference between

adjacent transmit channels. In order to reduce the out of band power, windowing can be used and applied to individual OFDM symbols. In this work, the waveforms are passed through an ideal rectangular window.

The baseband waveform is then upconverted to a carrier frequency depending on which band the MB-OFDM symbol to be sent on. Power spectral density of the output pass band signal is obtained as shown in Figure 2. 7. . Based on a Time Frequency Interleaving (TFI) pattern of $f_1 f_2 f_3 f_1 f_2 f_3$, the time-frequency graphical representation (spectrogram) of the first 15 MB-OFDM symbols is given in Figure 2. 8

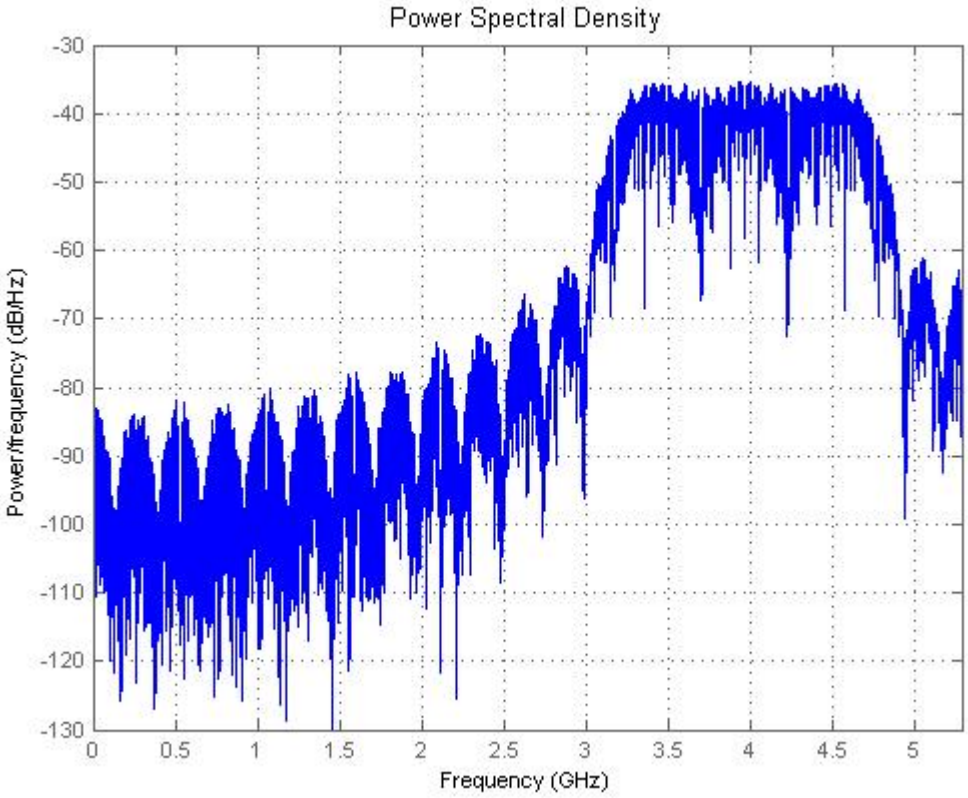

Figure 2. 7 Power spectral density of the transmitted signal

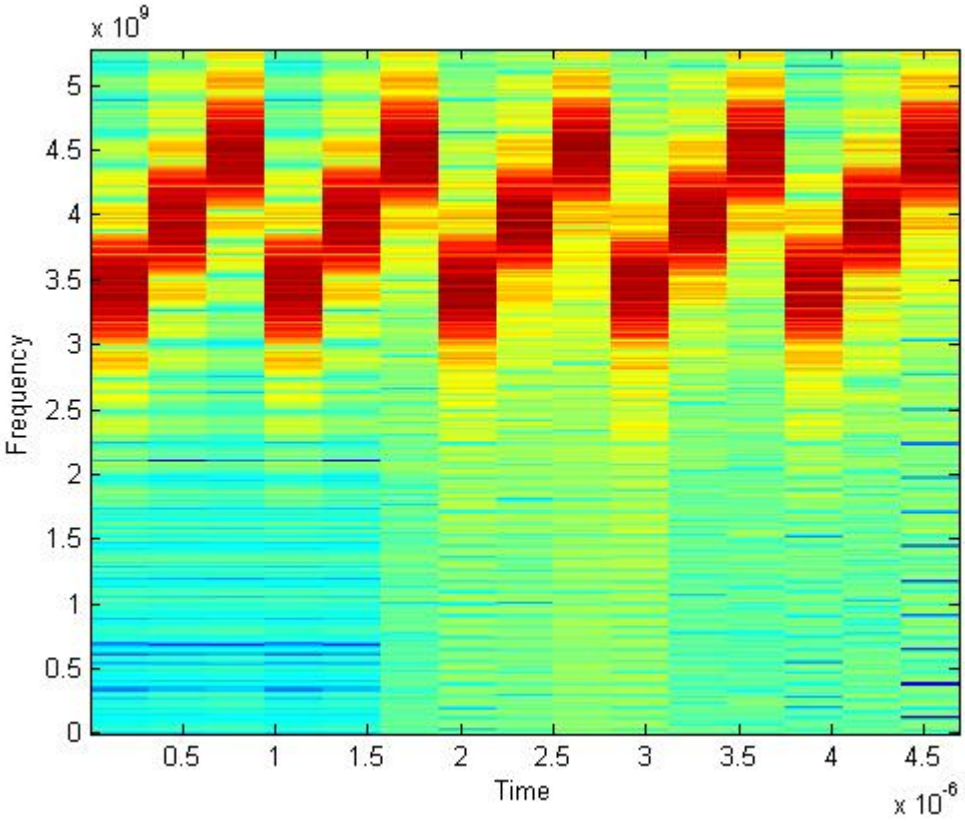

Figure 2. 8 Spectogram of the transmitted waveform using 15 MB-OFDM symbols

2.2. Channel Model

In this section, we describe the IEEE's channel model for Multipath propagation and path loss model according to MB-OFDM proposal.

2.2.1. UWB Channel Model for Indoor Multipath Propagation

For extremely wide-band signals, such as the MB-OFDM signal that has a bandwidth of 528 MHz, the central limit theorem will not be valid because the number of irresolvable multipath components at the receiver reduces drastically. Hence, Rayleigh distribution model [33] of received signal amplitudes becomes inappropriate.

In an office or a residence, the multipath arrivals could originate from walls or furniture etc. in the environment. As depicted in Figure 2. 9, the receiver may first capture a

cluster of reflections originating from wall 2 and than it could capture another set of reflections originating from wall 1, as a result of highly resolvable multipath arrivals.

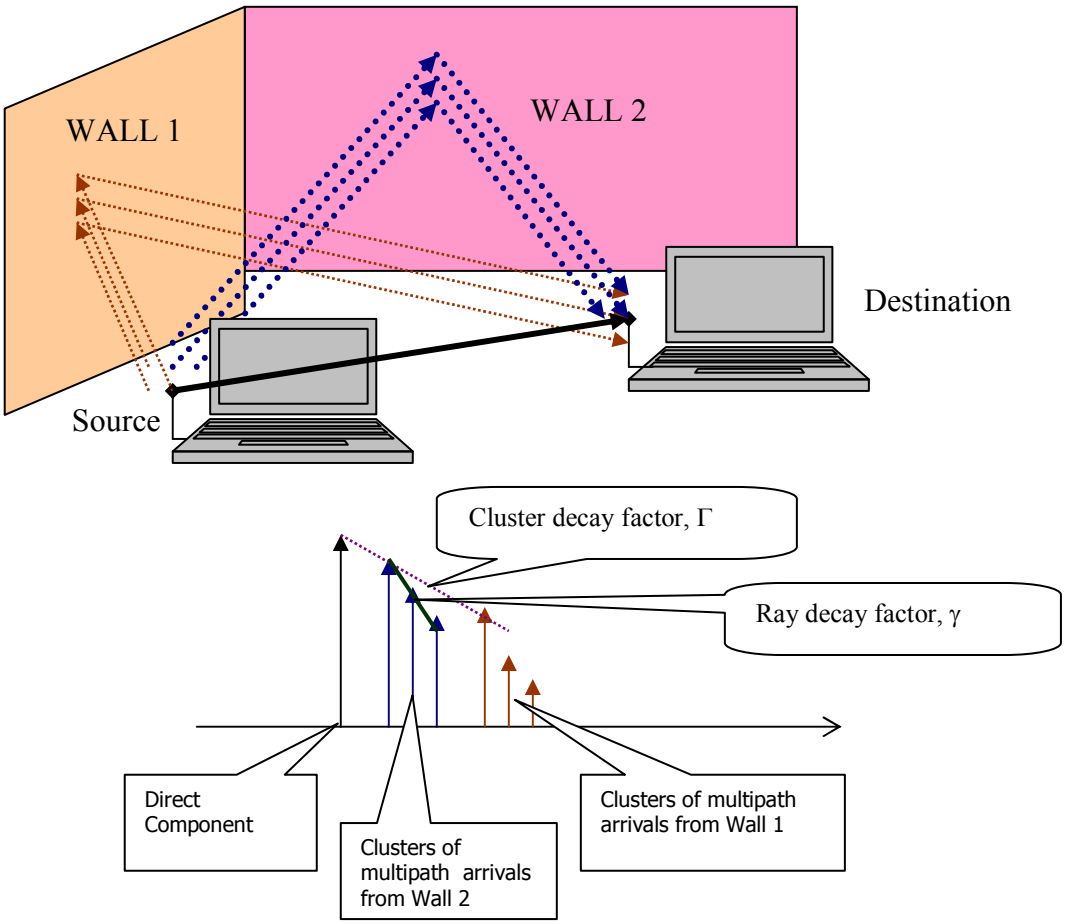

Figure 2. 9 Indoor multipath model

By considering such circumstances IEEE's UWB channel [34],[35] is based on the Saleh and Valenzuela's (S-V) pioneering work [36] where an arbitrary channel realization is defined by,

$$h(t) = X \sum_{l=0}^{L} \sum_{k=0}^{K} \alpha_{k,l} \delta(t - T_l - \tau_{k,l}) \qquad (2.9)$$

In the above equation, X denotes the log-normal shadowing for the channel realization, T_l denotes the arrival time of the l^{th} cluster of reflections, $\tau_{k,l}$ denotes the arrival time of the k^{th} multipath component (ray) within the l^{th} cluster, and $\alpha_{k,l}$ denotes the amplitude

of the k^{th} ray within the l^{th} cluster. According to the S-V model, the interarrival time between two successive cluster and ray is exponentially distributed with parameters Λ and λ respectively

$$P(T_l \mid T_{l-1}) = \Lambda e^{-\Lambda(T_l - T_{l-1})}$$
$$P(\tau_{k,l} \mid \tau_{k-1,l}) = \lambda e^{-\lambda(\tau_{k,l} - \tau_{k-1,l})} \tag{2.10}$$

The amplitude of the multipath arrivals $\alpha_{k,l}$ is defined by

$$\alpha_{k,l} = p_{k,l}\xi_l\beta_{k,l} \tag{2.11}$$

where $p_{k,l}$ is ± 1 with equal probability denoting the inversions because of the reflections, ξ_l and $\beta_{k,l}$ are the terms which represent the corresponding fading on each cluster and ray. The term $\xi_l\beta_{k,l}$ is lognormal distributed with parameters $N(\mu_{k,l}, \sigma_1^2 + \sigma_2^2)$ where σ_1, σ_2 denote the standard deviation of cluster ξ_l and ray $\beta_{k,l}$ lognormal fading terms. $\mu_{k,l}$ is calculated from the expression given in,

$$\mu_{k,l} = \frac{10\ln(\Omega_0) - 10T_l/\Gamma - 10\tau_{k,l}/\gamma}{\ln 10} - \frac{(\sigma_1^2 + \sigma_2^2)\ln(10)}{20} \tag{2.12}$$

In the above expression, Ω_0 is the mean energy of first ray of first cluster, Γ and γ are the decaying factor for the clusters and the rays within the clusters respectively. Finally, the lognormal shadowing term is modeled by the expression,

$$20\log(X) \propto N(0, \sigma_x^2) \tag{2.13}$$

Using the all above described parameters, references [16] and [35] present four different channel models, which characterize different channel conditions. First set of parameters named as Channel Model 1 (CM1) models a LOS channel for transmitter and receiver distances up to 4 meters, second set of parameters referred as Channel Model 2 (CM2), models a NLOS channel for transmitter and receiver distances between 0 and 4 meters ,

third set of parameters models a NLOS channel for transmitter and receiver distances between 4 and 10 meters which is called Channel Model 3 (CM3), and fourth set of parameters referred as Channel Model 4 (CM4) models a disperse channel having a rms delay spread of 25 ns.

Table 2-4 Parameters of UWB Channels

Model Parameters	**CM1**	**CM2**	**CM3**	**CM4**
Λ (1/nsec)	0.0233	0.4	0.0667	0.0667
λ (1/nsec)	2.5	0.5	2.1	2.1
Γ (Cluster decay factor)	7.1	5.5	14.00	24.00
γ (Ray decay factor)	4.3	6.7	7.9	12
σ_1 (dB)	3.3941	3.3941	3.3941	3.3941
σ_2 (dB)	3.3941	3.3941	3.3941	3.3941
σ_x (dB)	3	3	3	3
Model Characteristics				
Mean excess delay (nsec) (τ_m)	5.0	9.9	15.9	30.1
RMS delay (nsec) (τ_{rms})	5	8	15	25
Channel energy mean (dB)	-0.4	-0.5	0.0	0.3
Channel energy std (dB)	2.9	3.1	3.1	2.7

Throughout this work, we considered the data rate of 480 Mbps, which is highest data rate, offered by the Multiband OFDM physical layer proposal. For this rate, physical layer shows poor BER performance for the distances greater than 4 meters [1]. Therefore, in our all simulations we used channel realizations from CM1 generated based IEEE UWB model [35] with the parameters given in Table 2-4.

For computer simulations, discrete channel model is obtained from the continuous time model of Eq.(2.9) as follows; The analog waveform at the output of the transmitter is modeled with time resolution (t_s) 94.6 ps (Sampling rate of the DAC is 10.56 GHz). The time axis of the continuous channel model is divided into bins with duration t_s. When multiple multipath components fall into the same time bin, their values are added to obtain the impulse response at that time-bin.

2.2.2. Path Loss Model

In radio communication systems, when a transmitter antenna radiates isotropically in free space at a power level of P_T, the received power P_R is calculated from [30] as,

$$P_R = \frac{P_T G_T G_R}{(4\pi d/\lambda)^2} \tag{2.14}$$

where G_T is the gain of the transmitter antenna, G_R is the gain of the receiver antenna, d is the distance between transmitter and receiver and λ is the wavelength of transmitted signal. The factor $L = (4\pi d/\lambda)^2 = (4\pi f_c/c)^2$ is the free space path loss. Equivalently, the received power can be calculated in dB as,

$$P_R\big|_{\text{dBW}} = P_T\big|_{\text{dBW}} + G_T\big|_{\text{dBW}} + G_R\big|_{\text{dBW}} - L\big|_{\text{dBW}} \tag{2.15}$$

Table 2-5 summarizes the important parameters of the MB-OFDM PHY's link budget [10]

Table 2-5 Important parameters of the path loss model of an MB-OFDM link

Parameter	Value
Average Tx power (P_T)	-10.3dBm
Tx antenna gain (G_T)	0 dB
$f_c = \sqrt{f_{\min} f_{\max}}$: Geometric center frequency of waveform ($f_{\min}$ and $f_{\max}$ are the -10 dB edges of the waveform spectrum)	3882 MHz
Path loss at 1 meter ($L_1 = 20\log_{10}(4\pi f_0/c)$) $c = 3\times10^8$ m/s	44.2 dB
Path loss at d m ($L_2 = 20\log_{10}(d)$)	6 dB (d = 2 meters)
Rx antenna gain (G_R)	0 dB
Rx power ($P_R = P_T + G_T + G_R - L_1 - L_2$ (dB))	-60.5 dBm
Average noise power per bit	-87.2 dBm
Rx Noise Figure (N_F)[1]	6.6 dB
Average noise power per bit ($P_N = N + N_F$)	-80.6 dBm

2.3. Receiver Architecture

The MB-OFDM UWB receiver performs the reverse operations of the transmitter as shown in Figure 2. 10. Received analog waveform is first down converted to baseband by multiplying the pass band signal with the corresponding carrier on which the signal is transmitted. An anti-aliasing filter of bandwidth 528 MHz then filters the signal. The baseband analog waveform is then resampled at 528 MHz in order to obtain the discrete signal samples. Hence, ADC provides the faded and noisy baseband input samples.

Under perfect synchronization, the channel impulse response can be estimated prior to the FFT operation using the PLCP preambles. Since we already know the content of the training symbols (channel estimation preambles) in frequency domain we assume that their time-domain form is also available at the receiver. The time-domain packet synchronization and frame synchronization preambles which are defined in Section 2.4 can be further used to estimate the channel's impulse response.

After the removal of the guard intervals FFT is performed to obtain the data symbols on each subcarrier. Channels response to each subcarrier can be also determined from the pilot tones in each training symbol. Using the channel estimates, the information carrying symbols are equalized. After the equalization, soft information bits are obtained and they are converted to serial to feed the deinterleaver block. Finally the deinterleaved soft information bits are decoded using a modified Viterbi Algorithm. At the receiver, channel estimation and Viterbi decoding are crucial functions that influence the physical layer performance significantly.

As previously pointed out, perfect synchronization is assumed in this thesis so that the receiver finds precisely the timing information when individual OFDM symbols start and end. Also, it is assumed that receiver samples analog waveform at perfect sampling frequency. We also assumed that the transmitter and receiver oscillators are perfectly matched to each other. So there is no need to perform a frequency offset correction. Timing delays result significant phase shifts at subcarriers at the output of the FFT block.

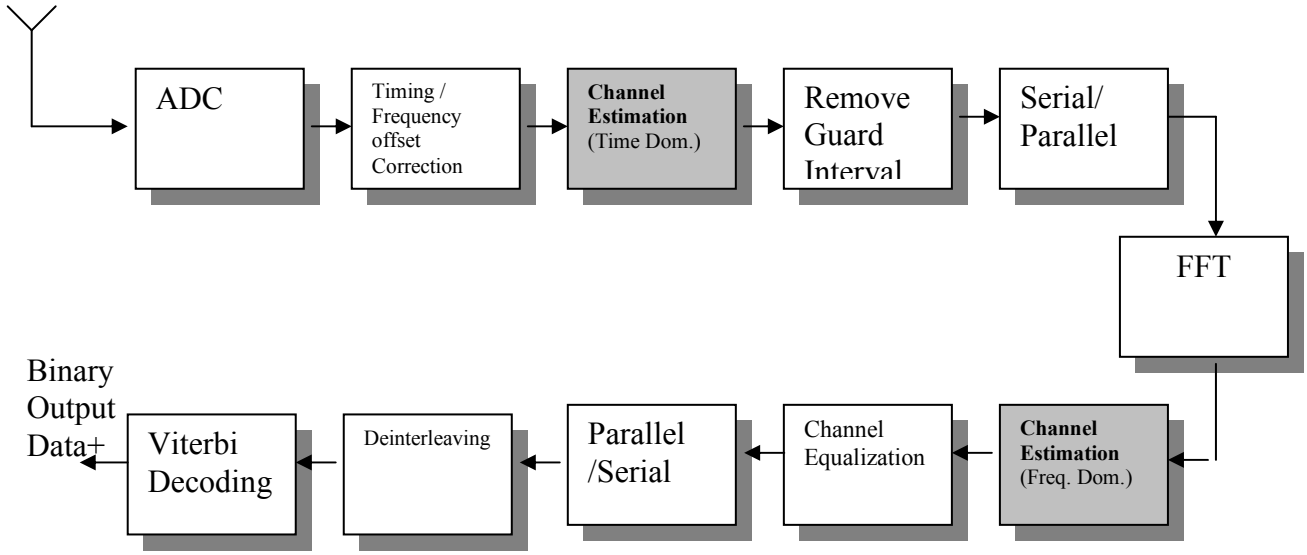

Figure 2. 10 MB-OFDM receiver block diagram

An error in the sampling frequency brings slightly incorrect sampling instants and the subcarriers orthogonality is lost. Hence inter-carrier interference occurs. A mismatch between transmitter and receiver oscillating frequencies introduces a frequency offset, which also results inter-carrier interference. Intended readers can refer [37],[38] for sample clock tracking. In packet transmission schemes, symbol timing and frequency offset correction is usually performed through data-aided algorithms. These algorithms are based on special training symbols appended into the beginning of the transmitted signal. [39]-[44].

In the next subsections, we are going to analyze the functions of each block in the receiver.

2.3.1. Channel Estimation

Following the removal of guard intervals and serial to parallel conversion, receiver performs FFT to get the frequency domain symbols. In our study, the multipath fading channel and the additive white noise affects the received MB-OFDM symbols. Since the channels excess delay is shorter than the duration of the cyclic prefix, following to the FFT process, the received symbols at each data subcarrier has the form.

$$R_{n,k} = X_{n,k}H_{n,k} + w_{n,k} \qquad \begin{matrix} k = 1,2,..,N_{SC} \\ n = 1,....,\infty \end{matrix} \tag{2.16}$$

where on the k^{th} subcarrier of the n^{th} MB-OFDM symbol, $R_{n,k}$ is the received symbol, $X_{n,k}$ is the transmitted data symbol, $H_{n,k}$ is the response of the channel for that subcarrier and $w_{n,k}$ is the additive noise.

If the channel introduces Additive White Gaussian Noise (AWGN) with distribution $N(0,\sigma_z^2)$, the Fourier transform of the noise samples z_n is,

$$w_k = \frac{1}{\sqrt{N}}\sum_{n=0}^{N-1} z_n e^{-j(\frac{2\pi}{N})kn} \tag{2.17}$$

where the mean ($E[w_k]$) of w_k is,

$$\begin{aligned} E\left[w_k\right] &= E\left\{\frac{1}{\sqrt{N}}\sum_{n=0}^{N-1} z_n e^{-j(\frac{2\pi}{N})kn}\right\} \\ E\left[w_k\right] &= \frac{1}{\sqrt{N}}\sum_{n=0}^{N-1} E\left[z_n\right] e^{-j(\frac{2\pi}{N})kn} \\ E\left[w_k\right] &= 0 \end{aligned} \tag{2.18}$$

and variance (σ_w^2) of the w_k is,

$$\sigma_w^2 = E[w_k^2] - \left(E[w_k]\right)^2 \tag{2.19}$$

Since $E\left[w_k\right] = 0$,

$$\begin{aligned} \sigma_w^2 &= E[w_k^2] \\ \sigma_w^2 &= E[\left|w_k\right|^2] \\ \sigma_w^2 &= E[w_k w_k^*] \\ \sigma_w^2 &= E[(\frac{1}{\sqrt{N}}\sum_{n=0}^{N-1} z_n e^{-j(\frac{2\pi}{N})kn})(\frac{1}{\sqrt{N}}\sum_{m=0}^{N-1} z_m^* e^{j(\frac{2\pi}{N})km})] \\ \sigma_w^2 &= \frac{1}{N}\sum_{n=0}^{N-1}\sum_{m=0}^{N-1} E[z_n z_m^*] e^{j(\frac{2\pi}{N})(m-n)k} \end{aligned} \tag{2.20}$$

Since z_n and z_m are uncorrelated noise samples

$$E[z_n z_m^*] = \begin{cases} 1 & n = m \\ 0 & n \neq m \end{cases} \tag{2.21}$$

and

$$\sigma_w^2 = \frac{1}{N}\sum_{n=0}^{N-1} E[z_n^2] = \sigma_z^2 \tag{2.22}$$

So the noise samples at the output of the FFT have the same statistics with that in the channel.

As presented in Section 2.1.4 the Multiband OFDM PHY specification reserves 6 training symbols for channel estimation. Therefore two training symbols are utilized to estimate the frequency response of each MB-OFDM operating band. We first estimate the frequency response of the channel to each subcarrier using the least squares (LS) method of [32]. In order to find the frequency response at the output of the FFT block, training symbols transmitted on the same band are first averaged. The frequency domain channel estimates are then obtained according to,

$$\widehat{H}_{LSF_{k,n}} = \frac{R_{k,n}}{X_{k,n}} \tag{2.23}$$

where at the k^{th} subcarrier of the n^{th} MB-OFDM symbol, $R_{k,n}$ is the average of two received training symbols for a given band, $X_{k,n}$ is the transmitted pilot symbol and $\widehat{H}_{LSF_{k,n}}$ is the estimated frequency response. This method estimates the channel response of N_{SC} data subcarriers simultaneously.

Since we have the exact timing information, channel's impulse response can be estimated in time domain more precisely using least squares [45]. Under perfect timing, each received OFDM training symbol in time domain $r[n]$, have the form,

$$r[n] = \sum_{l=0}^{m} x[n-l]h[l] + n_n \tag{2.24}$$

where m is the desired length of the channel's to be estimated impulse response and $x[n]$ is the original OFDM training symbol in time.

Due to the noise in the system, it is impossible to find a **h** vector satisfying below equation [46],

$$\vec{\mathbf{r}} = \mathbf{A}\vec{\mathbf{h}}$$

$$\begin{bmatrix} r_0 \\ r_1 \\ r_2 \\ \vdots \\ \vdots \\ r_{N-1} \end{bmatrix} = \begin{bmatrix} x_0 & x_{-1} & .. & .. & x_{-m+1} \\ x_1 & x_0 & .. & .. & x_{-m+2} \\ x_2 & x_1 & .. & .. & x_{-m+3} \\ \vdots & \vdots & \vdots & \vdots & \vdots \\ \vdots & \vdots & \vdots & \vdots & \vdots \\ x_{N-1} & x_{N-2} & .. & .. & x_{-m} \end{bmatrix} \begin{bmatrix} h_0 \\ h_1 \\ \vdots \\ \vdots \\ h_{j-1} \end{bmatrix} \tag{2.25}$$

Since $\mathbf{A}$ is a non-symmetric size $N \times m$ matrix, we can find a $\vec{\mathbf{p}}$ vector that is the projection of $\vec{\mathbf{r}}$ on to the column space of $\mathbf{A}$, which minimizes the error norm $\vec{\mathbf{e}}$ between $\vec{\mathbf{r}}$ and $\vec{\mathbf{p}}$.

Since $\vec{\hat{\mathbf{h}}}_{LS}$ denotes the estimated impulse response, we define $\vec{\mathbf{p}}$ as,

$$\vec{\mathbf{p}} = \mathbf{A}\vec{\hat{\mathbf{h}}}_{LS} \tag{2.26}$$

using the advantage of the cyclic prefix ($x(-l) = x(N-l)$), columns of $\mathbf{A}$ becomes,

$$\vec{\mathbf{a}}_0 = \begin{bmatrix} x_0 \\ x_1 \\ x_2 \\ \vdots \\ \vdots \\ x_{N-1} \end{bmatrix} \quad \vec{\mathbf{a}}_1 = \begin{bmatrix} x_{N-1} \\ x_0 \\ x_1 \\ \vdots \\ \vdots \\ x_{N-2} \end{bmatrix} \quad .. \quad \vec{\mathbf{a}}_{N-1} = \begin{bmatrix} x_{N-m+1} \\ x_{N-m+2} \\ x_{N-m+3} \\ \vdots \\ \vdots \\ x_{N-m} \end{bmatrix}_{\partial} \tag{2.27}$$

Since $\vec{\mathbf{e}}$ and $\vec{\mathbf{p}}$ are orthogonal to each other, columns of $\mathbf{A}$ is also orthogonal to $\vec{\mathbf{e}}$

$$\vec{\mathbf{p}}^{\mathrm{T}}\vec{\mathbf{e}} = \mathbf{0}$$

$$\vec{\mathbf{p}}^{\mathrm{T}}(\vec{\mathbf{r}} - \mathbf{A}\vec{\hat{\mathbf{h}}}_{LS}) = \mathbf{0}$$

$$\begin{bmatrix} \vec{\mathbf{a}}_0^T \\ \vec{\mathbf{a}}_1^T \\ \vec{\mathbf{a}}_2^T \\ \vdots \\ \vec{\mathbf{a}}_{N-1}^T \end{bmatrix} (\vec{\mathbf{r}} - \mathbf{A}\vec{\hat{\mathbf{h}}}_{LS}) = \mathbf{0} \tag{2.28}$$

$$\mathbf{A}^T(\vec{\mathbf{r}} - \mathbf{A}\vec{\hat{\mathbf{h}}}_{LS}) = \mathbf{0}$$

$$\mathbf{A}^T\vec{\mathbf{r}} = \mathbf{A}^T\mathbf{A}\vec{\hat{\mathbf{h}}}_{LS}$$

So the LS estimate of the impulse response can be obtained from,

$$\vec{\mathbf{h}}_{\mathbf{LS}} = (\mathbf{A}^{\mathbf{T}}\mathbf{A})^{-1}\mathbf{A}^{\mathbf{T}}\vec{\mathbf{r}} \tag{2.29}$$

Having the impulse response at each transmission band, the frequency response of the channel on each subcarrier can be found by simply taking the Fourier transform of (2.29) as,

$$\hat{\mathbf{H}}_{\mathbf{LST}} = FFT_{128}(\vec{\mathbf{h}}_{\mathbf{LS}}) \tag{2.30}$$

where $\mathrm{FFT}_N(.)$ denotes N point Fast Fourier Transform.

The norm of normalized error (NNE) is a useful to quantity the success of each estimation method and it is defined as,

$$\|e\| = \frac{\left\|\hat{H} - H\right\|}{\left\|H\right\|} \tag{2.31}$$

where H is the original channel response and $\hat{H}$ is the estimated channel response generated from frequency (H_{LSF}) or time (H_{LST}) domain training OFDM symbols.

To quantify the accuracy of the time domain and frequency domain estimation methods, we calculate the NNE as shown in Figure 2. 11. Time domain channel estimation estimates m taps of the channel's impulse response and channel estimation in frequency domain estimates the response to N_{SC} subcarriers simultaneously. Since the number of data subcarriers is large compared to the number of channel taps ($N_{SC} > m$), given a fixed amount of data (received training symbols in time/frequency domain), it is easier to estimate fewer parameters. Thus, the advantage of the time domain approach is its better performance. The drawback of the time domain estimation is that complex calculations are required and symbol timing has to be well determined. In our work, we employed channel estimation in time domain with LS with $m = 32$ channel taps.
After obtaining the channel estimates, received data symbols on each subcarrier are equalized as according to,

$$Y_k = \frac{\hat{H}_k^*}{\left|H_k\right|^2} R_k \tag{2.32}$$

We use the same channel estimates in all the MB-OFDM symbols inside one frame, since the channel is assumed to be constant over one frame duration. After equalizing the data symbols, the pilot and training symbols are removed.

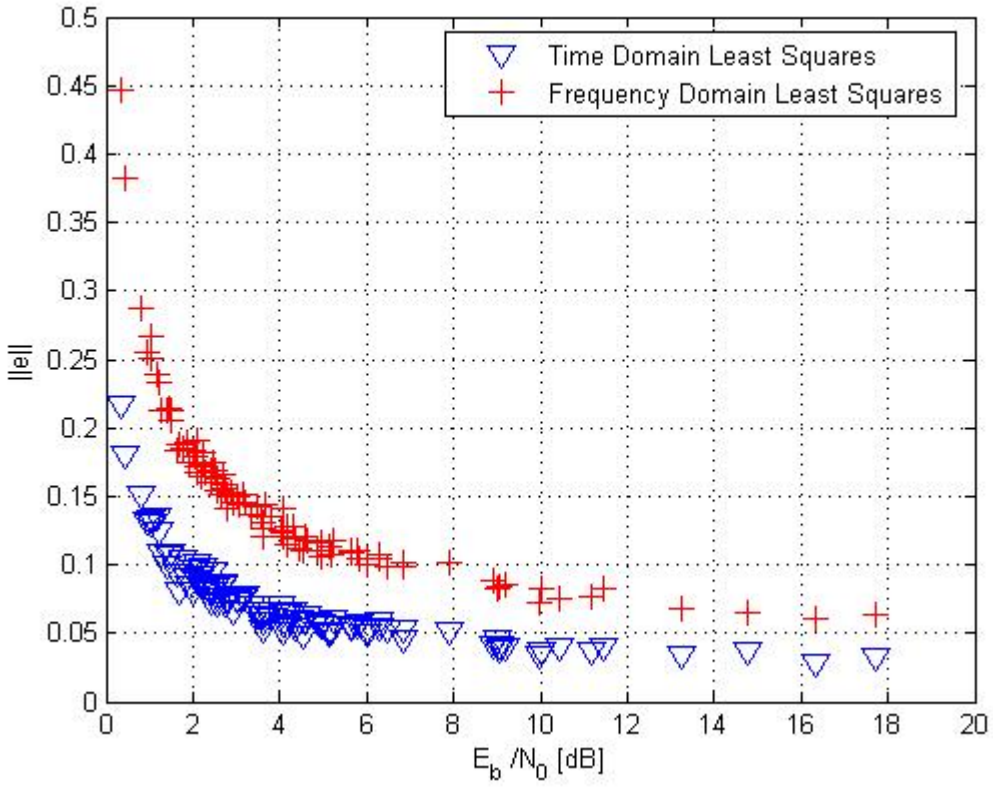

Figure 2. 11 Performance comparison of the channel estimation methods

2.3.2. Viterbi Decoding

In an uncoded OFDM system, each subcarrier's bit error rate can be determined by measuring the signal to noise ratio of each subcarrier. Then, the bit error rate for the whole data signal is obtained by averaging the BER's of all subcarriers. For instance, the bit error rate for MB-OFDM signal with N_{SC} data subcarrier and QPSK modulation can be obtained from,

$$P_{b,uncoded} = \frac{1}{N_{SC}} \sum_{k=0}^{N_{SC}-1} Q\left(\sqrt{\frac{|H_k|^2}{\sigma_n^2}}\right) \tag{2.33}$$

where the term inside the $Q(\sqrt{.})$ function gives the signal to noise ratio of each subcarrier. Figure 2. 12 shows the squared amplitude of an arbitrary frequency selective channel.

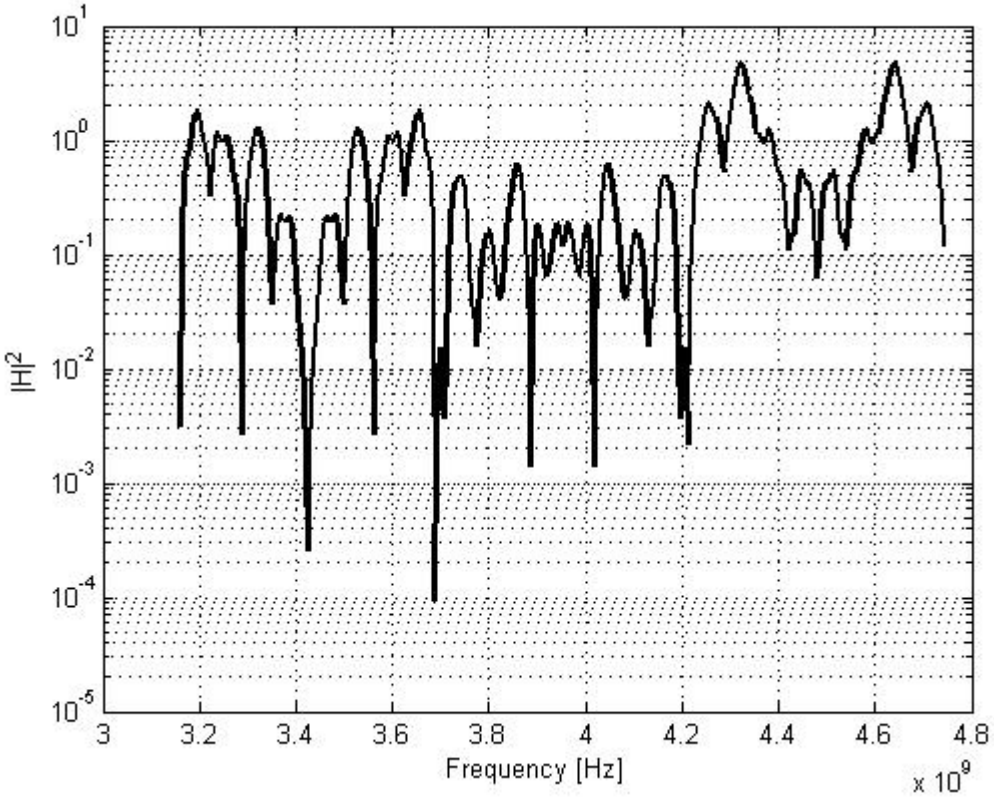

Figure 2. 12 An example channel response to MB-OFDM subcarriers

Following the symbol equalization, I and Q symbols are directly mapped to soft decision bits going into the deinterleaver. Tone deinterleaving is performed before the symbol deinterleaving to reverse the operations performed at the transmitter. The receiver performs maximum-likelihood sequence decoding using the Viterbi algorithm [30].

For soft-decision Viterbi decoding bit error probability is bounded by,

$$P_e \leq \sum_{d=d_{free}}^{\infty} a_d P_2(d) \tag{2.34}$$

where d is the distance between two merging paths inside the trellis, a_d is the distance spectrum defined as the total number of information bit errors for all events of length *d*. and $P_2(d)$ is the pair-wise error probability that a correct path and incorrect path differ in *d* positions. Note that the first summation term in Eq.(2.33) gives the minimum error bound where $a_{dfree} = 1$. For Rayleigh Fading Channels *P2(d)* is calculated from [30],

$$P_2(d) = p^d \sum_{k=0}^{d-1} \binom{d-1+k}{k} (1-p)^k \tag{2.35}$$

with,

$$p = \frac{1}{2}\left(1 - \sqrt{\frac{rE_b / N_0}{1 + rE_b / N_0}}\right) \tag{2.36}$$

The E_b/N_0 is defined as [21]

$$\frac{E_b}{N_0} = \frac{E[|X_k H_k|^2]}{E[|w_k|^2] \times \log_2 M \times r} \tag{2.37}$$

Since QPSK is the modulation type, M=4 and $E[|X_k|^2] = 1$, as shown previously noise power is selected as $E[|w_k|^2] = \sigma_z^2$.

The minimum free distance (d_{free}) for the mother r *=1/3* code is 15 and its distance spectrum can be obtained from MATLAB7's "distspec" command [47]. After puncturing, we find that d_{free} reduces to 7.

Since the trellis structure of the Viterbi algorithm to decode rate 1/3,K=7 convolutional codes, contains 64 (2^{K-1}) states, it is hard to give all trellis structure. Instead Figure 2. 13 shows some of the state transitions and the associated output bits on each state transition. The full trellis can be obtained by using the *poly2trellis* function inside the MATLAB7© 's Communication Toolbox [47].

When the Viterbi algorithm receives a soft bit, it finds a branch metric, which is the Euclidean distance between the soft bit and the transmitted bit. At t=0, branch metrics B_0 and B_1 are calculated from,

$$\begin{aligned} B_0 &= \left|\hat{b}_0 - (-1)\right|^2 \\ B_1 &= \left|\hat{b}_0 - 1\right|^2 \end{aligned} \tag{2.38}$$

where $\hat{b}_0$ is the received soft decision bit, and -1, 1 corresponds to transmitted bits 0,and 1 respectively.

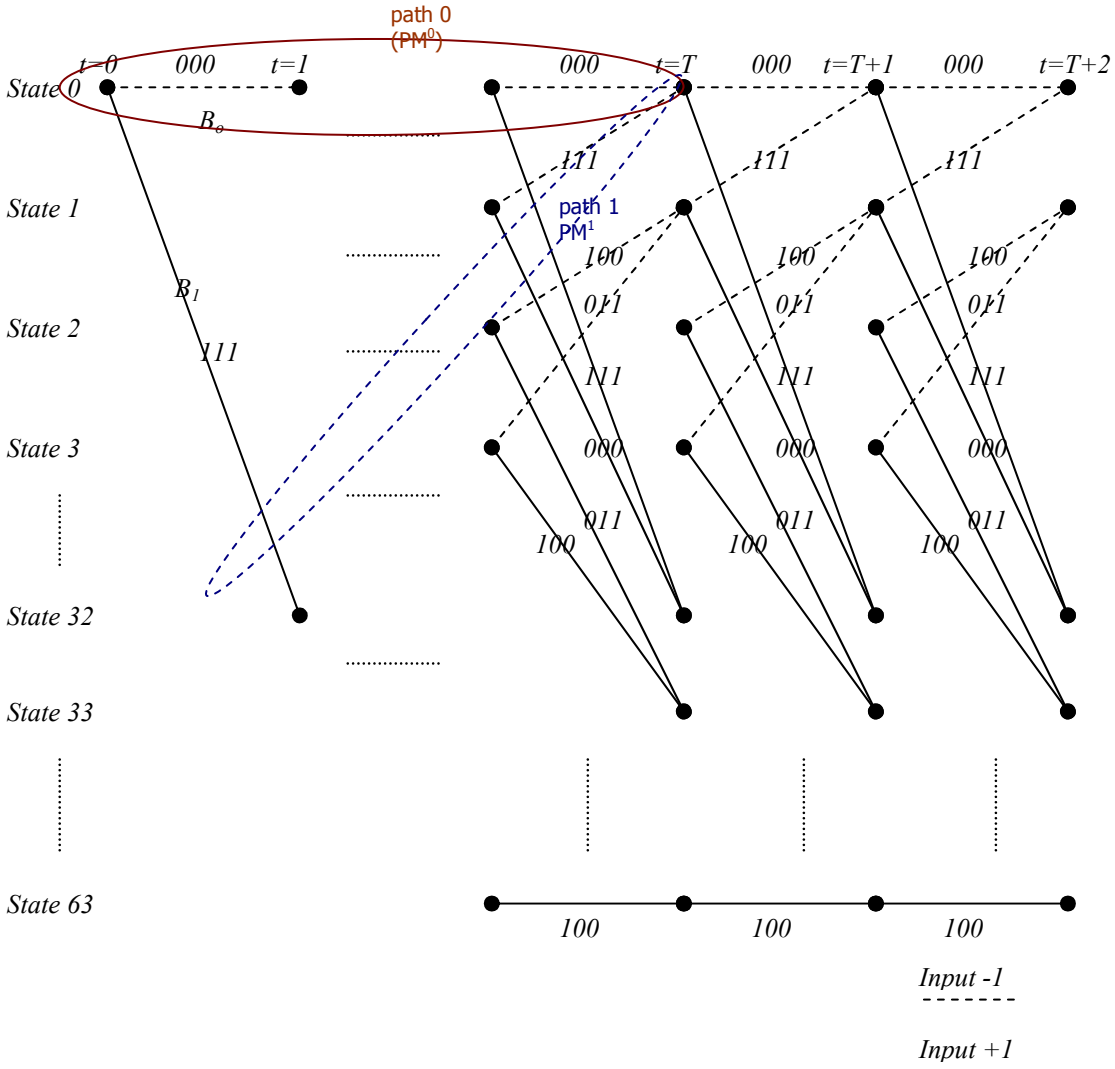

Figure 2. 13 Viterbi Trellis Structure for decoding r=1/3,K=7 convolutional code.

In the Viterbi trellis, a metric for the i^{th} path consisting of B branches (e.g. path 0, path 1 with T branches in Figure 2. 13) through the trellis is defined as,

$$PM^{(i)} = \sum_{j=1}^{B} B_j \tag{2.39}$$

At $t=T$, two paths merge at state 0. The selection criterion between two paths through the trellis is to select the one having the smaller path metric. The path with the larger path metric is discarded and algorithm resumes with the survivor path at the subsequent branches. This rule maximizes the probability of a correct decision. At the end of the trellis, the output bit streams that correspond to the minimum path metric minimizes the probability of error for the sequence of information bits.

On the other hand, when data are modulated onto multiple carriers as in MB-OFDM, the subcarriers experience different signal to noise ratios. The soft decision bits are then obtained from the equalized $\hat{Y}_k$ symbols as,

$$\hat{Y}_k = X_k + \frac{\hat{H}_k}{\left|\hat{H}_k\right|^2} n_k \tag{2.40}$$

The noise power contributed to each subcarrier becomes $\sigma_n^2 / \left|\hat{H}_k\right|^2$ where $\left|\hat{H}_k\right|^2$ is the estimated channel gain at subcarrier k. A subcarrier, which falls into a notch, comprises mostly noise. Using this observation, and having good channel estimate, we can conclude that the bits transmitted on the subcarriers having high gain are more reliable than the bits transmitted on the subcarriers having low gain. We define the information of channels gains at each subcarrier as the Channel State Information (CSI).

The CSI can be incorporated into the Viterbi algorithm to provide performance improvement, [46], [48], [49]. In this approach, the gain of the channel, that the bit is transmitted, weights the branch metric as,

$$B_n = \left|\hat{H}_k\right|^2 \left|\hat{b}_n - b_n\right|^2 \tag{2.41}$$

When a bit is transmitted on a notch subcarrier at $t=T$, the branch metric defined in Eq.(2.38) introduces a large branch metric for all possible transmitted bits at this instant and consequently reduces the decoding performance. On the other hand, since the deep-faded subcarrier has a relatively small gain, Eq.(2.41) scales the branch metric to almost zero at the notch subcarriers. Namely, the bits that are transmitted on deep- faded subcarriers will have reduced effect on the decision that the Viterbi algorithm makes. Finally, we have inserted a zero branch metric in places of the punctured bits, so puncturing does not affect the path decisions.

To observe the Final BER versus E_b/N_0, at d=3m TX-RX separation, Empirical BER values are obtained from 100 independent channel realizations from CM1 as shown in Figure 2. 14. We then fit an exponential curve (Exp. Fit) to this BER distribution using the MATLAB's curve fitting toolbox [47]. Non-Linear Least Squares method [50] is

used to minimize the sum of square error between the fitted curve and the empirical BER values. The fitted curve ($f(E_b/N_0)$) has an exponential form as,

$$f(\frac{E_b}{N_0}) = \sum_{i=1}^{G} a_k \exp(-\left(\frac{\frac{E_b}{N_0} - b_k}{c_k}\right)^2) \qquad (2.42)$$

with G = 3. The additional function parameters are given in the table below.

Table 2-6 Curve fitting Parameters

a_1	0.0618	b_1	-1.472	c_1	0.7554
a_2	-0.02135	b_2	-0.6494	c_2	0.4101
a_3	0.04802	b_3	-1.247	c_3	3.906

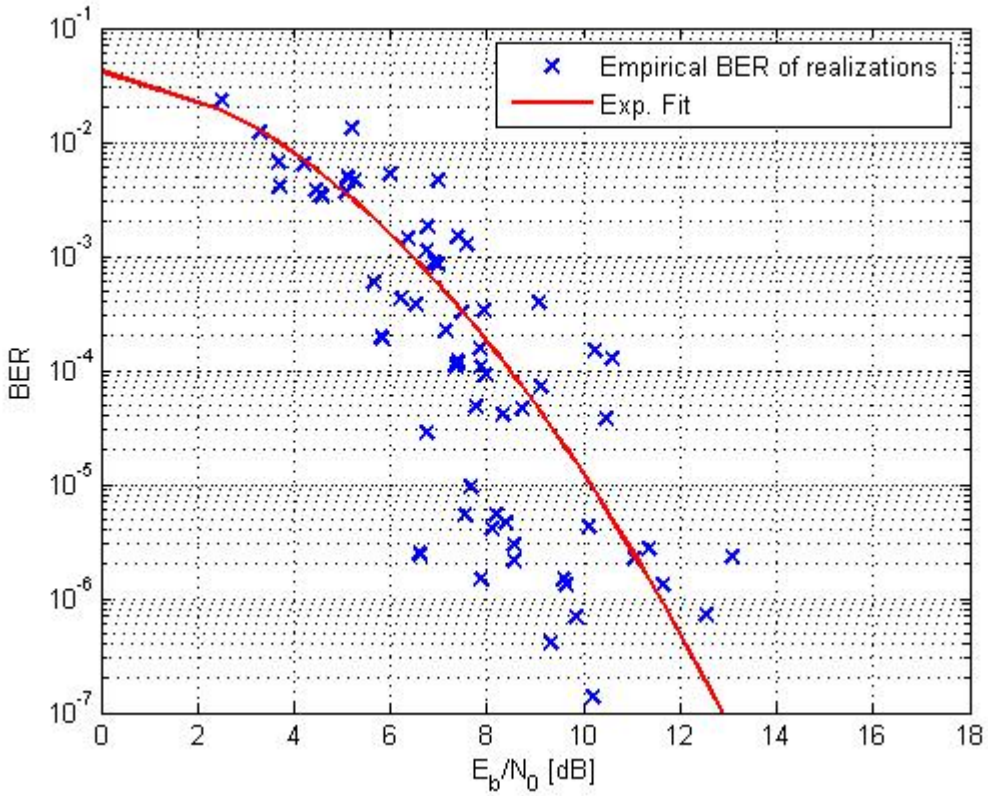

Figure 2. 14 BER vs E_b/N_0 performance for a number of MB-OFDM links with independent channel realizations

2.4. Frame Format

In this subsection we explain the Multiband Frame format defined in the MB-OFDM PHY proposal

A MB-OFDM frame is composed of PLCP (physical layer convergence procedure) preambles, MAC preambles, frame payload, Frame Check Sequence (FCS), tail bits and pad bits as shown in Figure 2. 15.

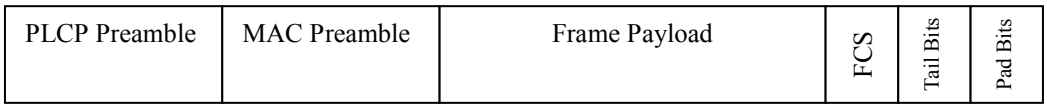

Figure 2. 15 MB-OFDM Frame format

Receiver can use the PLCP preamble at the beginning of the frame to perform frame detection, synchronization, frequency-offset recovery and channel estimation. The PLCP preamble consists of three parts: packet synchronization sequence, frame synchronization sequence and channel estimation sequence. First frame of the transmission carries 21 identical time-domain training symbols and streaming packets carries 6 training symbols where each signal has duration of one MB-OFDM symbol (T_{SYM}). Frame synchronization sequence is composed of 3 training signals where each signal is the inverse of the signal used in packet synchronization sequence. Frame synchronization sequence is used for internal synchronization purposes such as estimating the beginning of the channel estimation sequence. Finally channel estimation sequence is consisting of 6 training symbols composed of 128 pilot tones. In this thesis, we used this portion of frame to obtain the channel's response both in time and frequency domains. First and fourth training symbol is averaged and used to estimate the channel's response at sub-band 1, second and third OFDM symbol is averaged and used to estimate the channel's response at sub-band 2, and third and sixth OFDM symbol is averaged and used to estimate the channel's response at sub-band 3. Totally, The PLCP preamble elapses $N_{PR} = 30$ OFDM symbol duration for the first frame of transmission and $N_{PR} = 15$ OFDM symbol duration for the streaming frames.

The MAC preamble informs the receiver about the data rate of the transmission, and size of the frame in terms of bytes. The data rate field tells the receiver that the data on the frame payload will be transmitted at 480 Mbps. Packet length field indicates the number of bytes in the frame payload excluding the FCS, tail bits, pad bits. Frame payload has variable length between 0-4095 bytes. The MAC preamble is always transmitted at 55 Mbps and it has 7 OFDM symbol duration (N_{MAC}).

Frame payload and MAC preamble is protected with CCITT CRC-16 frame check sequence. This cyclic redundancy check informs the receiver about the frame is in error or not. Since *K* denotes the convolutional code's constraint length, tail bits are *K*-1 bits of zero appended to the end of information bits per each frame. Tail bits satisfy the Viterbi decoder return to zero state. Pad bits are inserted after the convolutional encoding and puncturing to ensure that the frame carries integer number of MB-OFDM symbols. Since the interleaving procedure accepts 3 N_{CBPS} bits at a time. Number of data OFDM symbols at the output of the receiver N_{DATA} becomes,

$$N_{DATA} = 3 \times ceil(\frac{round(\frac{N_{f,bits}}{r})}{3 \times N_{CBPS}}) \tag{2.43}$$

where r is the coding rate and $N_{f,bits}$ is,

$$N_{f,bits} = 8 \times N_{FRAME} + N_{FCS} + K - 1 \tag{2.44}$$

where N_{FRAME} is the number bytes written in the MAC preamble, N_{FCS} is the number of redundant bits for the CRC check and r is the coding rate.

In this section we model a single MB-OFDM link with its fundamental building blocks. In the subsequent chapter, we try to maximize the individual link's efficiency with dynamically and optimally selected frame sizes based on the channel conditions.

3. LINK ADAPTATION FOR MB-OFDM BASED UWB SYSTEMS

The fundamental characteristic of mobile wireless links is the time variation of the channel quality as a result of factors such as multipath propagation, path loss, shadowing and interference. To mitigate with these adversive effects inherit in wireless channel, ARQ schemes are employed to make sure reliable information transfer between communicating devices. Basically, ARQ protocols combine error detection and retransmission to ensure that the data is accurately delivered to the destination device. As shown in Figure 3. 1 Stop and Wait (SW) ARQ protocol, the transmitter and receiver work on the delivery of one frame at a time. The transmitter (A) sends an information frame to receiver (B). The transmitter stops and waits for an acknowledgement (ACK). If the transmitter cannot capture any ACK within some period, it resends its current frame. SW ARQ works well on channels that have low propagation delay. On the other hand the protocol becomes inefficient when the propagation delay is much greater than the time to transmit each frame. This problem is later overcome by allowing the transmitter to continue sending enough frames so that the channel is kept busy while the transmitter waits for acknowledgements. Figure 3. 2 shows the Go-Back N ARQ protocol. The transmitter (A) fills its pipeline with W_S frames (W_S is selected to ensure that channel is kept full), and sends all of them to the receiver. When transmitter realizes frame 0 is received correctly by capturing ACK1, it removes frame 0 from the pipeline and inserts a new frame. When frame 3 is in error, the receiver ignores all the subsequent frames. Meanwhile the transmitter pipeline cannot accept new packets since frame 3 has not been confirmed yet. Hence transmitter resends frame 3. Selective Repeat ARQ accepts out-of order but error-free frames. As shown in Figure 3. 3, when receiver cannot capture frame 3 within some period, it sends a negative acknowledgement (NAK3) frame to transmitter. During the propagation time of NAK3 frame, receiver captures frames 4 and 5 without error. When receiver captures frame 3 correctly, it sends an ACK for frame 6 verifying that frame 4 and frame 5 is received correctly [51].

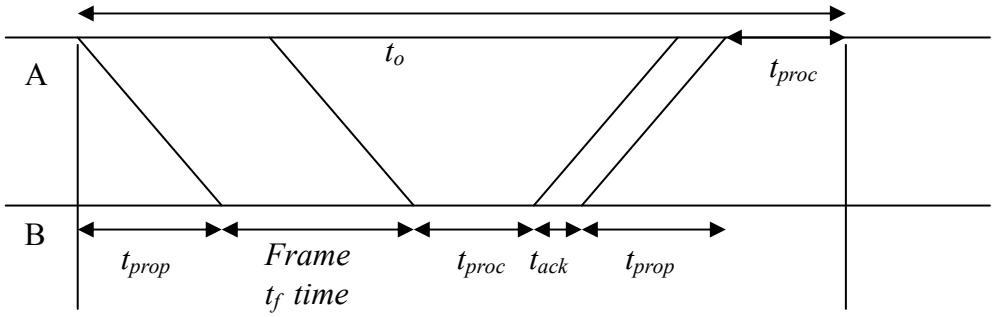

Figure 3. 1 SW-ARQ Protocol

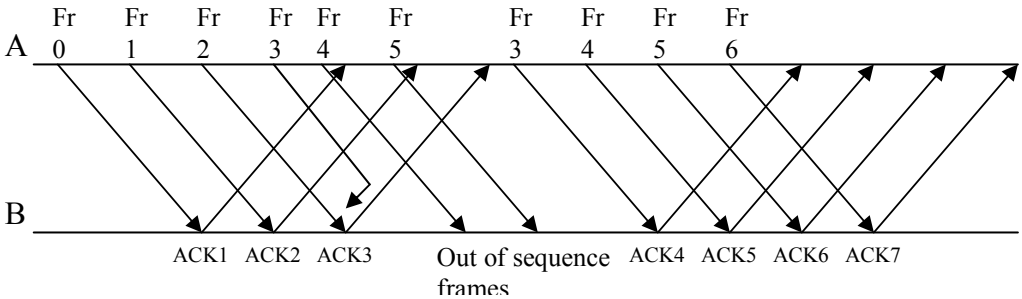

Figure 3. 2 Go-Back N ARQ Protocol

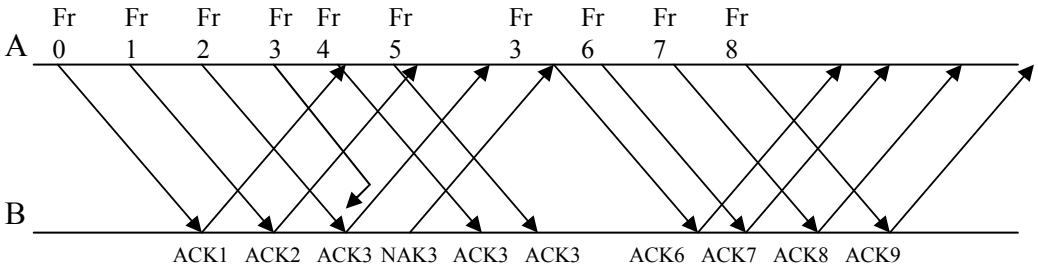

Figure 3. 3 Selective Repeat ARQ Protocol

In IEEE's 802.15.3 WPAN standard [4], the delivery of a frame through a connection between devices can be verified using one of the acknowledgement (ACK) policies: No-ACK policy, immediate ACK (Imm-ACK) policy and delayed ACK policy (Dly-ACK). No-ACK policy is suitable for the transmissions that do not need guaranteed delivery. In No-ACK policy transmitter accepts the frame is always delivered correctly and proceeds to the next frame. Imm-ACK policy provides an ACK for each individual transmitted. Thus Imm-ACK policy is alike to the SW-ARQ protocol. In the Dly-ACK, the transmitter sends multiple frames to the receiver. The acknowledgement for those frames is grouped and sent back to the transmitter when requested. The Dly-ACK process decreases the overhead in the Imm-ACK policy. Hence from this point of view it is similar to the Go-Back N and Selective Repeat ARQ protocols.

Fortunately, Imm-ACK policy is practical for such MB-OFDM channels that have low propagation delay. For example, excluding the frame processing periods at the transmitter and receiver, the total time that elapses from the beginning of the frame transmission to the receipt of its ACK is about 2.1μs when we transmit frames of 1000-bit size long over a 480Mbps MB-OFDM channel with TX-RX separation of 3 meters. The total number of bits that can be sent during is 2.1μs is 1008 bits, which corresponds to 99% link ARQ efficiency. Thus, in this thesis, the Immediate ACK policy is selected as the data link layer of our system.

For the packet (frame) transmission systems, while short frames are less likely to encounter errors than long frames, they are more encumbered by the frame overheads. The frame length, which maximizes the instantaneous throughput, is related with the dynamic channel conditions as a result of multipath fading, shadowing and propagation path loss. If the optimum frame size is selected adaptively by estimating channel condition, the maximum attainable throughput can be achieved continuously. In this chapter, we define the instantaneous channel conditions in terms of instantaneous BER and talk about methods to estimate the BER of an MB-OFDM UWB link.

This chapter is organized as follows. In Section 3.1, we review the SW-ARQ and explain the frame size optimization to improve ARQ efficiency. Section 3.2 and Section 3.3 are devoted for adaptation of frame sizes using Modiano's Algorithm and channel state information respectively. Finally, Section 3.4 includes simulation results regarding to frame size optimization methods.

3.1. Stop and Wait (SW) ARQ and Frame Size Optimization

In the absence of channel errors, the effective information transmission rate of this ARQ protocol R_{net}^{0} is given by,

$$\frac{\text{number of information bits delivered to the destination}}{\text{total time required to deliver the information bits}} \tag{3.1}$$

Then the transmission efficiency of the SW-ARQ protocol without errors is,

$$\eta_0 = \frac{R_{net}^0}{R} \tag{3.2}$$

where R denotes the bit rate of the channel .

When we neglect the ACK frame delivery duration (t_{ACK}) and propagation time (t_{prop}), processing durations (t_{proc}) of data and ACK frames, the total time required to deliver a single a single MB-OFDM frame , t_0 , becomes equal to a single frame duration (t_f) as,

$$t_0 = T_{SYM}(N_{PR} + N_{MAC} + N_{DATA}) \tag{3.3}$$

where as stated in Section 0, N_{PR} is the number of MB-OFDM symbols at the PLCP preamble ($N_{PR} = 30$ for the initial frame, $N_{PR} = 15$ for the streaming frames), N_{MAC} is the number of MB-OFDM symbols at the MAC preamble ($N_{MAC} = 7$), and N_{DATA} is the number of MB-OFDM symbols in the frame payload as calculated from (2.43).

Therefore η_0 can be rewritten as,

$$\eta_0 = \frac{1}{R} \frac{8 \times N_{FRAME}}{T_{SYM} \times (N_{PR} + N_{MAC} + 3 \times ceil(\frac{round(\frac{N_{f,bits}}{r})}{3 \times N_{CBPS}}))} \tag{3.4}$$

If the packets are transmitted over an erroneous channel with a bit error rate (BER) of ρ, the expected time to deliver a frame successfully; $E[t_{total}]$, can be directly determined from [51],

$$E[t_{total}] = \frac{t_0}{(1 - P_f)} \tag{3.5}$$

where P_f is the frame error probability and expressed as,

$$P_f = 1 - (1 - \rho)^{8 \times N_{FRAME} + N_{FCS}} \tag{3.6}$$

Then the efficiency of the MB-OFDM link using SW-ARQ (Imm ACK), η, can be determined as,

$$\eta = \frac{8 \times N_{FRAME}}{E[t_{total}] \times R} = \eta_0 \times (1 - \rho)^{(8 \times N_{FRAME} + N_{FCS})} \tag{3.7}$$

The optimum frame size N_{FRAME}^* that maximizes η can be found from,

$$N^{*}_{FRAME} = \arg\max_{N_{FRAME}} \eta \quad N_{FRAME} = 0,...,4095\,\mathrm{B} \tag{3.8}$$

where 0 and 4095B are pre-determined minimum and maximum frame payload sizes respectively in the TI's MB-OFDM PHY layer proposal.

For the data rate of 480Mbps, the optimal frame sizes can be selected according to the BER of the MB-OFDM channel as shown in Figure 3. 4. Also Figure 3. 5 shows the optimal link ARQ efficiency for the optimal frame size. At high bit error rates, small frame size selection increases the probability of correct delivery. On the other hand, a single MB-OFDM frame carries 43 preamble symbols, and the delivery of these overhead symbols dominates the transmission. Thus small frame size selection makes inefficient use of the ARQ protocol. As the BER of the link decreases, it is favorable to select a large frame size to keep the link ARQ efficiency maximum. Our calculations show that at maximum frame size including the frame preamble symbols, the link ARQ efficiency bounded to about 90 %.

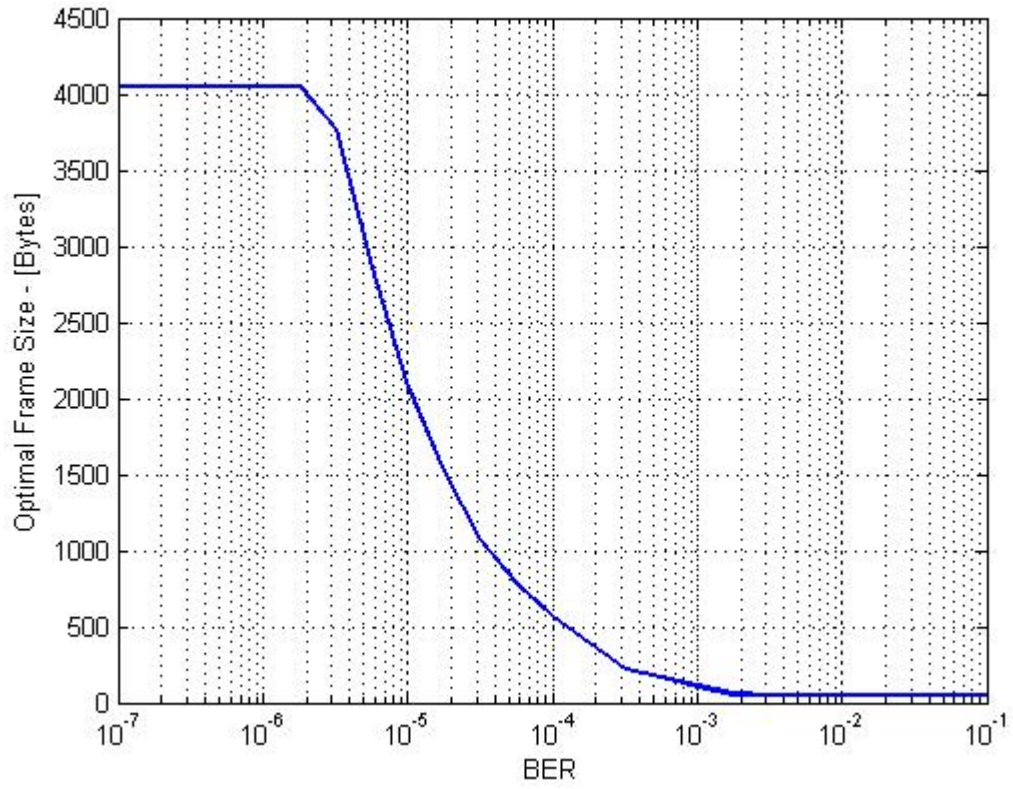

Figure 3. 4 Optimal Frame Size versus bit error rate (BER)

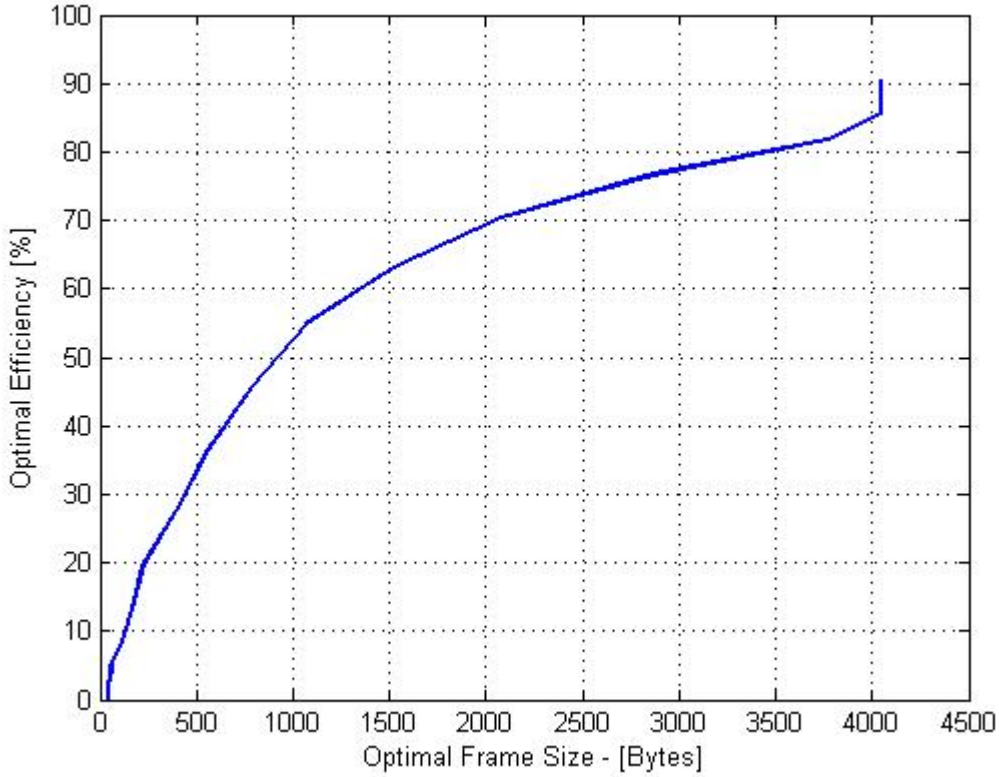

Figure 3. 5 Optimal Efficiency versus Optimal Frame Size

3.2. BER Estimation Using Modiano's Algorithm

Modiano's algorithm (MA) [24] is based on the maximum likelihood estimate (MLE) of ρ by monitoring the number of retransmission C, in the previous D transmissions. In this method, the BER estimate, $\hat{\rho}$, maximizes the probability that C retransmissions are observed in the previous D transmissions, which can be expressed as,

$$\hat{\rho} = \arg\max_{\rho} P[C \mid \rho] = \arg\max_{\rho} \binom{D}{C} P_f^C (1-P_f)^{(D-C)} \tag{3.9}$$

This maximization can be done by taking the log derivative of the above equation and setting equal to zero and solving for ρ, the MLE estimate of the BER ,$\hat{\rho}$, can be obtained as,

$$\hat{\rho} = 1 - \left(1 - \frac{C}{D}\right)^{\frac{1}{(8\times N_{FRAME} + N_{FCS})}} \tag{3.10}$$

By combining Eqs.(3.7), (3.8), and (3.10) the optimal frame size, N^*_{FRAME}, can be obtained to improve the link efficiency of MB-OFDM UWB channel.

However, MLE estimate of ρ tends to overestimate ρ when many errors occur and underestimate ρ when few errors occur. For example, when no errors occur in the previous M transmissions $\hat{\rho}$ becomes zero implying infinite frame size. On the other hand, when a frame size of 10^5 bits is used for a link with bit error rate 10^{-2}, the probability of retransmissions is close to one, producing all M frames need to be retransmitted. Therefore, optimum frame size scales down to zero. To avoid from such biases, the frame sizes are restricted to the range of payload sizes defined in the MB-OFDM PHY proposal. The frame sizes are then selected according to,

$$N_{FRAME} = \begin{cases} 1B & C = D \\ N^*_{FRAME} & 0 < \dfrac{C}{D} < 1 \\ 4095B & C = 0 \end{cases} \tag{3.11}$$

When the channel is clear, transmitter selects the maximum frame size to maximize the channel utilization. When the channel introduces some frame errors, transmitter uses (3.10) to estimate the channel BER and optimizes the frame size accordingly. When the link is in deep fade, namely all frames in the previous M frames are in error, transmitter selects the minimum frame size 1B instead of 0B defined in the PHY proposal to come up with a BER estimate.

Figure 3. 6 shows the BER estimation performance of MA. The empirical BER of the channel is previously recorded as $3\text{x}10^{-5}$. According to this figure, BER estimation accuracy mainly depends on two parameters: number of previous transmissions (D), and the frame size used in these transmissions (N_{FRAME}). Small frame sizes (50B) in low error channels result suboptimal a BER estimation value and a sub-optimal frame size, due to the insufficient number of encountered bits. Fortunately, if the channel remains static, at the next observation window algorithm works with a larger frame size and obtains to a more accurate BER estimate. Selecting a larger frame size (1024B) gives a BER estimate close to the ideal value. Moreover, the standard deviation of the BER estimates reduces as D increases. Shortly, when the D and N_{FRAME} are selected large enough, the ML BER estimate converges to the ideal BER value.

The BER estimate found in is valid when channel introduces independent bit-errors. Even though channel introduces many bit errors due to fading, the assumption of independent bit errors is justified through the use of two-stage interleaving operation as mentioned in Section 2.1.2. Throughout the manuscript, it is also assumed that the characteristic of the MB-OFDM link is invariant during the channel's coherence time. Hence, when a link just enters new fading conditions, MA selects the optimal frame size based on the ML estimate of the BER. As long as the channel's coherence time is long enough to track channel changes, MA algorithm converges near to the optimal frame size because the ML estimator variance is small enough to ensure the convergence.

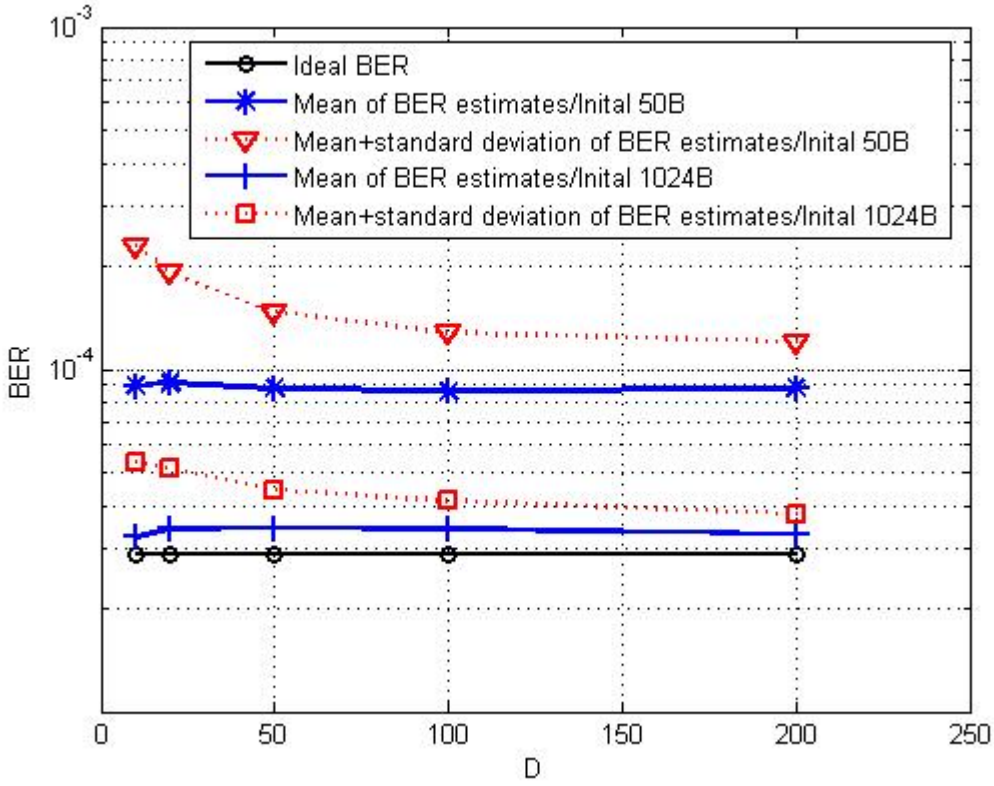

Figure 3. 6 Performance of MA under a BER=3x10^{-5} channel

MA does not consider PHY properties of the channel, i.e., it does not matter whether we estimate the BER of MB-OFDM UWB or of any other wireless system. However, the its main disadvantage is that it requires *D* frame duration for the BER estimation, as the channel coherence time decreases or the optimal frame size increases, BER monitoring becomes hard. To alleviate that problem, in this thesis, we develop another

method to estimate the instantaneous BER of the MB-OFDM link based on channel response as presented in the next subsection.

3.3. BER Estimation Based on the Channel State Information (CSI)

As previously pointed out, the main disadvantage associated with MA is the need for D frame duration to make an estimate the BER. However, as the channel coherence time decreases it becomes hard to track channel and to monitor and estimate the BER. MA also does not consider PHY layer structure of MB-OFDM UWB when estimating the BER. In the subsequent development we consider the building blocks of MB-OFDM UWB to estimate its BER.

First, we try to make a BER estimation based on the received E_b/N_0. According to Figure 2. 14, for E_b/N_0 < 5dB, fitted curve gives a good idea about the channel conditions. On the other hand, when E_b/N_0 is between 5dB and 12 dB, the observed coded BER values deviate from the fitted curve. For instance, around 7dB of E_b/N_0, coded link BER varies between $2\text{x}10^{-6}$ and $4\text{x}10^{-3}$. We define BER estimation error κ as,

$$\kappa = \frac{\left|\hat{\rho} - \rho\right|}{\rho} \tag{3.12}$$

where $\hat{\rho}$ is the estimated BER obtained from the fitted curve and ρ is the empirical BER value. For this approach, κ varies between $4\text{x}10^{-5}$ and 341.36, and average estimation error is 15.87 with standard deviation 47.7065.

On the other hand, we intuitively know that the number of small amplitude subcarriers dominates the BER of the channel. So we analyze the gain distribution of subcarriers rather than their average gain. We define the Carrier to Noise Ratio (CNR) for the k^{th} subcarrier as,

$$CNR_k = \frac{E\left[\left|X_k H_k\right|^2\right]}{\sigma^2} = \frac{\left|H_k\right|^2}{\sigma^2} \tag{3.13}$$

The CDF of subcarriers for a given threshold γ is also defined as,

$$F(\gamma) = P\left(\frac{|H_k|^2}{\sigma^2} < \gamma\right) \tag{3.14}$$

When the entire channel is in deep fade, number of small amplitude subcarriers increases which enhances the noise power and worsen the Viterbi soft decoding performance. To observe this effect, Figure 3. 7 shows CNR_k's cumulative distribution function (CDF) for three independent MB-OFDM links with 3 meters TX-RX separation.

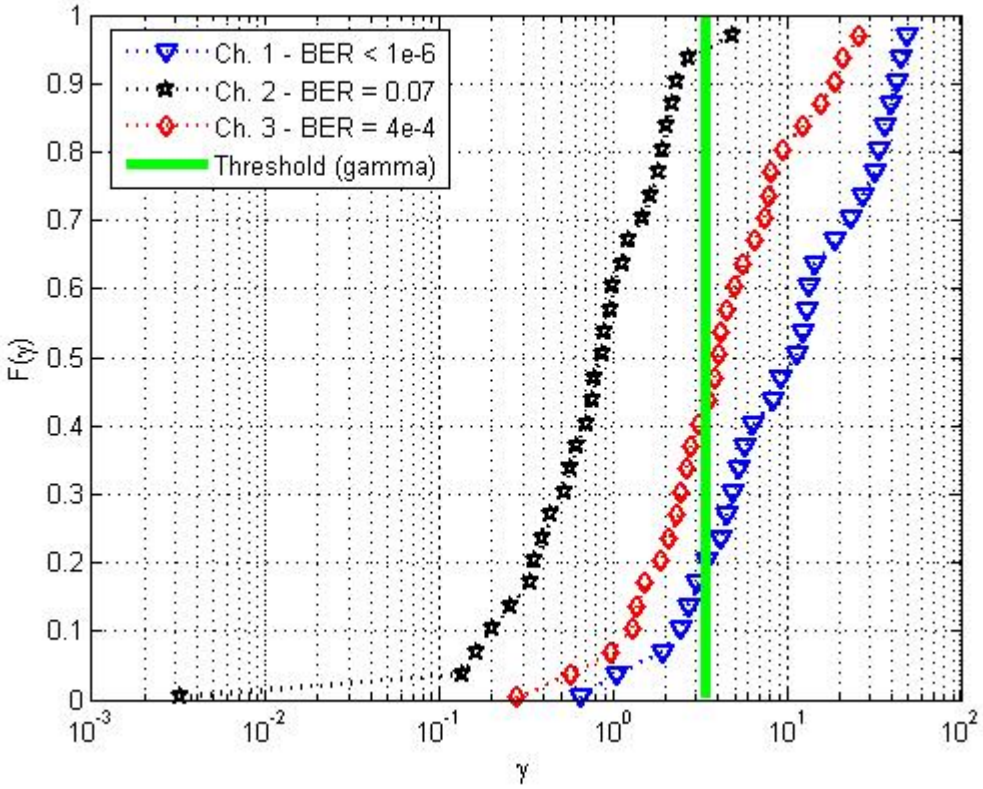

Figure 3. 7 CDF of CNR_k 's of three independent channel responses at d=3m separation distance

The BER of the MB-OFDM link 1 is less than 10^{-6} and the BER of the link 2 and 3 are experimentally found as $7\text{x}10^{-2}$ and $4\text{x}10^{-4}$ respectively. The important observation from this figure is that for a given threshold γ , the CDF value of the worst channel is highest among others. Intuitively, we propose that for a properly selected threshold, γ , the BER of the system is an increasing function of number of subcarriers whose gain is less than this threshold.

Similarly, using a specific channel realization, we vary the TX-RX separation and plot $F(\gamma)$ versus γ graph as shown in Figure 3. 8. As one can see from this figure,

increasing the TX-RX separation decreases the overall signal to noise ratio, and, $F(\gamma)$ shifts to left, implying an increase on channel BER.

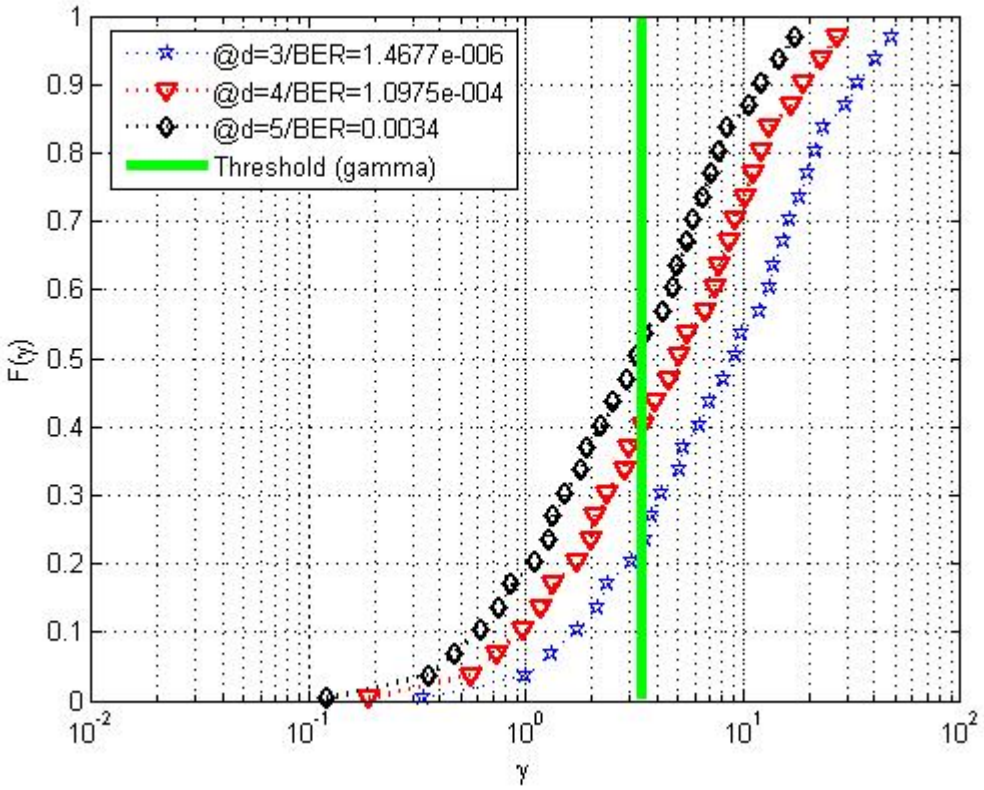

Figure 3. 8 CDF of CNR_k of a specific realization at different TX-RX distances

$F(\gamma)$ takes values between 0 and 1. To increase the dynamic range from now on we use $1/F(\gamma)$ as the decision variable for BER estimation which denotes the number of subcarriers where SNR of one of them is below the threshold value. The empirical bit-error rates of individual channel realizations versus $1/F(\gamma)$ are obtained for arbitrary selected thresholds $\gamma = 1$ and $\gamma = 10$ as shown in, Figure 3. 9 and Figure 3. 10 respectively. When a small threshold ($\gamma = 1$) value is selected, as one can see from Figure 3. 9, a good correlation is obtained between $1/F(\gamma)$ values of each realization and empirical BERs for high error rate channel realizations but this is not true for channels with low BER since their CDFs scale down to zero. On the other hand, large threshold value ($\gamma = 10$) results in $1/F(\gamma)$ of each realization vary within a small range although their BERs are significantly different from each other.

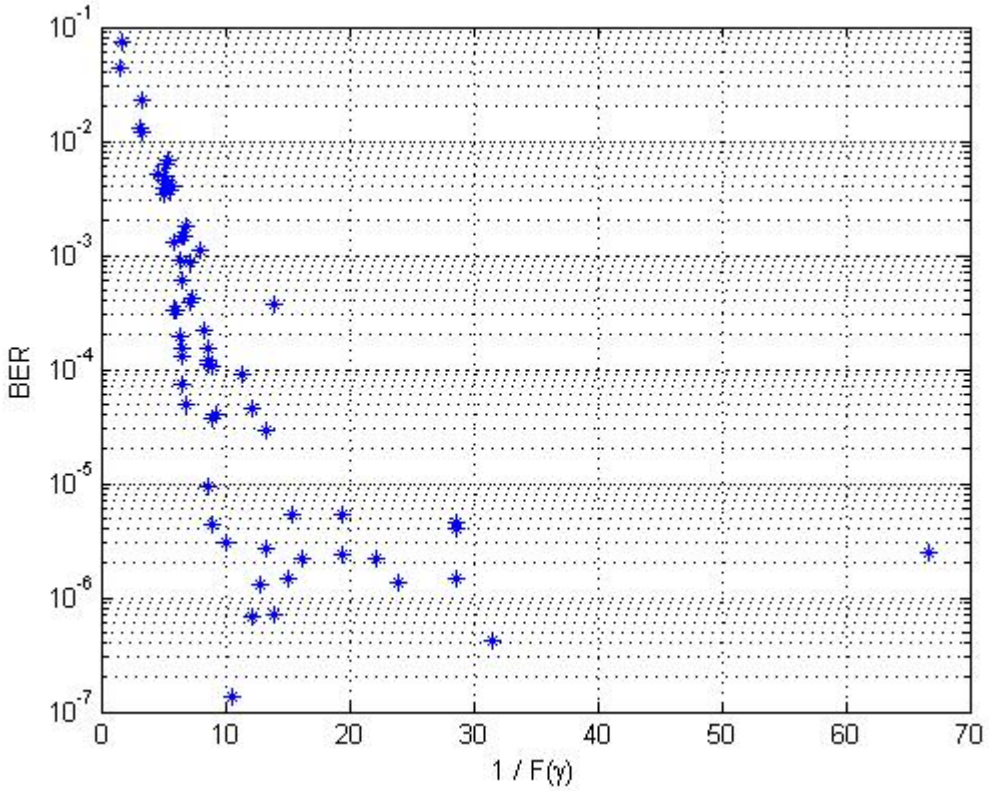

Figure 3. 9 BER versus 1/F(γ) (γ = 1)

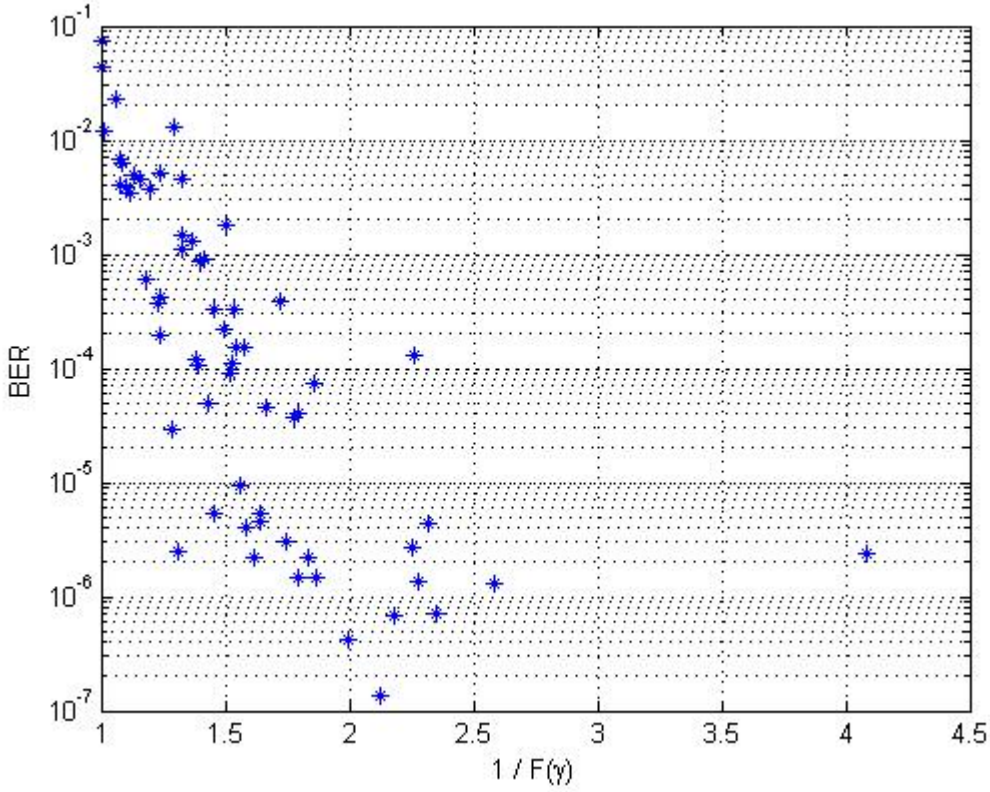

Figure 3. 10 BER versus 1/F(γ) (γ = 10)

Since BER performance of OFDM links is highly correlated with the subcarriers signal to noise ratio distribution, increase in BER implies increase in $F(\gamma)$. Hence, to find an optimal threshold value we look for the normalized cross-correlation between the realization BERs and associated $1/F(\gamma)$ and search for the threshold value γ for which the correlation is minimum. To do that, the empirical BERs are recorded and sorted in ascending order and for each BER value, decision variables $1/F(\gamma)$ are calculated for γ and the differences between two consecutive empirical bit error rates are recorded inside the $\Delta(BER)$ vector and the corresponding differences between two decision variables are also recorded inside the $\Delta\left[1/F(\gamma)\right]$ vector. Since we expect that $\Delta(BER)$ and $\Delta\left[1/F(\gamma_i)\right]$ be negatively correlated, we search for the gamma value that minimizes the correlation coefficient, ξ, as

$$\gamma^* = \arg\min_{\gamma} \ \xi(\gamma) = \arg\min_{\gamma} \frac{\Delta(BER) \times \left[\Delta\left[\frac{1}{F(\gamma)}\right]\right]^T}{\left\|\Delta(BER)\right\| \times \left\|\Delta\left[\frac{1}{F(\gamma)}\right]\right\|} \tag{3.15}$$

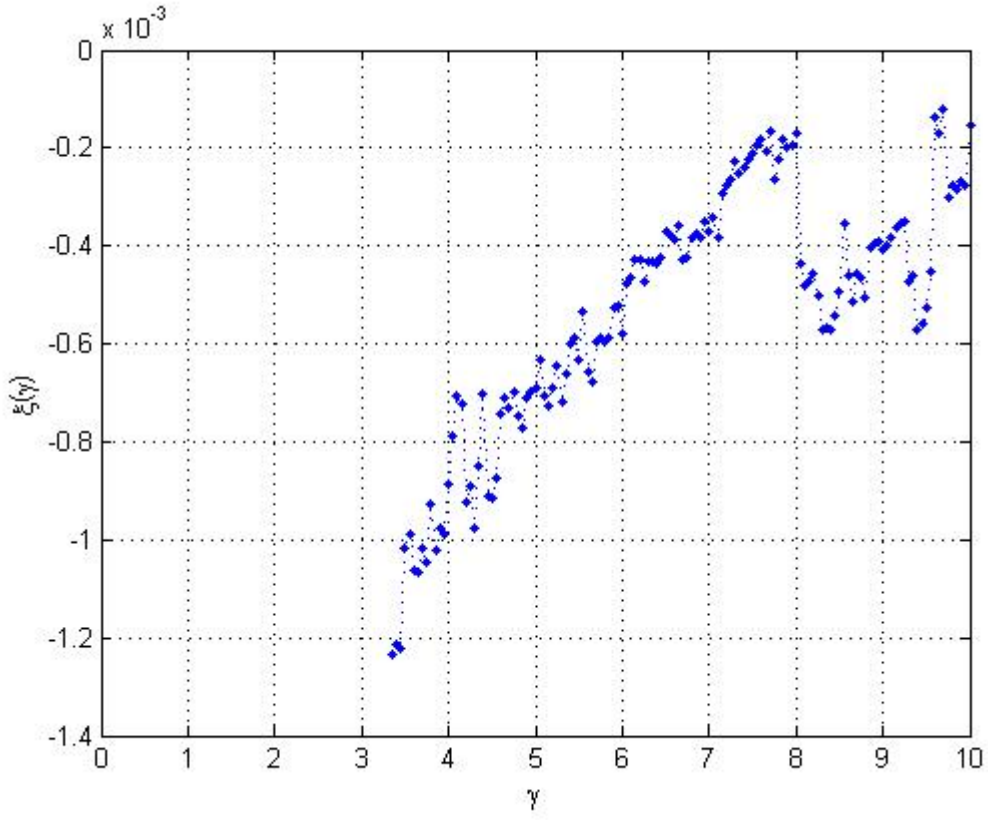

Figure 3. 11 Cross-correlation between BER of each realization and 1/ F(γ)

As shown in Figure 3. 11, Eq. (3.15) is not defined for $\gamma < 3.4$ because for some number of realizations $F(\gamma) = 0$ makes the correlation coefficient infinite. The normalized cross-correlation is minimized for $\gamma = 3.4$ and then increases towards to zero.

For $\gamma = 3.4$, BER versus $1/F(\gamma)$ graph is depicted in Figure 3. 12. It is interesting to note that the relationship between the $1/F(\gamma)$ and the channel BER resembles a Q(.) function with appropriate scaling coefficients. Hence, we find out a curve which models the graph very well as expressed as,

$$\hat{\rho} = 5 \times Q(2.32\sqrt{\frac{1}{F(3.4)}}) \tag{3.16}$$

which is also shown in Figure 3. 12.

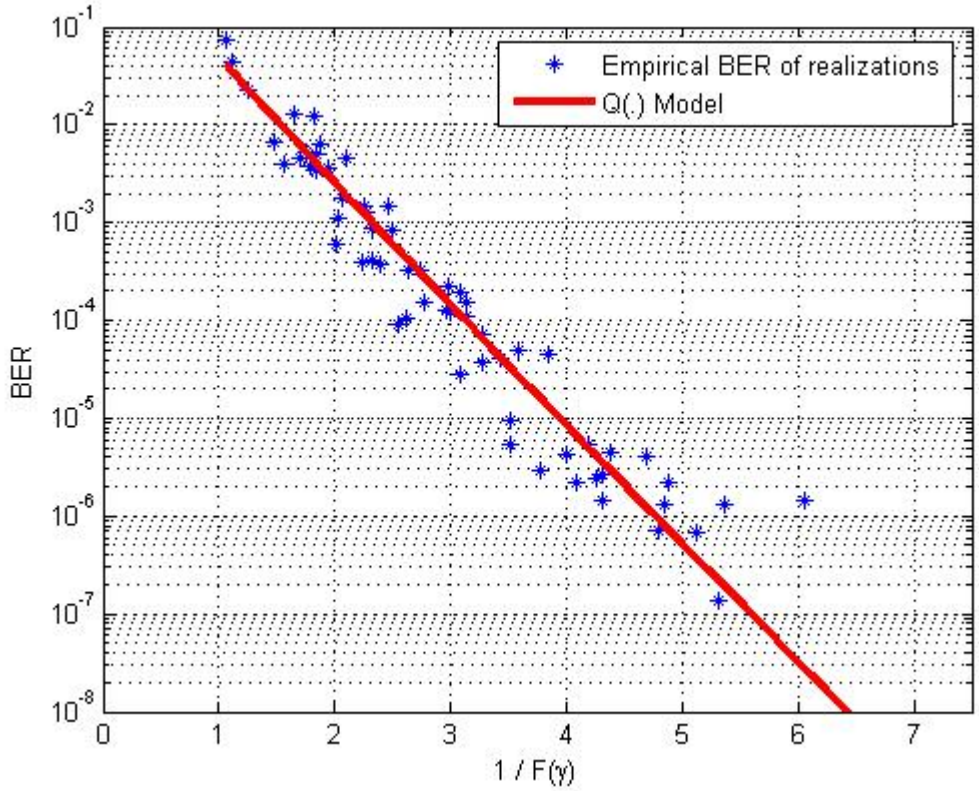

Figure 3. 12 BER versus F(γ) at γ = γ* = 3.4

According to Figure 3. 12, κ now varies between 7.2×10^{-4} and 5.49 .Moreover, using subcarrier to noise ratio distribution rather than their average reduces the average BER estimation error from 15.87 to 0.93 and the standard deviation from 47.7065 to 1.2036.

Note that the curve in (3.16) is obtained for independent channel realizations at same TX-RX separation distance of 3 meters. Figure 3. 13 shows again that the behavior remains same as the overall SNR decreases as the TX-RX distance increases and realizations BER performance of shifts up along.

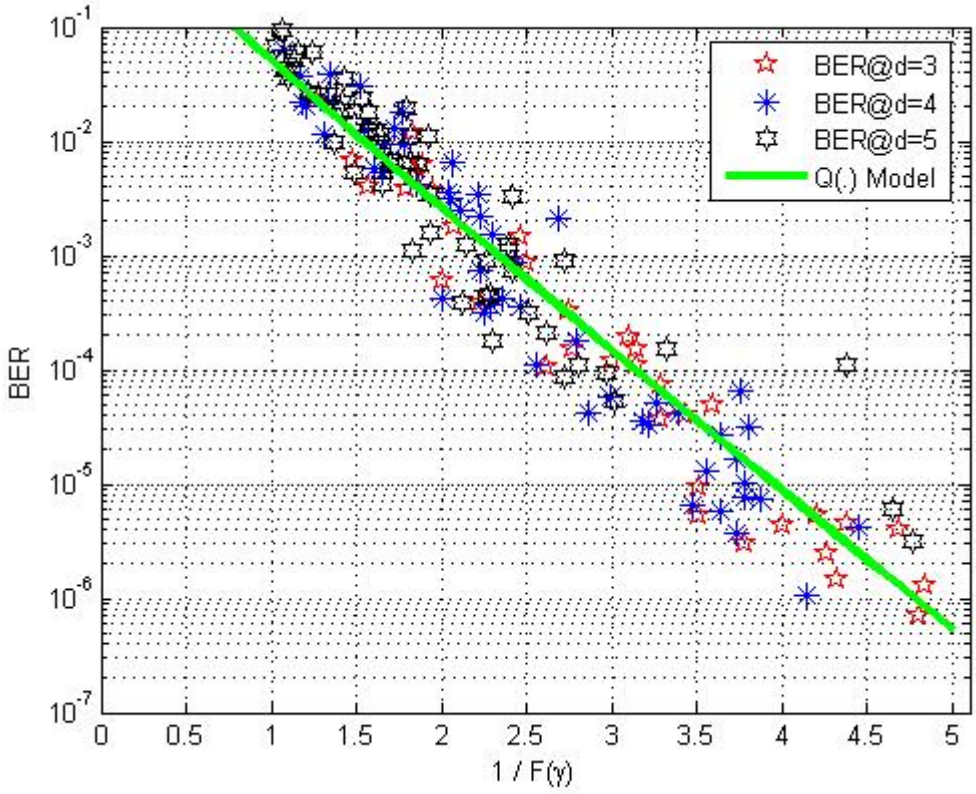

Figure 3. 13 Behavior of the realization BER's at different TX-RX separation distances at γ =3.4

3.4. BER Estimation and Frame Size Optimization Simulation Results

In order to analyze the effect of frame size adaptation based on channel BER estimates, we use 100 channel realizations from Channel Model 1. As a benchmark, we obtain the BER of this realization via extensive simulation and calculate the associated optimal frame sizes. We refer this benchmark as ideal channel adaptation. Time-varying nature

of the wireless-system is simulated by switching to different realizations according to the channel's coherence time T_C as defined in Section 2.1.4.

The final link ARQ efficiency (η_F) is obtained as,

$$\eta_F = \frac{\dfrac{\text{Number of bits delivered to receiver in } 100 \times T_C \text{ second.}}{100 \times T_C}}{R} \qquad (3.17)$$

Figure 3. 14 shows the final link ARQ efficiency at variable user speeds. At human walking speed ($v = 1.35$ m/s), coherence time of the channel (T_{coh}) becomes 10 ms. At *d=3* meters, using fixed 4095B frames gives 21% performance improvement against the frame size that is optimized for the channel's average BER (784B). When the channel is in good condition, the transmission link is better utilized for 4095B frames rather than small size frames. Using frame size adaptation with exact channel knowledge improves the link efficiency against 4095B frames about 11% as a theoretical bound. (MA) with tracking previously transmitted *D*=50 frames, brings 5,38 % performance improvement. On the other hand, link adaptation using CSI using the channel estimates found in Section 2.3.1, brings 7.32% performance enhancement against 4095B frames.

While user speeds increase, the coherence time of the channel and the number of frames transmitted inside the channel coherence time reduces. Thus channel tracking becomes hard for MA. Above some speed, the selected frame sizes do not represent the instantaneous channel conditions. Simulation results show that link adaptation based on MA only produces performance improvement against fixed frame size (4095B) links for user speeds slower than $v = 3\ m/s$. Since link adaptation based on CSI requires a single frame to adapt on new fading conditions, it produces only 3% performance loss from the theoretical bound. At faster user speeds, small number of frames is sent inside the channel's coherence time. So at low BER conditions receiver does not capture enough number of erroneous frames to converge the optimal efficiency for this BER. Hence system slightly overestimates the final link efficiency for ideal and proposed frame size adaptation methods.

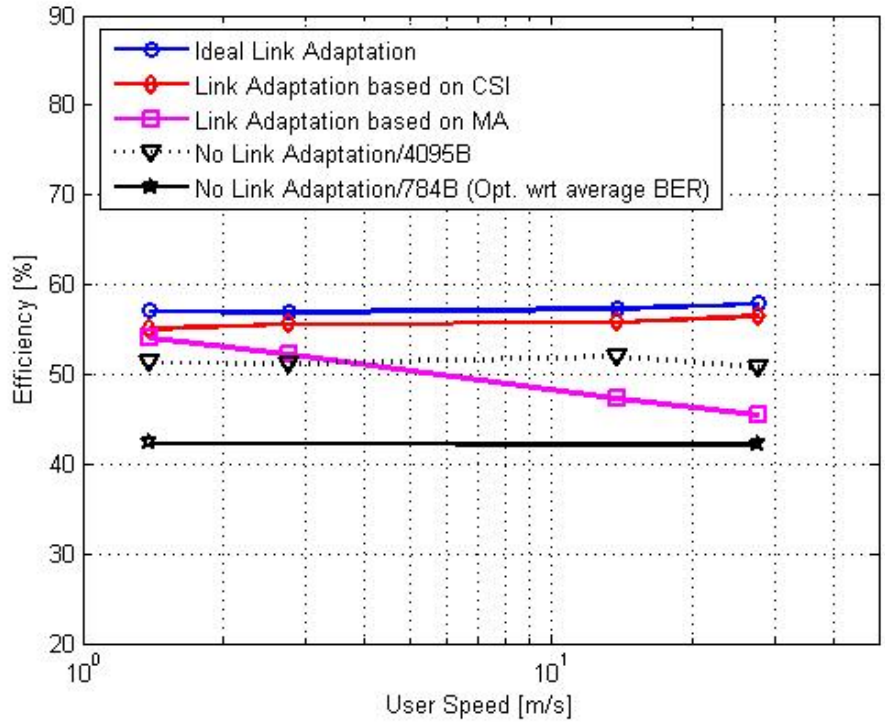

Figure 3. 14 Data Link ARQ Efficiency vs. User Speed at d=3m separation distance

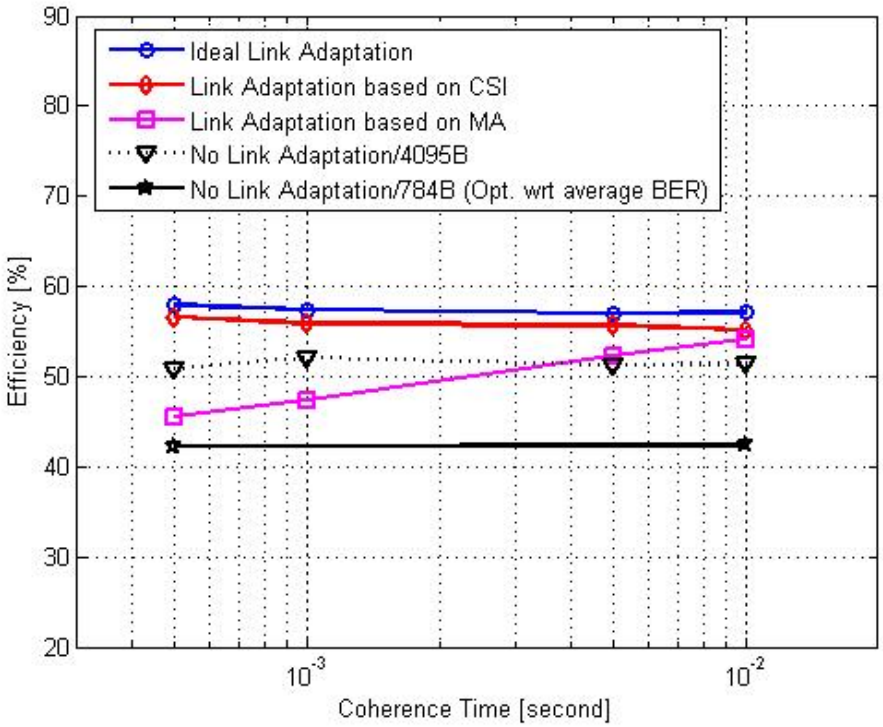

Figure 3. 15 Data Link ARQ Efficiency vs. Coherence Time at d=3m separation distance

At human walking speeds both Modiano's algorithm and the proposed method offers efficiency improvements. Since faster user speeds is irrelevant in applications, in a multi-user scenario connections perceive some portion from the coherence time. So as the number of operating connections increase, the transmission duration inside the coherence time decreases. So a rapid frame size adaptation technique is required for dense number of connections. In Figure 3. 15 the decrease on the transmission duration is shown alike the decrease on the channel's coherence time. As the perceived time from the channel's coherence time decreases, the proposed method still provides efficiency improvement.

In this chapter we show that in time-varying environments the efficiency of a link can be increased with frame size adaptation. In the subsequent chapter we focus on the network performance where individual links compete to access a single MB-OFDM channel. We further try to improve the total network performance by utilizing the already estimated instantaneous channel conditions.

4. WPAN THROUGHPUT IMPROVEMENT BASED ON AN OPPORTUNISTIC SCHEDULING SCHEME

In the previous chapter, we propose and analyze methods to estimate and to monitor the instantaneous BER of the MB-OFDM links, and accordingly optimize the frame size through ARQ policies. The efficiency of wireless links can be further increased through multi-user scheduling methods that take channel conditions into account. Opportunistic multi-user scheduling makes use of these variations and prioritizes the users with the best channel conditions, resulting in improvements in the total throughput performance [27],[28],[29]. Hence, in this chapter, we focus on the total network performance of MB-OFDM based WPANs. At first, we give the medium access structure of IEEE 802.15.3 standard. Based on this standard, we apply equal bandwidth share for all channel requesting links. Following that, we propose an opportunistic channel access scheme by utilizing the already estimated channel conditions in order to maximize the overall network performance. Simulation results finally conclude the chapter.

4.1. IEEE 802.15.3's Medium Access Structure

IEEE 802.15.3 MAC standard has been initially defined for high data rate WPANs that uses radio transmissions at 2.4 GHz [3]. Recently, the standard has been considered for the WPANs that use MB-OFDM in their physical layer [25].

A WPAN is named as "piconet" which allows a number of independent data devices to communicate with each other in a spontaneous (ad-hoc) manner. A piconet confines the communications to a small area around a person or object, which typically covers around 10 meters in all directions and envelops the person or an object whether it is stationary or in motion.

An 802.15.3 piconet is composed of several components as shown in Figure 4. 1, the basic component is "*device*" (DEV). In a piconet, one DEV is required to assume the role of the piconet coordinator (PNC). The PNC provides basic timing, power control and medium access. It also manages the Quality of Service (QoS) requirements of individual transmissions.

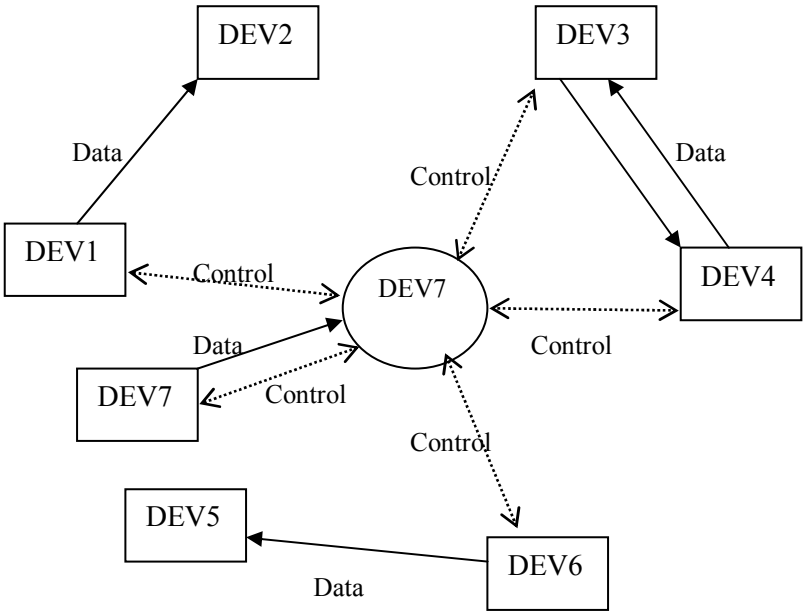

Figure 4. 1 A 802.15.3 Piconet

The 802.15.3 Medium Access is based on a centralized and connection-oriented network topology. A DEV that is capable to operate as a PNC scans the medium for an empty channel. If it finds one, it starts the piconet by sending the beacon after making sure that the channel has remained empty for a specified period of time. Following the receipt of the beacon, the DEVs send channel requests to the PNC. After that, in a time division multiple access fashion, the PNC assigns time slots to requesting links prior to their data communication. A link between two DEV is than established on its allocated time-slot on a peer-to-peer fashion.

In order to perform these operations, the PNC divides the channel time into superframes as shown in Figure 4. 2. The 802.15.3 superframe structure is composed of three major parts.

1. **Beacon:** The DEVs inside the piconet synchronize with the PNC, when the beacon is broadcasted. The beacon carries information elements to inform the DEVs about the duration of the current superframe, beginning-end of the contention access period, start of the contention free period, and the locations of each channel time allocations inside the contention free period. The superframe duration is selected between 0 and 65 ms.

2. **Contention Access Period (CAP):** CAP is used for authentication request/response and channel time request, as well as data transmission. CAP uses random medium access. In this period, when a DEV desires to initiate a link with another DEV, it sends a channel request frame to the PNC. To avoid frame collusions, the standard defines Carrier Sense Medium Access with Collision Avoidance (CSMA/CA). According to CSMA/CA, a DEV first senses the medium. If the medium is empty; it begins transmission. If the medium is busy, the transmission is deferred to a later randomly selected time [50].

3. **Contention Free Period (CFP):** CFP is composed of channel time allocations (CTA) and management channel time allocations (mCTA). CTA is an isolated time-slot, which is dedicated for ongoing communications. If the PNC accepts the channel time request of a DEV, it informs the DEV about the location and duration of the reserved CTA inside the CFP in the following beacon. The communication between two DEVs than take place inside this CTA without interference. The mCTA's are special time-slots that are used for the transmission between DEVs and the PNC. The mCTA can be located everywhere inside the CFP.

Unlike 802.11 networks [3],[46], once time is reserved for the channel requesting links, the PNC is no longer involves the data communications. The data transfer resumes in a peer-to-peer manner inside the CTA as shown in Figure 4. 3.

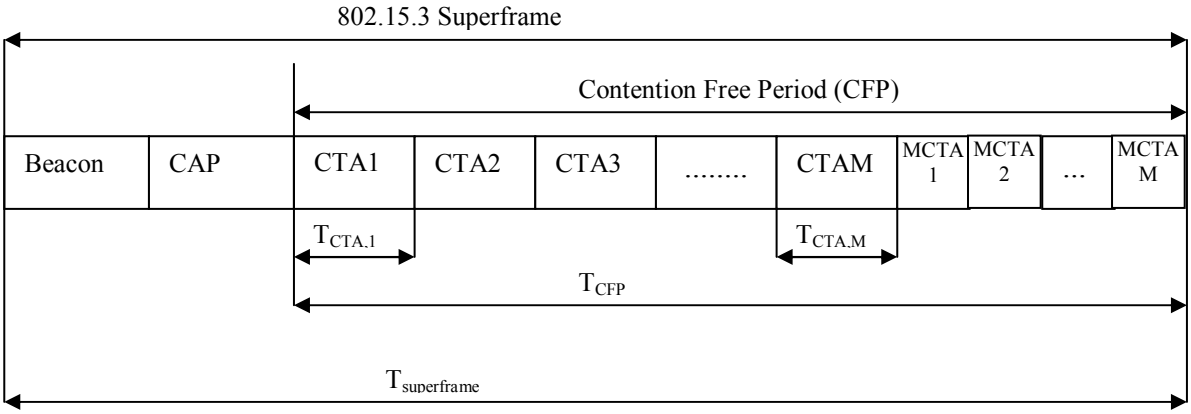

Figure 4. 2 IEEE 802.15.3 Superframe Structure

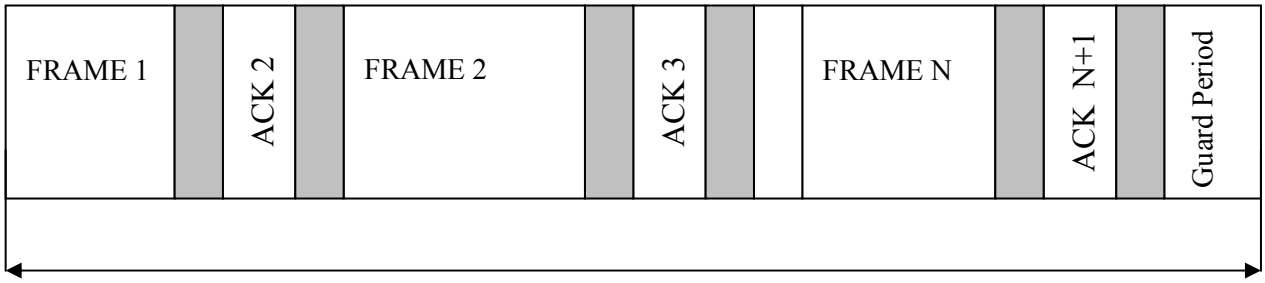

Figure 4. 3 Channel Time Allocation of the i^{th} link inside the contention free period

Frame size adaptation can be performed to increase the link efficiency. When a frame is received successfully, receiver waits for a specific period and it sends back an ACK frame to request the next frame. In our network model, the transmitter calculates the time for delivering a single frame throughout the CTA. If transmitter ensures that the frame delivery can be completed before the end of the CTA, it sends the current frame. If it realizes that frame cannot be delivered without violating the end of the CTA, in order to avoid collisions with the next CTA, the transmitter stops frame transmission and waits for the next superframe. Here, we define the CTA utilization, γ_{CTA}, as,

$$\gamma_{CTA} = \frac{\sum_{i=1}^{P} T_{FRAME,i}}{T_{CTA}} \tag{4.1}$$

where $T_{FRAME,i}$ is the duration of the i^{th} frame and P denotes the number of transmitted frames inside the CTA period (T_{CTA}).

The current form the IEEE 802.15.3 superframe structure does not include any scheduling scheme that manages the time allocations of channel requests inside the contention free period. In this study we consider a single MB-OFDM channel as the resource to be shared between the connection requests. We first share the channel equally to the requesting links. In order to improve the total network performance, we then present an opportunistic channel-sharing scheme based on the instantaneous channel conditions.

4.2. Equal Time Sharing Scheme

As a reference case, we suggest that PNC has no information about the conditions of the independent channel requesting links. Therefore, the PNC assigns the time allocations of each link equally in a round-robin fashion. We name this medium access scheme as "*Equal Time Sharing*" where the assigned T_{CTA} for the i^{th} requesting link is given as,

$$T_{CTA,i} = \frac{T_{CFP}}{M} \quad i = 1, 2, .., M \tag{4.2}$$

T_{CFP} denotes the duration of the contention free period and M is the total number of channel requesting links.

When the communication links inside the piconet experience similar channel conditions, equal time-sharing provides fairness in terms of delivered net data throughput. On the other, when one of the links is in a deep fade, its frame fails, and the frames will have to be retransmitted numerous times until the channel recovers. Therefore, the entire time allocated for the faded link becomes wasted.

The links quality can be measured in terms of number of erroneous frames, and when the link is in deep fade fragmentation can be applied to reduce frame errors. Also we can use the already estimated channel BER from the sub-carrier to noise ratio

distribution. Time allocation using the channel knowledge can increase the performance.

4.3. Proportional Time Sharing Scheme

Since wireless channels have time-varying characteristics, different wireless links perceive different channel quality at the same time because of shadowing, path losses due to the channel environment, and user mobility. These variations in the channel conditions can be exploited to increase the total network performance. The basic idea behind exploiting the channel variations is to schedule more of the resources to a link or a user at a given time. In literature, such scheduling mechanisms are called "Opportunistic Scheduling" [27]-[29].

In this work, we define an access scheme where the time allocations of each link is determined proportionally according to the link's instantaneous efficiency as,

$$T_{CTA,i} = \frac{\eta_i}{\sum_{i=1}^{M} \eta_i} T_{CFP} \quad i = 1, 2, .., M \tag{4.3}$$

where η_i can be the estimated or measured link efficiency inside the last CTA of i^{th} link. We name this approach as "*Proportional Time Sharing*" scheme. This scheme is opportunistic because when the link is in good condition, the PNC allocates more time to transmissions with high link-ARQ efficiency. Unlike most of the opportunistic schemes in the literature, this scheme also allocates some time for deep faded links. This modification provides the PNC to track the network conditions. If the scheduling scheme does not allocate some time for deep-faded links, the PNC cannot be aware when the faded links recover.

When the link is in a very deep fade, namely $\eta_i \approx 0$, mathematically the channel time allocation period for this link goes down to zero. To track channel conditions, the channel time allocations needs to guarantee at least one frame transmission. For such cases the measured efficiency has to be raised up to some value to guarantee at least one frame delivery.

For the worst scenario, namely (*M-1*) links have good channel conditions ($\eta_i = \eta_{\max} = 0.9064$) and one deep faded link with efficiency $\eta_f \approx 0$, the allocated time for the faded link becomes,

$$T_{FRAME} = \frac{\eta_f}{\left(\sum_{i=1}^{M-1} \eta_i\right) + \eta_f} \times T_{CFP} \tag{4.4}$$

Then solving the above equation for $\eta_{\min} = \eta_f$,

$$\eta_{\min} = \frac{0.9064 \times (M-1)}{\frac{T_{CFP}}{T_{FRAME}} - 1} \tag{4.5}$$

When the link layer operates with fixed 4095B frames, the frame duration T_{FRAME} is about $80\mu s$. Similar to that, when link adaptation is performed via MA, the last frame inside the CTA may have been stopped at 4095B. For both cases, the required time to make frame delivery (T_{FRAME}) must be selected as $80\mu s$. When link adaptation is performed via CSI, a deep-faded link operates on significantly smaller frame sizes compared to 4095B frames. Thus, operating on such small frame sizes reduces the required time to track deep-faded links. According to Figure 3. 5, while the link-ARQ efficiency is between 0% and 10%, the optimal frame size varies between 0B and 128B. For our proposed scheme, we select 128B frame duration, $10\mu s$, for T_{FRAME}.

When we have multiple operating links, the minimum required efficiencies are obtained as in Figure 4. 4. When the link layer operates with fixed 4095B frames, the minimum required efficiency increases drastically as the number of operating links increases. Finally, for *M*=25 links, $\eta_{\min}$ has to be selected about 90%, which is equal to the maximum link-ARQ efficiency obtained from MB-OFDM PHY at 480 Mbps. In other words, the PNC has to ignore the fading conditions to guarantee channel tracking. On the other hand when the link adaptation is performed via CSI, for *M*=25 links, selecting the minimum required efficiency about 10% becomes enough for channel tracking.

In order to obtain performance improvements from the proportional time-sharing scheme, the superframe duration has to be selected smaller than the coherence time of the channel. Unlike most other multi-user systems, the PNC cannot directly measure the quality of each link in an ongoing communication. To provide a channel feedback, the transmitter device of each link needs to send its link status back to the PNC. For this purpose, mCTAs in the contention free period can be utilized, and the PNC can make the scheduling decisions accordingly.

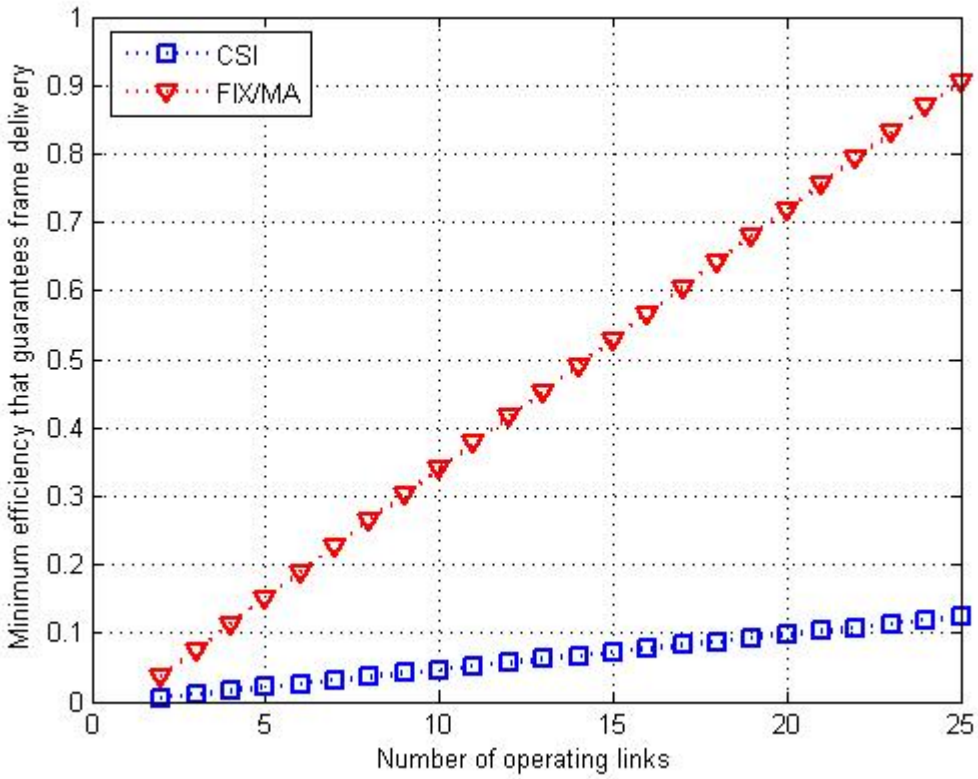

Figure 4. 4 Minimum Efficiency required for frame delivery

4.4. Multiple Link Scheduling Simulation Results

In order to evaluate the performance of our proposed link adaptation and access schemes, namely optimal frame size adaptation and proportional time-sharing, we have simulated MB-OFDM UWB PHY and IEEE 802.15.3 WPAN MAC described in Chapter III. We test the performance of the access schemes, when all links inside the piconet experience similar channel conditions under 480Mbps data rate and the TX-RX separation of all links is selected as 3 meters. For the wireless channel, we consider channel model 1, with multipath fading, AWGN and path loss effects, and no

interference. Time-varying properties of the channel are modeled by switching channel realizations with respect to the coherence time that is determined by the user speed. In order to obtain the steady state performances, channel response of each link is varied at least 100 times within the simulation time. Coherence time of the UWB channel is selected as 10 ms., which corresponds to human walking speed (about 1,35 meters/second) at UWB frequencies. Beacon and the contention periods are not modeled explicitly ($T_{superframe} = T_{CFP}$) and we assumed that connection requests and management packets are delivered correctly inside the CAP. We selected the superframe duration as 2 ms, so that the channel remains static during five successive superframes. 4095B frames are selected to compare the performance of the link-ARQ efficiency between the fixed frame size selection and the adaptive frame size selection.

In order to test the performance of the proportional time-sharing scheme with and without frame size adaptation we calculate the instantaneous the link efficiencies of (4.3) as follows:

1. *PTS-CSI (Proportional time sharing / link adaptation with channel state information):* The instantaneous BER for each frame is estimated according to Eq.(3.16). i^{th} link's current CTA period is determined according to Eq.(3.7) and Eq.(3.8) based on the last BER estimate obtained at the i^{th} link's previous CTA.

2. *PTS-FIX (Proportional time sharing / Fixed 4095B frames):* When opportunistic channel sharing is implemented with fixed frame sizes, i^{th} link's current CTA period is determined according to the link-ARQ efficiency measured inside the i^{th} link's previous CTA.

3. *PTS-MA (Proportional time sharing / Modiano's Algorithm):* When opportunistic channel sharing is implemented with MA, we consider a reverse method. As M increases, time assigned for each link and number of frames transmitted inside the channel time allocation period's decreases. Hence channel adaptation becomes hard. To alleviate this problem, we first measure the link-ARQ efficiency as described in 2. Frame adaptation is performed subsequent to the channel time management. Since good links capture more time, their frame

adaptation facilitates. When the receiver counts D=50 frames over successive CTAs, it performs frame size adaptation.

To obtain the theoretical bound for PTS, we use the previously recorded 100 channel realizations where their associated BER is known explicitly. Thus, peer-to-peer links use ideal frame sizes throughout their data transmission. We also assume that the PNC knows the exact channel conditions prior to the channel time management. So, the efficiencies of the deep-faded links are not raised to a minimum value for tracking the channel conditions.

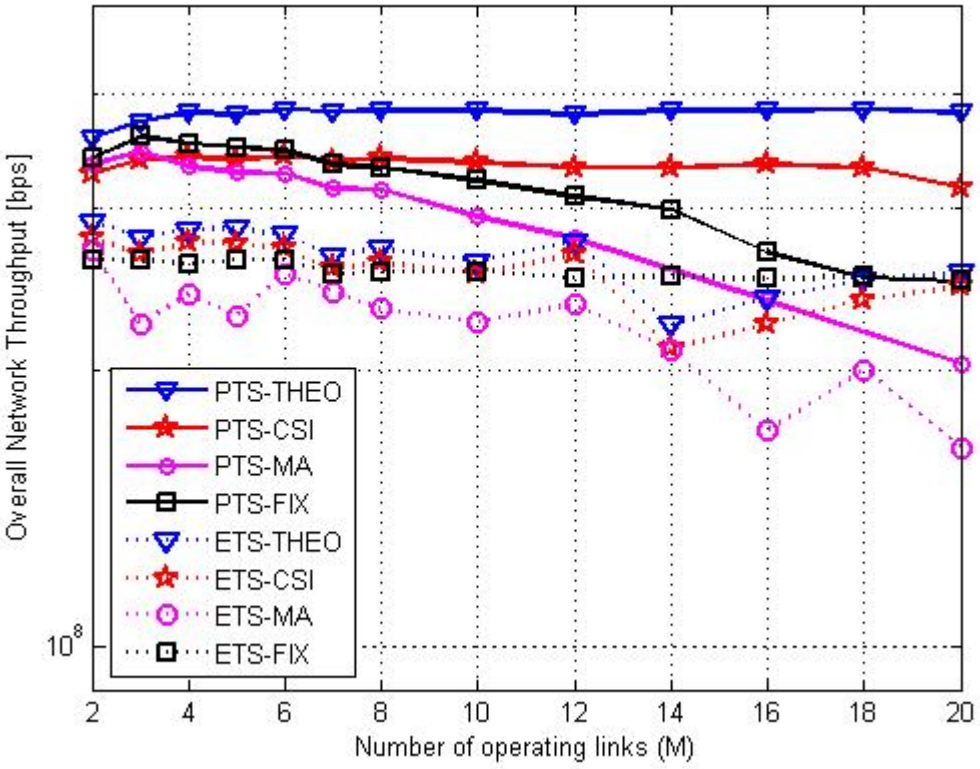

Figure 4. 5 Piconet's overall throughput vs. the number of operating links

Figure 4. 5 show the piconet's overall encountered throughput with respect to number of simultaneously operating links while employing ETS and PTS schemes both using frame size adaptation and fixed frames. Under ETS scheme, when the data link layer uses fix 4095B frames, all links inside the piconet undergo similar channel conditions and the overall network throughput retains stable about 264 Mbps. Under ETS with low number of operating links ($M \le 6$), frame size adaptation in link layer theoretically brings about 10% performance improvements against using 4095B frames. For the same

number of links, link adaptation with CSI brings performance improvements up to 5%. Link adaptation with MA brings performance improvement about 2.5% against fixed size frames only for M=2 links. For M>2, number of frames sent within each channel time allocation period decreases and channel cannot be tracked. For large M values, algorithm selects random frame sizes resulting random network performance.

Under proportional time-sharing scheme with ideal BER knowledge, the overall efficiency increases with the number of operating links for M<4. Increasing M also increases the probability of finding a link with a good channel conditions. For $M > 4$, the network's overall throughput is measured about 384 Mbps as a theoretical limit. At the theoretical performance, the PNC does not schedule the links with $\eta_i \approx 0$ inside the contention free period. Hence the overall network performance is not affected by the number of operating links. Due to the channel estimation errors, and mis-scheduled superframes that occur when individual links just experience new fading conditions; PTS/CSI offers 336 Mbps network throughput for $M > 4$. Since deep-faded links consume very small time inside the superframe, the overall network performance remains stable as M increases. Eventually, for M>18, the time consumed by deep-faded links becomes significant inside the contention free period and the time allocated to good links reduces. Thus the performance begins to decrease.

PTS/FIX offers maximum 360 Mbps network throughput for M=3 links In order to make a proportional time-scheduling, the link's instantaneous efficiency in a given CTA has to be determined first. Thus PTS requires at least one frame transmission inside each CTA to measure the instantaneous link efficiency. So with fixed frame size selection as M increases the time allocated for the deep faded links becomes a significant overhead inside the CFP and CTA durations of each connection becomes equal. Hence, the performance of the PTS converges to the performance of ETS. Eventually, about M=20, the performance of the PTS/FIX becomes equivalent to ETS/FIX.

On the other hand PTS/FIX provides more total network throughput against PTS/CSI for low number of connections (M<6*)*. Since 4095B frame size is not the optimal size for the conditions that have BER greater than 10^{-6}, the link's measured efficiency is

much smaller than the optimal efficiency value obtained with CSI. So at these instants, PTS/FIX assigns rather smaller CTA durations to these links as compared to PTS/CSI. Instead PTS/FIX increases the CTA durations of the links that have BER<10^{-6} where the optimal frame size is 4095B.

The PTS/MA provides the maximum total network throughput at M=3 links as 345Mbps. PTS/FIX's performance is superior against PTS/MA because PTS/FIX does not include the frame adaptation of D frame duration to make a frame size decision on the states where BER is less than 10^{-6}. On the other hand, PTS/MA still provides significant performance improvement against ETS schemes up to M=8 operating links. Beyond this, PTS/MA looses its channel tracking capability because of the insufficient CTA durations and the time allocated for the deep faded links becomes a significant overhead. For increasing M, the performance of PTS/MA decreases linearly.

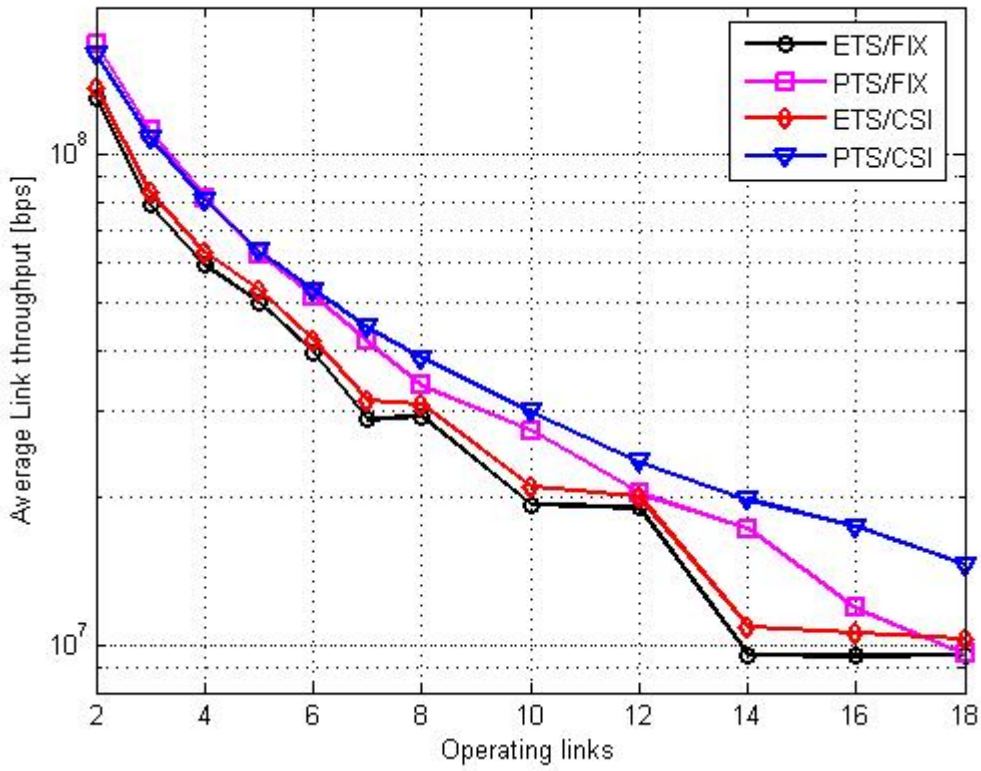

Figure 4. 6 Individual links average throughput vs. number of operating links

Figure 4. 6 shows individual connections average data throughput with and without the proposed frame size adaptation and time-scheduling methods. Since a single MB-OFDM channel is shared to the operating connections, increasing M decreases the

user's net data throughput. Similar to the results found in the previous chapter, frame size adaptation with CSI improves the data throughput about 7% as compared with fixed frame size selection. For low number of connections ($M<7$), under frame size adaptation with CSI, PTS further improves the average individual link throughputs about 23% as compared to ETS.

Under equal time sharing schemes with and without frame size adaptation, simulation results show that the average throughput remains stable for some number of operating links. To explain this behavior, the number of transmitted frames inside each CTA has to be counted. As an example, for M=14 to M=18 operating links, the CTA durations of each link varies between 142 μs and 111 μs. When a channel is under good condition, for these numbers of connections transmitter can only send one 4095B frame with duration 80 μs inside each CTA. Since the number of bits delivered to the receiver inside the entire simulation duration is nearly equal, the average data throughput per user does not change. The CTA utilization factor defined in Eq. (4.1) is lowest (0.56) for M=14 which means a huge silence time inside each CTA. This wasted time causes the notch in Figure 4. 5 (ETS-THEO/CSI with M=14) As M further increases the wasted time inside the CTA reduces and the overall network throughput increases. When the CTA utilization is minimum for M=14 PTS/CSI provides 110% performance improvement on the average data throughput per user as compared to ETS/FIX.

The time allocated to deep faded connections inside the CFP is insignificant for low number of operating links, and a 4095B frame is the optimal size at the channel instants that offers highest efficiency. As a result of these two properties PTS/CSI and PTS/FIX yield similar individual data throughput performances. On the other hand as M increases, the average data throughput obtained with PTS/FIX decreases to the value obtained with ETS/FIX while for M=18 PTS/CSI still provides 50% improvement as compared to ETS/FIX.

Under PTS/CSI scheme, there is a trade-off between the number of schedulable links inside the contention free period and the scheduling performance received from the piconet. According to Figure 4. 7 at $T_{coherence} / T_{superframe}=5$, M=18 simultaneously operating links are schedulable inside the contention free period while keeping the overall network efficiency around 70% (overall network throughput=336 Mbps). Similarly if we want to schedule more links keeping the same ratio, link's mobility

needs to be decreased, which allows the PNC select larger superframe durations. On the other hand, as the superframe duration decreases ($T_{coherence}$ / $T_{superframe}$=10), the mis-scheduled superframes that occur when channel just experiences new fading conditions consumes less time. So selecting superframe durations of 1 ms enhances the maximum network throughput performance slightly around 2%. Unfortunately, selecting small superframe duration decreases the number of schedulable links inside the contention free period. PTS/CSI schedules up to 10 links with network efficiency above 70%. For $M \geq 10$, the overall network throughput begins to decrease and finally for $M > 12$, PTS/CSI scheme cannot schedule all channel requesting links inside the contention free period.

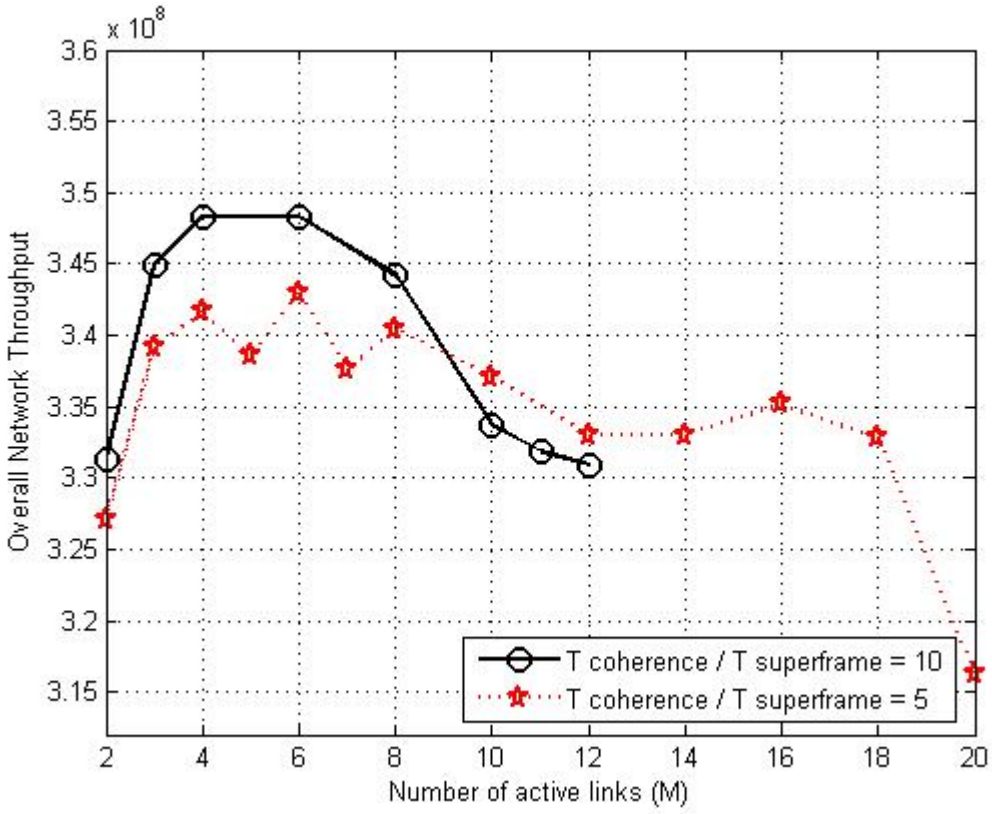

Figure 4. 7 Effect of $T_{coherence}$ / $T_{superframe}$ on the overall network performance

5. CONCLUSIONS and FUTURE WORK

In this thesis, the complete MB-OFDM physical layer with the IEEE's UWB channel model is examined through the simulator we develop in MATLAB environment.

Under erroneous multipath fading channels, we analyze the performance of MB-OFDM links and try to maximize the link efficiency through the ARQ policies. In order to maximize the throughput per link, frame sizes used in the data link layer is selected optimally and dynamically based on the instantaneous BER of the channel. The coded BER performance is first examined in terms of E_b/N_0. In order to obtain a iBER estimate based on the channels instantaneous E_b/N_0, we fit a curve to the empirical BER versus E_b/N_0 results. Unfortunately, this curve does not provide an accurate BER estimate. Empirical BERs deviate much from the estimation value with the mean normalized absolute error of 15.87. We also show that when the observation period is long and the size of the transmitted frames within the observation period is large enough, Modiano's BER estimation algorithm converges to the link's ideal BER

To obtain a more accurate iBER estimate, we analyze the CNR distribution of a number of channels and showed that the channel BER is highly correlated with the number of subcarriers whose CNR is less than some specific threshold. Using correlation between the CDFs and BERs, the optimum CNR threshold is found as 3.4. We then accurately model the empirical BERs as a function of number of subcarriers where CNR of one of them is below the optimum threshold using a Q function with appropriate scaling factors. We find that the new model provides a means of the estimate BER accurately with the mean of normalized absolute error of 0.93.

The BER estimation is then used in the frame size optimization. At 3 meters TX-RX distance where ideal frame size selection enhances the link layer efficiency about 11% against most favorable fixed frame size (4095B), MA increases the efficiency 5% against 4095B frames. Since MA requires D frame transmission prior to make an iBER estimate, it results poor performance against fixed 4095B frames at fast fading channels. Since the proposed iBER estimation method requires a single frame to make an iBER

estimate, under realistic user speeds frame size selections based on these estimates enhances the link efficiency about 7% against selecting a fixed frame.

In Chapter IV, the overall network throughput performance of IEEE 802.15.WPAN is examined first where MB-OFDM is the underlying physical layer. Under equal time-sharing, simulation results show that ideal frame size selection brings 10% and link adaptation with CSI brings about 5% performance improvements on network throughput against using fixed 4095B frames. For both cases, we show that as M increases CTA utilization becomes an important factor on the overall network throughput. We also show that link adaptation with MA output poor performance against using fixed frame size for $M>2$, since it is hard to track the channel changes inside the given channel allocation period.

Without frame size adaptation PTS scheme offers maximum 360 Mbps network throughput as ETS offers 260 Mbps network throughput around. On the other hand, under fixed 4095B frame size selection, as M increases the performance of the PTS converges to the performance of ETS. Under given simulation settings, priory knowledge of ideal iBER, bounds the overall network throughput performance of PTS around 384 Mbps. PTS/CSI keeps the overall network throughput around 336 Mbps up to $M=18$ operating links. As M further increases allocated time for the deep faded links consume a significant overhead inside the CFP which result a decrease on the overall network throughput performance. PTS/MA gives maximum network throughput 345Mbps, for $M=3$ operating links, but as stated in the previous paragraph, its performance decreases as the number of operating links increases.

The individual links average data throughput inside the IEEE 802.15.3 WPAN is than measured. Similar to the recently obtained results, under ETS, frame size adaptation with CSI improves the average data throughput per user about 7% against using fixed 4095B frames. Given that frame size adaptation is performed based on the proposed iBER estimates, PTS further improves the average data throughput by 23% as compared to ETS for low number of operating links. Simulation results show that when the CTA utilization factor of ETS is minimum (0.56) for $M=14$ links, PTS/CSI brings maximum 110% performance improvement on the data throughput against ETS/FIX.

As some suggestions for future work, the results presented so far can be recalculated for other possible data rates and channel models. The BER performance of MB-OFDM links can be further analyzed under non-perfect symbol synchronization. Having the complete physical layer model available, the Gilbert-Elliot Model [50] of UWB channels can be obtained for a given frame size. This model can be further used in network simulations to describe the entire physical layer. Moreover, link BER estimation using CSI can be used in power management to keep the instantaneous BER around a desired value. In this work, the channel introduces only multipath fading and additive white noise. The performance of the MB-OFDM links can be further examined under simultaneously operating piconets. For this purpose, using the techniques in literature, the transmitted MB-OFDM symbols can be spread in time to avoid from the collisions.

REFERENCES

[1] Prasad, R.; “OFDM for Wireless Communications Systems”, Artech House Publishers, 2004

[2] Pahlavan, K., Krishnamurthy, P. “Principles of Wireless Networks”, Prentice Hall, 2002

[3] IEEE Standards Department, "Wireless LAN medium access control (MAC) and physical layer (PHY) specifications", IEEE standard 802.11-1997

[4] IEEE Std 802.15.3-2003 IEEE standard for information technology - telecommunications and information exchange between systems - local and metropolitan area networks - specific requirements part 15.3: wireless medium access control (MAC) and physical layer (PHY) specifications for high rate wireless personal area networks (WPANs)

[5] Swiak, K; McKeown, D: "Ultra Wideband Radio Technology". John Wiley & Sons, 2004

[6] Federal Communications Commission, “First report and order 02-48,” 2002.

[7] IEEE 802.15 WPAN High Rate Alternative PHY Task Group 3a (TG3a) “http://www.ieee802.org/15/pub/TG3a.html”

[8] Fisher R., Kohno R., Mc Laughlin M, Welborn M., “DS-UWB physical layer submission,” 2004. Document IEEE 802.15-03.

[9] Aiello, G.R.; Rogerson, G.D.; “Ultra-wideband wireless systems” Microwave Magazine, IEEE Volume 4, Issue 2, June 2003 Page(s):36 – 47

[10] Batra et al., “Multi-band OFDM physical layer proposal,” 2003. Document IEEE 802.15-03.

[11] Batra, A.; Balakrishnan, J.; Aiello, G.R.; Foerster, J.R.; Dabak, A.; **“**Design of a multiband OFDM system for realistic UWB channel environments” Microwave Theory and Techniques, IEEE Transactions on Volume 52, Issue 9, Part 1, Sept. 2004 Page(s):2123 – 2138

[12] A. Rajeswaran, V. S. Somayazulu and J. R. Foerster, “Rake performance for a pulse based UWB system in a realistic UWB indoor channel,” Proc. IEEE ICC’03, vol.4, pp.2879–2883, 2003.

[13] D. Cassioli, M. Z. Win, F. Vatalaro, and A. F. Molish, “Performance of low-complexity Rake reception in a realistic UWB channel,” Proc.IEEE ICC’03, vol.2, pp.763–767, 2003.

[14] Roberto Aiello et al. "Multi-band performance tradeoff". IEEE P802.15 Working Group for Wireless Personal Area Networks, IEEE P802.15-03/209r3, May 2003.

[15] Win, M.Z.; Scholtz, R.A.; "Impulse radio: how it works" Communications Letters, IEEE Volume 2, Issue 2, Feb. 1998 Page(s):36 - 38

[16] Seung Young Park; Gadi Shor; Yong Suk Kim; "Interference resilient transmission scheme for multiband OFDM system in UWB channels" Circuits and Systems, 2004. ISCAS '04. Proceedings of the 2004 International Symposium on Volume 5, 23-26 May 2004 Page(s) 373 - 376

[17] Kumar, N; "MAC and Physical Layer Design for UWB Communications", MSc Thesis, Virginia Polytechnic Institute, 2004

[18] Ramachandran, I.; Nakache, Y.-P.; Orlik, P.; Molisch, A.F.; Jinyun Zhang; "Symbol spreading for ultrawideband systems based on multiband OFDM" Personal, Indoor and Mobile Radio Communications, 2004. PIMRC 2004. 15th IEEE International Symposium on Volume 2, 5-8 Sept. 2004 Page(s):1204 - 1209 Vol.2

[19] Joo Heo; KyungHi Chang; "Exploitation of extra diversity in UWB MB-OFDM system" Wireless Communications and Applied Computational Electromagnetics, 2005. IEEE/ACES International Conference on 3-7 April 2005 Page(s):9 – 12

[20] Chebl, R; "Performance of Multiband OFDM in IEEE UWB Channels", MSc Thesis, Chalmers University of Technology, Sweden, 2004

[21] M.-O. Wessman, A. Svensson and E. Agrell, "Frequency diversity performance of coded multiband-OFDM systems on IEEE UWB Channels," IEEE Veh. Tech. Conf. fall, Los Angeles, CA, USA, Sept. 2004. pp.1197–1201.

[22] Siew, C.K.; Goodman, D.J.;"Packet data transmission over mobile radio channels" Vehicular Technology, IEEE Transactions on Volume 38, Issue 2, May 1989 Page(s):95 – 101

[23] Hara, S.; Ogino, A.; Araki, M.; Okada, M.; Morinaga, N.;"Throughput performance of SAW-ARQ protocol with adaptive packet length in mobile packet data transmission" Vehicular Technology, IEEE Transactions on Volume 45, Issue 3, Aug. 1996 Page(s):561 – 569

[24] Modiano,E. "An adaptive algorithm for optimizing the packet size used in wireless ARQ protocols". Wireless Networks (1999), 279–286.

[25] Rangnekar , A.; Sivalingam, K.M.;"Multiple channel scheduling in UWB based IEEE 802.15.3 networks" Broadband Networks, 2004. BroadNets 2004. Proceedings. First International Conference on 2004 Page(s):406 – 415

[26] Ranran Zeng; Geng-Sheng Kuo; "A novel scheduling scheme and MAC enhancements for IEEE 802.15.3 high-rate WPAN" Wireless Communications and Networking Conference, 2005 IEEE Volume 4, 13-17 March 2005 Page(s):2478 - 2483 Vol. 4

[27] Xin Liu; Chong, E.K.P.; Shroff, N.B.; "Optimal opportunistic scheduling in wireless networks"Vehicular Technology Conference, 003. VTC 2003-Fall. 2003 IEEE 58th Volume 3, 6-9 Oct. 2003 Page(s):1417 – 1421

[28] Xin Liu; Chong, E.K.P.; Shroff, N.B.; "Opportunistic transmission scheduling with resource-sharing constraints in wireless networks" Selected Areas in Communications, IEEE Journal on Volume 19, Issue 10, Oct. 2001 Page(s):2053 - 2064

[29] Zhang,Z; He, Y; Chong, E.K.P.; "Opportunistic downlink scheduling for multiuser OFDM systems" Wireless Communications and Networking Conference, 2005 IEEE Volume 2, 13 March 2005 Page(s):1206 - 1212.

[30] Proakis J.G.; "Digital Communications", McGraw-Hill 4th ed, 2001.

[31] Richard Van Nee, Ramjee Prasad, "OFDM for Wireless Multimedia Communications", Artech House Publishers, Boston, London, 2000.

[32] Coleri, S., Ergen, M., Puri, A., Bahai, A; "A Study of Channel Estimation in OFDM Systems" Vehicular Technology Conference, 2002. Proceedings. VTC 2002-Fall. 2002 IEEE 56th, Volume 2, 24-28 Sept. 2002 Page(s):894 - 898 vol.2

[33] Rappaport, T.; "Wireless Communication: Principles and Practice", Prentice Hall, 2002.

[34] Molisch, A.F.; Foerster, J.R.; Pendergrass, M.; "Channel models for Ultrawideband personal area networks" Wireless Communications, IEEE Volume 10, Issue 6, Dec. 2003 Page(s): 14 – 21

[35] J. Foerster et al., "Channel modeling sub-committee report final," IEEE P802.15 Wireless Personal Area Networks, P802.15-02/490r1-G3a,Feb. 2003.

[36] Saleh, A.;Valenzuela, R.; "A statistical model for indoor multipath propagation," IEEE Journal on Select. Areas Commun., vol. 5, pp. 128–137, Feb. 1987

[37] Fetchel, S. A.; "OFDM carrier and Sampling Frequency Synchronization and its performance on stationary and mobile channels", IEEE Transactions on Consumer Electronics, Vol 46, No 3, August 2000.

[38] Kim, D.K. et.al. "A new joint algorithm of symbol timing recovery and sampling clock adjustment for OFDM systems", IEEE Transactions on Consumer Electronics, Vol 46, No 7, July 1998.

[39] Byungjoon Park; Hyunsoo Cheon; Changeon Kang; Daesik Hong; "A simple preamble for OFDM timing offset estimation", Vehicular Technology Conference, 2002. Proceedings. VTC 2002-Fall. 2002 IEEE 56th , Volume: 2 , 24-28 Sept. 2002 Pages:729 - 732 vol.2

[40] Schmidl, T.M.; Cox, D.C; "Robust frequency and timing synchronization for OFDM" Communications, IEEE Transactions on , Volume: 45 , Issue: 12 , Dec. 1997 Pages:1613 – 1621

[41] Moose, P.H.; "A technique for orthogonal frequency division multiplexing frequency offset correction" Communications, IEEE Transactions on , Volume: 42 ,Issue: 10 , Oct. 1994 Pages:2908 – 2914

[42] Nandula, S.; Giridhar, K.; "Robust timing synchronization for ofdm based wireless lan system" TENCON 2003. Conference on Convergent Technologies for Asia-Pacific Region , Volume: 4 , Oct. 15-17, 2003 Pages:1558 – 1561

[43] Morelli, M.; Mengali, U.; "An improved frequency offset estimator for OFDM applications" Communications Letters, IEEE , Volume: 3 , Issue: 3 , March 1999 Pages:75 – 77

[44] Hlaing Minn; Bhargava, V.K.; Letaief, K.B.; "A robust timing and frequency synchronization for OFDM systems", Wireless Communications, IEEE Transactions on , Volume: 2 , Issue: 4 , July 2003 Pages:822 – 839

[45] Scharf, L.L. "Statistical signal processing:, estimation, and time series analysis", Addison-Wesley, Inc., 1991.

[46] Heiskala, J.,Terry, J.; "OFDM Wireless LANs: A Theoretical and Practical Guide", SAMS Publishing, 2002

[47] The Mathworks http://www.mathworks.com/

[48] Sari, H.; Karam, G.; Jeanclaude, I.; "Transmission techniques for digital terrestrial TV broadcasting", Communications Magazine, IEEE Volume 33, Issue 2, Feb. 1995 Page(s):100 - 109

[49] Kyu-Man Lee; Dong-Seong Han; Ki-Bum Kim; "Performance of the Viterbi decoder for DVB-T in Rayleigh fading channels" Consumer Electronics, IEEE Transactions on Volume 44, Issue 3, Aug. 1998 Page(s):994 – 1000.

[50] Griffiths, W. E.; Hill, R.C.; Judge, G.G.; "Learning and practicing econometrics" Wiley, 1993.

[51] Leon-Garcia, A.; Widjaja, I.; "Communication Networks: Fundamental Concepts and Key Architectures", McGRAW-HILL, 2004

[52] Tranter, W.H.;Shanmugan, K.S.;Rappaport, T.S.;Kosbar K.L. "Principles of Communication Systems with Wireless Applications" Prentice Hall 2003